Master thesis

# Studies and Optimization for Future Beam Dump Experiments in the K12 and P42 Beams at CERN

Florian Stummer

florian-stummer@live.at
Matr.Nr. 01526524
Date: May 21, 2021

*Supervised by*
Univ. Prof. Dipl.-Phys. Dr. Jochen Schieck
Dr. Alexander Gerbershagen



## Acknowledgements

First of all, I want to express my gratitude to my supervisors Alexander Gerbershagen, who guided me through the research for my thesis, and Jochen Schieck for supporting me in my thesis at CERN wherever he could on the university side.

I wish to extend my special thanks to Gian Luigi D'Alessandro who introduced me to the software used for the simulations and the various tools that are used by the BE-EA-LE section. His guidance was very valuable to me and without his support and the BDSIM model of the K12 beam line he designed the achievements made in the studies of this work could not have been accomplished.

Furthermore, I would like to thank Johannes Bernhard, Lau Gatignon, Gaia Lanfranchi and Simone Schuchmann for their input and ideas, as for their feedback on the model building for the optimization studies.

I wish to acknowledge the work that has been carried out by Maarten Van Dijk, whose FLUKA model of the ECN3 shielding geometry and field map generator helped a lot, and Marcel Rosenthal, who previously investigated the setup for NA62-BD and whose studies made with G4Beamline were of great use during the studies for this thesis.

Stefan Alexandru Ghinescu, Tommaso Spadaro and Babette Dobrich offered valuable data from the NA62 experiment which I used in the validation of the BDSIM model of K12 in beam dump mode and I would like to show my deep appreciation for their help.

Finally, I want to acknowledge the advice given by the members of the BE-EA-LE section. The discussions during the section meetings had great impact on my work. All of them did a great job in helping me to attain these results.

**Abstract**

During the beam operation years 2021-2025 at CERN the NA62 experiment is expected to reach its goal of making a more precise measurement of the branching ratio of the decay $K^+ \to \pi^+\nu\bar{\nu}$. There is a number of potential future experiments under consideration which could utilize the beam lines P42 and K12 that currently provide the beam for NA62. One possibility would be to operate the K12 beam line in a beam dump mode. The experiment taking data in such a beam line setting is called NA62 beam dump (NA62-BD) and would be able to use the NA62 detectors to search for dark matter decays downstream the beam dump thereby looking for physics beyond the Standard Model. Additionally, a possible off-axis experiment alongside the K12 beam line called SHADOWS is considered, which would be able to focus on the search for feebly interacting particles. Prior to these experiments preliminary studies need to be performed to optimize the setup and to reduce the backgrounds that blur the signals of the detectors. Therefore, simulations in the Geant4-based software BDSIM have been performed to gain insight on the expected backgrounds and to evaluate the possibilities for reducing them. The BDSIM model of the K12 beam line has been validated in beam dump mode and the simulation data is in good agreement with measurement data provided by NA62. It was confirmed that in beam dump mode the muon background will be the main background and that it needs to be minimized. An optimization study for the magnetic field configuration of BEND1, a dipole configuration near the beam dump in the K12 beam line, showed that the muon background for NA62-BD can be reduced by a factor of 20 compared to the setting that is currently used in $K^+$ mode. Furthermore, the simulations pointed out that the magnetic field optimization of BEND1 is not sufficient to minimize the muon background for SHADOWS and that an off-axis muon sweeping system will be necessary. Several possibilities for such a system have been evaluated and a configuration was found that achieves a muon background reduction by a factor of 7 compared to the simulations without a SHADOWS dedicated muon sweeping system.

# Contents

## List of Figures

## List of Tables

# 1. Introduction

This piece of paper will present the experiences made during six months of research in the world of particle physics. Selected experiments in the largest research facility on the planet will be discussed and the unknown mysteries of dark matter and physics beyond current understanding will be introduced. The collected insights gained during the six months at CERN will be shared and the results of these studies done within the BE-EA-LE section will be presented.
Prior to the description of the studies done for this section at CERN a short introduction to some helpful prerequisites is given. The introduction will start with an overview of particle physics and accelerator physics by paying special attention on kaon physics and dark matter, because those are most important for the experiments affiliated with this thesis. Then a description of the P42 and K12 beam lines, followed by a discussion of the NA62 experiment, its possible beam dump mode, better known as NA62-BD, and their goals in the search for rare kaon decays and dark matter will be presented. Finally, the option of adding a parasitic dark matter experiment off-axis to NA62-BD, which is part of current discussions, namely the SHADOWS experiment, will be explained.

## 1.1. Particle Physics

A physicist, who concerns himself with theories of the smallest constituents of the observed and unobserved universe, is called a particle physicist. Even though the word “particle” can refer to many different small objects, such as protons, alpha particles and so on, in particle physics it is frequently used for the most elementary objects yet known. They are the foundation of the world as it is known today, and the carriers of the fundamental interactions. This section gives a quick overview of these elementary particles and their interactions, which currently find their best description in the Standard Model of Particle Physics [2].
The Standard Model is a quantum field theory, which means that particles are interpreted as excitations of the quantum fields used to describe the fundamental interactions. It contains all elementary particles, which following the spin-statistic theorem are separable into bosons with integer spin and fermions with half-integer spin. Depending on their spin they are described via different probability distributions resulting in different quantum effects. Also, each particle has its own anti-particle, which has the same properties, except it is complementary charged under all fundamental interactions. For some particles like, for example, photons this means that they are their own antiparticle.
The fermions are further categorized in quarks and leptons of three generations yet known. While the quarks are either up-like or down-like particles, leptons are separated into charged leptons and neutrinos. In nature quarks will always appear in form of a combined state of several quarks, namely two of them, a quark and an anti-quark forming a meson ($q\bar{q}$) or in threes forming a baryon ($qqq$ / $\bar{q}\bar{q}\bar{q}$). Quarks are therefore called confined, which is a result of the strong interaction. Leptons on the other hand are not subject to the strong interaction and can therefore exist as free particles. Figure 1 provides an overview of the particles, their naming and some of their properties, which form the basis for this classification [3].

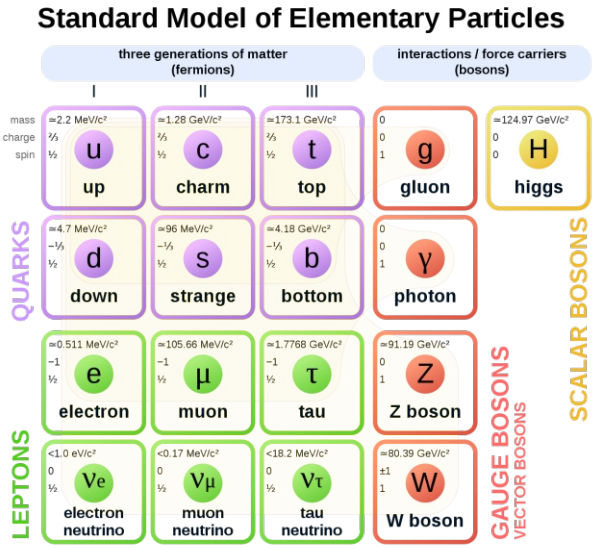


**Fig. 1:** Standard model of elementary particles: 12 fundamental fermions and 5 fundamental bosons. Retrieved from [3].

Bosons on the other hand are separated in gauge/vector bosons (spin 1) and scalar bosons (spin 0). The gauge bosons are affiliated with fundamental interactions, which is why they are called carriers of this interaction. The fundamental interactions of the Standard Model are electromagnetic, weak and strong interaction. While the electromagnetic and the weak interaction could already be unified in a theory, that considers them two sides of one coin, this was not yet possible for the strong interaction. Even though there are already theories, that manage to unify all three of them, namely so called Grand Unified Theories (GUT), the experimental evidence needed to verify one of them, has yet to be found. The strength of each interaction is described by their coupling constants, which is different by several orders of magnitude for the three interactions. These coupling constants cannot be predicted by the Standard Model and must be evaluated experimentally. This of course is a weakness for the Standard Model and can be interpreted as a hint for the existence of a more general underlying theory, that has yet to be discovered. Table 1 delivers a summary of the gauge bosons, the fundamental interactions and some of their properties [1].

| **Force** | **Strength** | **Boson** | **Spin** | **Mass [GeV]** |
|---|---|---|---|---|
| Strong | $\mathcal{O}(1)$ | Gluon ($g$) | 1 | 0 |
| Electromagnetism | $\mathcal{O}(10^{-3})$ | Photon ($\gamma$) | 1 | 0 |
| Weak | $\mathcal{O}(10^{-8})$ | W boson ($W^{\pm}$) | 1 | $80.379 \pm 0.012$ |
| | | Z boson ($Z$) | 1 | $91.1876 \pm 0.0021$ |
| Gravity | $\mathcal{O}(10^{-37})$ | Graviton* ($G$) | 2 | 0 |

*not part of the Standard Model

**Tab. 1:** Essential properties of the fundamental interactions [1].

The last particle that needs to be introduced is the Higgs particle, the only scalar boson discovered so far. Via the so-called Higgs mechanism, the Higgs field is responsible for the masses that each particle carries. This mass can be interpreted as the interaction strength of a particle with the Higgs field. It is the newest member of the observed elementary particles and even though it has been predicted already in the 1960s [4], it took until 2012 to build the necessary tools to create and detect it [5, 6], namely the LHC and its detectors. The reason for that was it's high mass of $125.10 \pm 0.14$ GeV [1], which only then became accessible.

## 1.2. Kaon Physics

Kaons are the lightest mesons with nonzero strangeness. In terms of the Standard Model this means, they are bound states of a strange quark (anti-quark) with a first-generation antiquark (quark). This definition results in four possible combinations $K^+(u\bar{s})$, $K^0(d\bar{s})$, $\bar{K}^0(s\bar{d})$ and $K^-(s\bar{u})$ [2].
Even though the neutral kaons are created via the strong interaction and are eigenstates in terms of the strong and electromagnetic force, they will decay via weak interaction processes. The most interesting one of them is the decay from one into the other (see Figure 2), which is more commonly known as neutral kaon mixing or kaon oscillation. The mixed neutral Kaons can be thought of as the superposition of $K^0$ and $\bar{K}^0$, which results in the two weak eigenstates, called $K_L$ and $K_S$. These two are the physical states of neutral kaons and are named after their different lifetimes, long and short. Table 2 delivers a brief overview of the properties of these particles [1].

| **Kaon** | **Anti** | **Mass [MeV]** | **Lifespan [s]** | **Decay modes (>5%)** |
|---|---|---|---|---|
| $K^+(u\bar{s})$ | $K^-(s\bar{u})$ | $493.677 \pm 0.013$ | $(1.2380 \pm 0.0020)\,10^{-8}$ | $\mu^+\nu_\mu, \pi^+\pi^0, 2\pi^+\pi^-, \pi^0 e^+\nu_e$ |
| $K^0(d\bar{s})$ | $\bar{K}^0(s\bar{d})$ | $497.611 \pm 0.013$ | | |
| $K_S(\frac{d\bar{s}-s\bar{d}}{\sqrt{2}})$ | $K_S(\frac{d\bar{s}-s\bar{d}}{\sqrt{2}})$ | $497.611 \pm 0.013$ | $(8.954 \pm 0.004)\,10^{-11}$ | $\pi^+\pi^-, 2\pi^0$ |
| $K_L(\frac{d\bar{s}+s\bar{d}}{\sqrt{2}})$ | $K_L(\frac{d\bar{s}+s\bar{d}}{\sqrt{2}})$ | $497.611 \pm 0.013$ | $(5.116 \pm 0.021)\,10^{-8}$ | $\pi^\pm e^\mp \nu_e, \pi^\pm \mu^\mp \nu_\mu, 3\pi^0, \pi^+\pi^0\pi^-$ |

**Tab. 2:** Kaon properties [1]. Note that the quark content of $K_S$ and $K_L$ is missing the small CP-violating term.

Due to CP-conservation, $K_L$ should have a different decay channel, than $K_S$, because they have separate, conserved phase spaces. As a result, $K_L$ should always decay into three pions ($3\pi$), while $K_S$ decays into two pions ($2\pi$). Intuitively it seems reasonable to write $K_1 = \frac{K^0+\bar{K}^0}{\sqrt{2}}$ and $K_2 = \frac{K^0-\bar{K}^0}{\sqrt{2}}$ and to identify $K_1$ with $K_L$ and $K_2$ with $K_S$, but measurements show, that in reality $K_L$ will also partially - about $10^{-3}$ - decay into $2\pi$ and $K_S$ into $3\pi$ by the same fraction [2]. This has tremendous physical consequences, namely that the CP-symmetry is violated for the weak interaction. The direct detection of CP-violation was observed in 1999 at the kaon experiment NA48 [7]. This experiment was located in the North Area of CERN and is the predecessor of NA62, which is one of the experiments that this thesis concerns itself with. While there already are well established methods for dealing with CP-violation, its underlying structure is not understood yet, which means introducing it to the Standard Model results in additional free parameters, that cannot be retrieved from the model, but only by input from experiments.

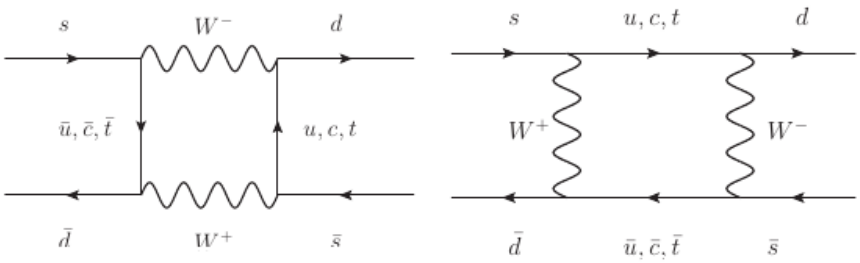


(a) First boxplot for Kaon oscillation

(b) Second boxplot for Kaon oscillation

**Fig. 2:** Feynman diagrams of kaon oscillations. Retrieved from [8].

So far, this effect has not only been found for kaons with their strange decays, but also the other quarks [2]. The most common method of dealing with this effect is by introducing the CKM-matrix. This is a matrix, which connects the observed superposition of the states - in this case $K_L$ and $K_S$ - with their theoretical counterparts called mass eigenstates - here $K_1$ and $K_2$. It contains information about the probability of detecting a certain decay product.

$$\vec{q}' = \widehat{CKM}\,\vec{q}_{mass} \longrightarrow \begin{bmatrix} d' \\ s' \\ b' \end{bmatrix} = \begin{bmatrix} V_{ud} & V_{us} & V_{ub} \\ V_{cd} & V_{cs} & V_{cb} \\ V_{td} & V_{ts} & V_{tb} \end{bmatrix} \begin{bmatrix} d \\ s \\ b \end{bmatrix} \tag{1}$$

The CKM-matrix is part of the Standard Model but cannot be naturally derived from it. It was found that the nine matrix elements are not entirely independent from each other, but that they can be reduced to four. This leads to introducing four additional free parameters, which are three mixing angles and a complex phase, that causes the CP-violation. These parameters must be found in experiments and added to the model separately. The idea is to measure the probabilities for mixed transformations, which are represented by the non-diagonal elements of the CKM-matrix and calculating the free parameters from it. This can be written in the Wolfenstein parametrization as [9]:

$$\widehat{CKM} = \begin{bmatrix} 1 - \frac{1}{2}\lambda^2 & \lambda & A\lambda^3(\rho - i\eta) \\ -\lambda & 1 - \frac{1}{2}\lambda^2 & A\lambda^2 \\ A\lambda^3(1 - \rho - i\eta) & -A\lambda^2 & 1 \end{bmatrix} + \mathcal{O}(\lambda^4)$$

$$\text{with } \lambda = 0.22453 \pm 0.00044,\ A = 0.836 \pm 0.015,\ \rho = 0.122^{+0.018}_{-0.017},\ \eta = 0.355^{+0.012}_{-0.011}$$

Developing a model able to already comprise this interesting phenomenon remains part of current research. Finally, one can have a deeper look at the most common decay products of kaons, which are again shown in Table 2.
One can see that the kaons mainly decay to muons, pions and electrons/positrons, since they are the only ones with a branching ratio larger than 5%. As a matter of fact, the charged pions will likely decay into muons too and the neutral pions will result in an additional fraction of photons [1]. So, if one is interested in detecting Kaons and wants to learn about its properties in more depth, one will also want to investigate its decay products and will therefore have to put special effort on their detection.

## 1.3. Dark Matter

Even though the Standard Model of particle physics is the most accepted theory mankind knows of today, there is a lot of evidence, that there must be a more general theory. The fourth fundamental force, gravity, cannot be described by the standard model or any model like it. On the large scale, where physics is governed by gravity, there are phenomena that do not find appropriate answers in the Standard Model, like for example the motion of galaxies as shown at the left side of Figure 3. Their explanation requires the introduction of some sort of additional matter, that has not yet been observed, namely dark matter [10]. Its share in the universe is expected to be even five times as high as all observed matter combined [1]. Only the share of dark energy, which is responsible for the expansion of the universe and can be thought of as vacuum fluctuations, is larger, as shown in Figure 3 on the right.

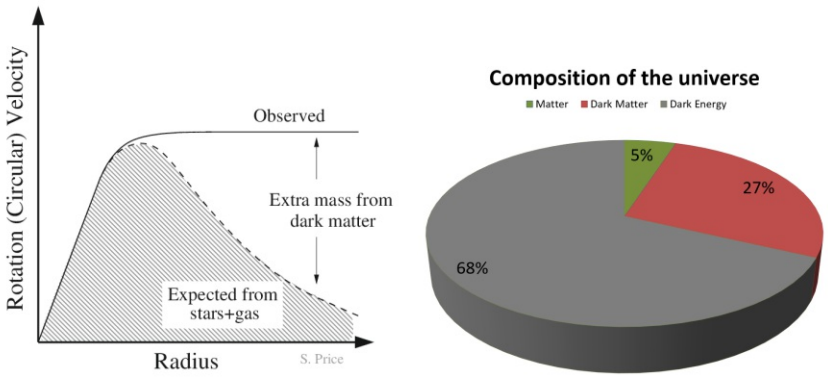


**Fig. 3:** Experimental evidence for dark matter (left). Composition of the observable universe (right). Retrieved from [11].

Dark matter is a name for every form of matter, which humanity was not yet able to detect and therefore every particle, that is not part of the Standard Model. The fact that it still remains hidden from scientists means, that such particles must only interact very weakly with matter and because of that high sensitivities will be needed to detect one or more of its candidates. After Vera Rubin found first evidence of this form of matter in her study of galactic motion [12], many theories have been developed that could explain the missing mass needed to explain this behaviour. Some of them seek for answers in the hidden parts of the universe, others introduce new particles. The following paragraphs give a brief overview of the most prominent candidates for dark matter:

**Primordial black holes**: Theoretical physicists like Stephen Hawking stated that during an inhomogeneous phase of the big bang, like the cosmic inflation, density fluctuations could appear thereby creating black holes with small masses [13]. Because of the rapid expansion of the universe during this period these primordial black holes would be widespread and distributed homogeneous and isotropic. It is even possible, that some of them are still in the milky way by today. Primordial black holes and other candidates like white, brown or black dwarfs all united under the term MACHOs (Massive Compact Halo Objects) could be discovered through the microlensing effect [14]. This effect describes the diffraction of light caused by the gravitation of a massive object. Today it is commonly accepted that a part of dark matter should consist of MACHOs, but experiments like "MACHO" or "EROS" pointed out that not more than 40% of the galactic halo can be explained by them [15].
There are of course more reasons to believe that the current theory is not the final one yet and after realizing this, the next step is to look for candidates beyond the Standard Model.

**Axions and Axion-like particles (ALPs)**: In 1977 the Peccei-Quinn theory suggested a hypothetical particle, which could solve the strong CP problem of quantum chromodynamics, which seeks for an answer to why the CP-symmetry holds in strong interactions. Therefore, the strong CP-violating term must vanish [16]. For that to be the case, it is necessary that the carrying particle, which is called axion, is massless at temperatures above the QCD phase transition. In theory it is possible that at low temperatures $T < 1$ GeV the axion develops a mass, which is why it is a candidate for cold dark matter [17].
When Pierre Sikivie modified the Maxwell's equations for stable axions, he found that in a strong magnetic field it theoretically should be possible to convert them into photons [18]. This effect is used to search for axions on earth. Modern experiments that are looking for axions or axion-like particles are for example CAST (CERN) [19], ADMX (University of Washington) [20] or ALPS II (DESY) [21]. Calculations estimate that the mass of an axion could be only a few $\mu$eV [22] and because of that it has not been detected yet.

**Sterile neutrinos and Heavy Neutral Leptons (HNLs)**: The standard model includes three types of neutrinos (active neutrinos). All of them have left-handed chirality and are therefore charged under the weak interaction [2]. Sterile neutrinos on the other hand are hypothetical particles with right-handed chirality, which means that the weak interaction would not affect them so that they only interacted gravitationally. However, it is theorised that a mixing of active and sterile neutrinos could lead to a decay of a sterile neutrino into an active neutrino and a photon or into three active neutrinos. So far scientists are trying to estimate the range in which these processes occur and currently these HNLs are expected to have masses from below 1 eV up to $10^{15}$ GeV [23], which of course is not yet a very restrictive estimate. So far there is still a vast spectrum to investigate and the effort to search for HNLs increased steadily in recent years.

**Weakly Interacting Massive Particles (WIMPs)**: WIMPs are classic candidates to explain all of dark matter. They are hypothetical particles, that would be subject to a yet unknown fundamental force with a strength, that is even lower than the weak interaction [24]. This definition leaves a vast latitude to what the particle's properties could be, how they behave and how many different sorts of them exist. Because of that, when looking for a WIMP it is necessary to search at all scales of mass, which cannot be done with only one experiment. Therefore, there are many different groups that search for WIMPs with various masses, like for example CRESST [25], XENON [26] or CDMS [27]. Most likely the mass of a WIMP is quite high meaning at least above 10 GeV and more likely even up to several TeV because otherwise the particles perhaps would already have been found at the LHC. Of course, LHC results might not have been sensitive enough to observe them, which legitimates also low energetic WIMP searches.

**Dark Photons**: The dark photon is a hypothetical spin-1 gauge boson and therefore the carrier particle of a new force [28]. It would have similar properties as the photon and would also be described by an abelian U(1) gauge symmetry, but the strength of this force would be very weak, leading to the fact that nobody yet found it. It might pose the solution for the anomalous magnetic dipole moment of electromagnetism, where experiments show that the expected value for electrons, muons and tauons is about 0.1% off the value calculated in QED. The explanation would be a mixing between the photon and the dark photon, which could also be the interaction enabling scientists to detect it [29].

Of course, there are a variety of other theories to explain dark matter, but the introduced candidates cover the most prominent ones.
Great effort has been and will be undertaken to reveal their mysteries. Large machines were built giving mankind the opportunity to uncover, what is still hiding in the shadows. Most of these machines are based on the same principle. First of all stable particles are accelerated to an extremely high energy, so high, that their kinetic energy is a multitude of the mass of the particle itself. As soon as they reach the maximum reachable energy, they are only a small fraction apart from the speed of light. In the next step they are led into collision with either another accelerated particle or some block of material called a fixed-target. The next section will give an insight on how this can be achieved.

## 1.4. Accelerator Physics

The field of physics that studies the motion, manipulation and observation of charged particles and their electromagnetic interactions is called accelerator physics. The accelerator physicist's mission is to design, build or operate particle accelerators and to use them for research purposes. In general, accelerators are classified as linear and circular accelerators. Both bare up- and downsides, which must be taken into consideration when deciding on which one to build. Before these two most prominent types of accelerators are discussed, an overview of the most common constituents of an accelerator beam line and what they are needed for are presented.

**Bending magnets**: Bending magnets, short "bends", are dipole magnets, which open up the opportunity to change the direction of a charged particle beam. As their name already suggests, they have two poles and thereby create a homogeneous magnetic field along the magnet's length. The most important property of a bending magnet are its magnetic field and its length. They hold the information on how big its impact can be on the beam. In the region where a linear approximation of the magnetic field is still valid, its field strength is given by [30]

$$s = BL[Tm] \tag{2}$$

and as a result, the angle about which the trespassing particles are bent is calculated with [30]

$$\theta[mrad] = \frac{299.79\, BL[Tm]}{p[GeV]}$$

Bends are a vital part of every non-linear beam line and even linear ones often contain several of them for momentum selection purposes.

**Quadrupole magnets**: A quadrupole or short "quad" is used for focussing and defocussing of the beam. It has four poles, where the north and south poles are opposite of each other. While in the centre of a quadrupole the magnetic field is about zero, it then grows linearly with the radius. The maximal radius is called the aperture radius. Its strength is defined by [30]

$$s = \frac{BL}{r_{aperture}}[T] \tag{3}$$

Of course, there are also other magnets than bends and quads, but they are not as frequently used and for the purposes of this thesis, introducing only those two will be enough.

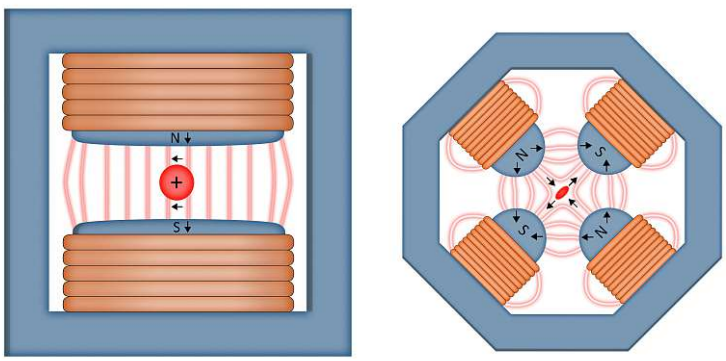


**Fig. 4:** Schematic descriptions of bending (left) and quadrupole (right) magnet. Retrieved from [31].

**Collimators**: A collimator is used to shape or to limit the transverse size of the particle beam. It often is a massive object with holes inside of it, where only particles that pass the hole will be seen downstream of it. This can be used to reduce the beam size or in combination with a bending magnet for momentum selection. Since the sorted out particles that hit the collimator material undergo scattering processes, there might be secondary particles created in it, which often leads to the introduction of a second, so-called cleaning collimator, where these are dumped. Like light in a prism, magnetic bending of the beam results in a dispersive effect, that separates the single particles of the beam by their momentum resulting in a momentum spectrum after the bend. While this will have a negative impact on the beam size, which is the key element in the detector area, it is the ideal situation if one is looking for momentum selection hence this momentum selection technique is being frequently applied. The easiest way to perform a proper momentum selection is with a setup called achromat. In an achromat there at first is a bending magnet before the collimator and one after it. The first magnet makes sure, that the particle with the momentum one wants to select will go directly through the collimator's hole after splitting up the beam in its momentum components. All the other particles with the wrong properties are dumped in the surrounding material and will not be seen downstream the collimator. Finally, the momentum component selected will appear as a narrow outgoing beam and all the particles go into the same direction making it easy to work with downstream.

**RF-cavities**: Radio-frequency cavities are the actual accelerators of the particle. They generate a strong alternating electric field inside this cavity, which accelerates the particles in one half of the period and decelerates them in the second half of the period. Because only the accelerated particles will fulfil the conditions necessary to stay in the beam line, the decelerated particles will be lost. This results in the effect, that the beam will be separated in so-called bunches. All the RF-cavities must be synchronized to always push the particles at the right time, which at high frequencies, like those in particle accelerators, becomes a challenging task with still some potential for improvement in the upcoming years.

**Beam dumps**: A beam dump is the final element of every fixed-target beam line. It consists of a dense material, where the beam particles are dumped. There they will undergo a lot of scattering processes to lose most of their remaining energy, which can still be very high.

**Targets and secondary beam lines**: Even though they are not directly part of an accelerator these terms shall also be quickly introduced, because they are of great importance for experiments and in particular the experiments this thesis concerns itself with. A target is an object made from a material that fulfils certain properties that are satisfactory for the experiment. The primary beam hits the target and the particles will interact with the material. Depending on the material, different interactions become available and different particles are created. These particles, which are now called secondary beam, are then available for the experiment. The interactions in the material and the subsequent collimation to limit the emittance and momentum spread of the beam lead to an intensity loss of about $10^4$ [30] and the beam line downstream the target will then be called secondary beam line, to differentiate between the transported beams and their properties. Targets are the sources for certain types of particles, which one wants to do measurements on. Because some of those particles are only short-lived it is important to only create them near the detector.

Now that the integral parts of an accelerator have been introduced, it is possible to properly describe the two most prominent types of particle accelerators:

**Linear accelerators** (LINACs) accelerate particles in a straight line by generating a high frequency alternating electric field. They get faster and faster via the use of RF-cavities, that push the particles to higher and higher energies. Since there of course is only a certain number of RF-cavities the experiment can use or afford, the length of a LINAC is limited and thereby its maximal reachable energy. In the end, the length of such an accelerator decides about how fast the accelerated particle can get. However, in principle the length could be as long as one wishes it to be, which is why they are still considered in new proposals for future colliders, like CLIC [32].

In **circular accelerators** on the other hand the RF-cavities can be used more than once due to the circular shape, which of course is a major advantage of circular accelerators, which are often built in a certain structure called synchrotron. However, the circular shape bares other problems, namely that in addition to the accelerating RF-cavities, high magnetic fields are needed to keep the relativistic particles on track. This restricts the maximal reachable energy of massive particles like protons or antiprotons, since the voltage, with which even superconductive magnets can be driven with today's methods, is limited and therefore their bending power. For lighter particles like electrons or positrons the magnetic fields are not a restriction any more, but for them another effect poses a threat, namely the synchrotron radiation. Synchrotron radiation is emitted whenever charged particles at relativistic velocities are accelerated radially. The emitted radiation results in an energy loss of the accelerated particle. At a certain velocity this energy loss is so big, that it equals the energy added by the RF-cavities, which means the particle reaches its maximum speed. Because the higher the synchrotron radius, the lower the beam curvature per length, the energy loss decreases with rising circumference of the synchrotron ring. This again means, that going for higher energetic particles leads to the need of bigger machines and therefore once more financial limitations play a role. The main disadvantage of circular colliders is, that once built it is not possible to increase their circumference any more, while extending a linear accelerator at a later point is less problematic.

Despite those limits, the energies reachable in modern particle accelerators are enough to have a severe impact on the scientific landscape. With their help it was possible to create all the Standard Model particles and to examine their properties. The last of them, the Higgs particle, could only be created in the largest synchrotron mankind ever built, namely the LHC at CERN. CERN is the largest particle and accelerator physics facility in the world and has had a huge impact on particle physics in the past sixty years. Because of that the following section shall introduce this international institution, where the research for this master thesis has been done.

## 1.5. CERN

The "Conseil Europeén pour la Recherche Nucléaire", short CERN or vaguely translated the "European Organization for Nuclear Research", is a European project, which focuses on basic research by the use of particle accelerators. It has 23 member states and is located in the suburbs of Geneva at the border between France and Switzerland. Its main goals are defined via the so-called four pillars, research, innovation, collaboration and inspiration. Its scientists aim for boosting the scientific progress in the field of particle physics, information technology and whatever else is necessary to achieve that, and therefore CERN provides the infrastructure needed for high energy physics experiments, which means the design, installation and maintenance of particle accelerators and the needed resources for computation. At the moment it hosts the worlds largest particle accelerator, the LHC.
The laboratories are used by a variety of different experiments, which work on particle physics,

accelerator physics, astrophysics and many more. Because of this CERN staff possesses a vast spectrum of knowledge in these fields of research and therefore it is constantly used by the member states as a gateway to education, knowledge transfer and internationalization of their students and scientists.

The particle detectors of the various experiments hosted by CERN create an enormous amount of data, which has to be stored and processed. The LHC experiments alone produce about 90 petabytes of data per year and all the other ones another 25 [33]. Because of that, CERN has always been a global player in the computation frontier, which in 1990 even led to the invention of the world wide web.

The particle accelerators at CERN are built in a staged way, meaning that the created particle will be accelerated to the maximum velocity of one accelerator until it will gain more speed in the next larger accelerator ring. The stages that the particles will pass on its way to the LHC will now be briefly discussed. Figure 5 therefore gives a schematic overview.

At the moment the accelerator complex is used to speed up low energetic protons. They are created in LINAC4, go throught the BOOSTER (PSB) and are then being transferred to the Proton Synchrotron (PS). PS is the oldest synchrotron at CERN and there the protons are accelerated to an energy of 28 GeV before they are guided to the larger Super Proton Synchrotron (SPS). The SPS is a 7 km long circular accelerator, where the protons reach energies up to 450 GeV. It was finished in 1976 and at this time was one of the most modern machines on the planet. It also had a huge impact from the physics point of view, where it enabled the discovery of the W- and Z-bosons and of the CP-violation. From the SPS the already high energetic protons are induced into the LHC, a 27 km long ring collider pushing them to 7 TeV, the highest speed ever reached by a particle accelerator. The LHC then collides the high energetic particles against each other, where they undergo high energetic scattering processes and thereby create possibly yet unknown particles, like the Higgs until 2012. The collision energy can reach up to 14 TeV, which is hotter than the sun's core. The collisions are constantly monitored by the experiments CMS, ATLAS, LHCb and ALICE, which therefore nowadays hold a key role in the discovery of new particles.

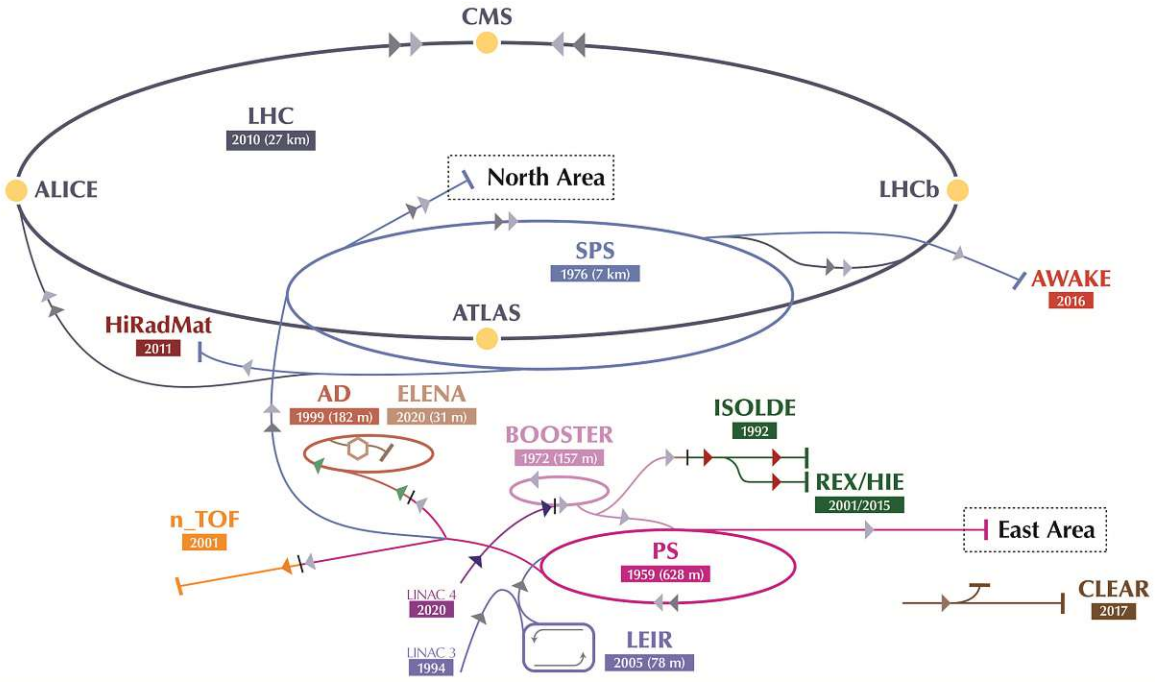


**Fig. 5:** CERN accelerator complex. Retrieved from [34].

However, as can be seen in Figure 5, there are also other stations, that end without reaching another circular accelerator. These are facilities and experiments, that use the beam extracted from the colliders otherwise, like for material testing or more often fixed-target experiments. The North and East Areas of CERN are even hosting several experiments, which share the extracted beam for different purposes. The responsibility for delivering these beams to the experiments with the desired properties lies on the BE-EA-LE section. This section provides the beam for experiments like AMBER/COMPASS, NA61/SHINE, NA62/NA62-BD/KLEVER and NA64 in the North Area or for CLOUD in the East Area, as for AWAKE, HiRadMat and others. Also the irradiation facilities GIF++ in the North Area as IRRAD and CHARM in the East Area depend on the beam delivered by BE-EA-LE.
This is the section, where in the six month from October 2020 to March 2021 the content of this thesis was worked out and in where the research described in this thesis was done. The main focus of this thesis lies on the beam line optimization for NA62-BD and another possible off-axis experiment. The affected beam lines are called P42 and K12 and since they are so important for this thesis, they deserve their own section.

## 1.6. The P42 and K12 beam lines

In current runs the CERN's SPS accelerated protons reach energies of 400 GeV. These protons are extracted into the facility, at which the experiments are performed. As it was already pointed out, this can either be the LHC or other beam lines, that lead to different experiments. One possibility is the North Area and its P42 beam line, which transports the attenuated (in T4 target) primary proton beam to the T10 target.
Depending on the target material, the particles will undergo different processes and therefore create a different secondary beam. In case of P42, the primary proton beam hits a beryllium target called T10, where the interactions lead to the generation of a secondary beam with a high population of Kaons. Correspondingly, this secondary beam and the beam line downstream the T10 target is referred to as K12. This secondary beam is then focussed and momentum selected, so that the experiment, that is supplied with this beam, can optimize its results. In the K12 beam line there is only one user for this secondary beam line: NA62. This experiment shall be introduced in more detail in the next section, but beforehand it is helpful to look a bit deeper into the K12 beam line.

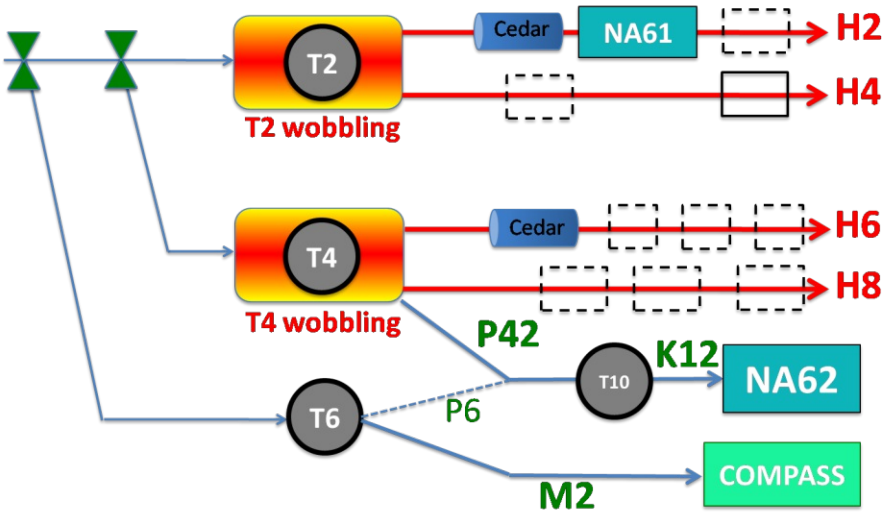


**Fig. 6:** North Area beam lines. Retrieved from [35].

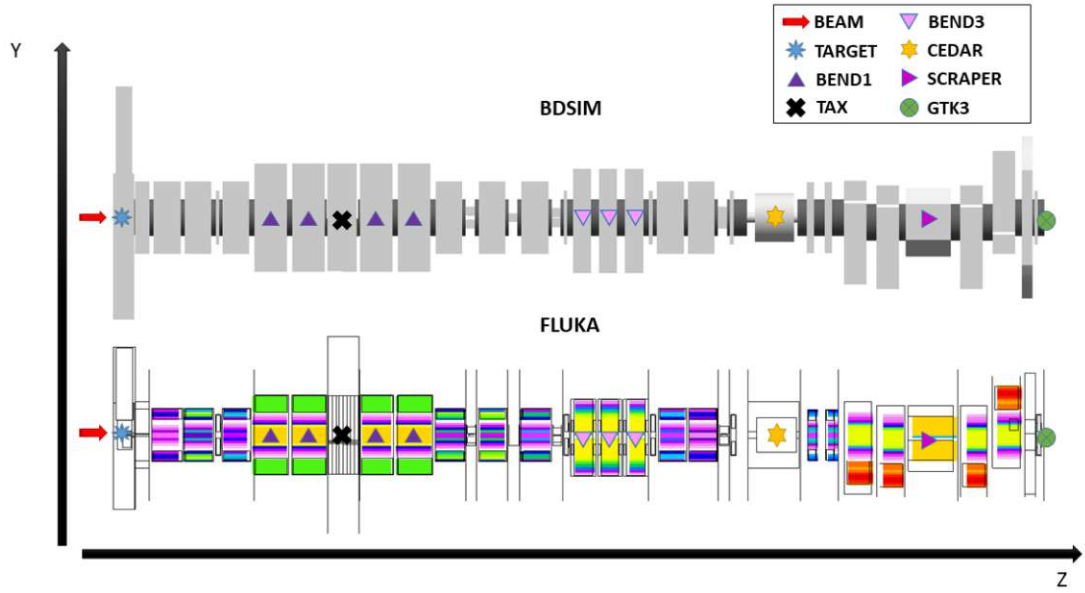


**Fig. 7:** K12 beam line models in BDSIM (top) and FLUKA (bottom). Retrieved from [36].

K12 is the beam line this thesis concerns itself with. It is located in CERN's North Area in a separate tunnel called TCC8, which leads to the ECN3 cavern. All simulations and the studies for experiments supplied by its beam are based on a model that represents this beam line. This shall be introduced in some more detail. Therefore, the K12 beam line setup K12HIKA+ will be explained [37].
The 400 GeV primary protons hit the T10 target, resulting in the generation of a secondary charged hadron beam. This hadron beam enters the first achromat, also referred to as BEND1, where the momentum selection takes place. BEND1 consists of four MTR bending magnets called BEND1A, BEND2, BEND1B, BEND1C and a collimator/beam dump called TAX. The TAX is placed between the central two bending magnets BEND2 and BEND1B. While all four magnets have the same field of 1.65 T, the central two have polarities different from the outer two bends. As a result, the incoming hadron beam bends down and due to dispersion only the particles with a momentum of 75 GeV can pass the TAX. Behind the TAX they get bent back to their original position in the beam line. After that one has a 75 GeV secondary beam, where about 6% of the remaining hadrons are positively charged kaons. Only a few meters downstream BEND1 there are another three bending magnets, which are called BEND3, whose purpose it is to sweep away as many of the muons created in the target or the TAX as possible. The kaons are then led to the decay volume. On their way there, the $K^+$ get identified by a differential Cerenkov counter called KTAG (kaon tagging) and their momenta and directions are measured by three silicon pixel tracking detectors called Gigatrackers (GTK 1,2 and 3). Before the vacuum tank there are also several quadrupole magnets, which are used for focussing and defocussing of the beam at certain points. The Kaons then enter the decay volume, a $10^{-6}$ mbar vacuum tank in which the so called LAVs (large-angle photon-vetoes) and four STRAWs (straw trackers) are placed. The LAVs will detect all photons up to an angle of 50 mrad, while the STRAWs can identify charged particles in the decay volume. Directly after the tank there is a RICH detector (ring-imaging Cerenkov detector), which enables the identification of charged pions, where two plastic scintillators called CHODs (charged-particle hodoscopes) are used for triggering and timing. In the last few meters of the beam line once more photons are identified in the latest stage of the detector via on the one hand a liquid krypton calorimeter, the LKr, and on the other hand two small angle detectors called IRC (intermediate ring calorimeter) and SAC (small-angle

calorimeter). While the SAC is the last element of the beam line before the dump, the three muon vetoes (MUV) are placed a few meters upstream of it. The muon vetoes aim for identifying muons and rejecting their associated signals. MUV1 and MUV2 are hadron calorimeters, which are followed by a 80 cm thick iron block, the MUV filter, that shields the plastic scintillator detector MUV3. The muon vetoes are used to detect remaining hadrons and muons, where it is expected that the MUV filter will eliminate most of the hadrons detected in MUV1 and MUV2 and thereby distinguish them from the muons, which swiftly pass the iron block.
It was part of this thesis to build the geometry of the NA62 detector for the simulation software BDSIM. More on how this was accomplished can be found in Section 3.3.2.
While collider experiments accelerate particles against each other with centre of mass energies up to 14 TeV [38], fixed-target experiments let the high energetic beam interact with a target of a certain material. Even though compared to collider experiments the collision energies are rather small, fixed-target experiments have a great advantage over them. The high energetic particles that hit the target show a much higher interaction rate and therefore the event rate is increased by a huge factor. This higher statistic is the key element of every fixed-target experiment. Where the high energy frontier, namely collider experiments, hit rock bottom due to their low statistic, they represent the ideal counterpart to test the limits of the standard model via rare decay searches or to look for particles, that only vaguely interact with those yet known.
K12 provides the opportunity to perform both searches. Depending on the position of the TAX different modes of the K12 beam line can be used [39]:

| **Mode** | **TAX1 position [mm]** | **TAX2 position [mm]** |
|---|---|---|
| $K^+$ mode (K12HIKA+) | -110 | -110 |
| $K^+$ mode $\frac{\Delta p}{p}$(rms)=1% | -110+2.5 | -110-2.5 |
| $K^-$ mode | +110 | +110 |
| $K^\pm$ mode | +110 | -110 |
| $K_L$ mode (K12HIK0L) | 0 | 0 |
| Beam dump mode (BD) | +140 | -140 |

**Tab. 3:** Modes of the K12 beam line at different TAX positions, where the position means the offset in vertical direction with respect to the T10 target, not the beam.

Which one to choose depends on the aim of the experiment using the provided beam and of course also on the results of the preliminary studies, which are performed to get a deeper insight already before the experiment is taking data.
Momentarily, these preliminary studies for the K12 beam line are carried out in a shared effort between the BE-EA-LE section and the NA62 experiment.

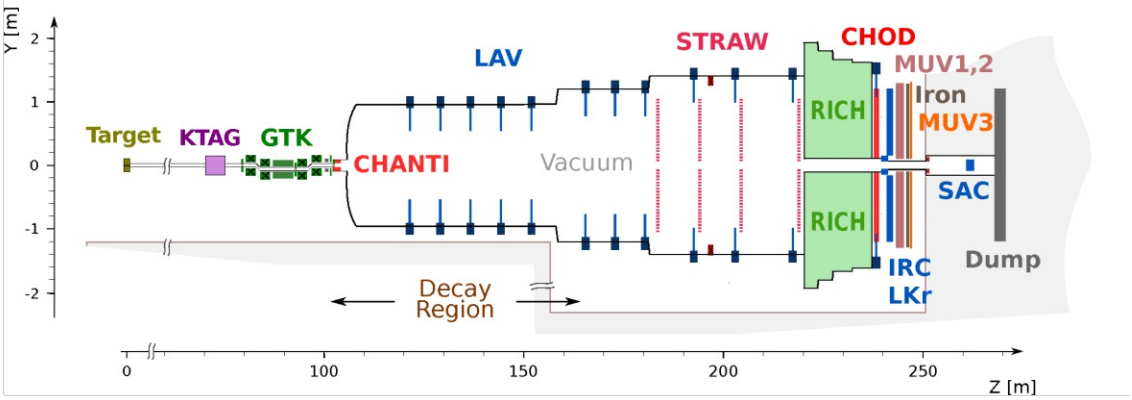


**Fig. 8:** NA62 detector. Retrieved from [37].

## 1.7. The NA62 experiment

NA62 is a fixed-target experiment in the North Area of CERN, which is specialized on Kaon physics. It uses the K12 beam to acquire the data needed for their searches.
Since 2016 the experiment is investigating the branching ratio of the process $K^+ \to \pi^+ \nu\bar{\nu}$, which from the Standard Model perspective is expected to be only around $10^{-11}$ [40]. This means it needs a high statistic to investigate it, which is only possible at fixed-target experiments. If in the search for this rare decay mode there would be found an irregularity in the branching ratio, this would be a hint for physics beyond the standard model.
To get an acceptable statistic in a reasonable time it is necessary to be extremely sensitive to kaons and to have a high fraction of them in the secondary beam. Therefore, the experiment is built as described above. With a $K^+$ rate of 6% in the secondary beam a goal like this should be achievable with data from several years of data taking. Because of the accurate Kaon identification and the particle rejection at the photon and muon vetoes NA62 can accomplish an extremely high accuracy in distinguishing between the different decay modes.
Additionally, with this data the NA62 collaboration can determine the $V_{td}$ element of Equation 1 at a high precision. This quantity will give physicists a deeper insight on the likelihood of the decay of a top quark to a down quark, a number that is very important for the Standard Model, since its value has fundamental impact on the four free parameters of the CKM-matrix.
The statistics needed for announcing the observation of this ultra-rare decay is tremendous, which means the needed beam time can only be achieved in several years. Up to now the NA62 collaboration found 20 candidate events in the data taken in 2016, 2017 and 2018 during Run 2. With this NA62 was able to claim first evidence for this rare decay events with a statistical significance of $3.4\sigma$ [40]. It follows that such a decay will be seen once every $10^{11}$ $K^+$ decays with an uncertainty of about 35%, which means the experimental value at the current precision is still in acceptance with the predictions of the Standard Model. It will take a higher statistics to reach the significance of $5\sigma$, which is needed to claim the observation of the process. This is expected to be achieved during the operation period starting in 2021.

## 1.8. The NA62-BD experiment

As it was explained in section 1.6 depending on the position of TAX1 and TAX2, it is possible to set the constraints for collimation. This means that depending on the positions of the two holes in each TAX different particles can move on to the other side.
As a result, the NA62 setup can be easily used for a variety of experiments. One possible option is to close the TAX, by setting the first on a position of +140 mm in y-direction and the second TAX on -140 mm. In this configuration, as showed in Figure 9 all the holes are closed, which means the TAX is then working as a beam dump. If additionally the Beryllium target is removed the primary proton beam will enter the K12 beam line and directly hit the copper and iron blocks of the TAX, where they undergo various scattering processes and almost all of the particles will be lost. The experiment using K12 in this way is called NA62-BD (NA62 beam dump).
Behind the TAX ideally there would be no particles of the Standard Model left to detect. However, if there was a detection of such a particle despite the expectations, the answer to that phenomenon could be that a dark matter particle was created in the beam dump collisions and that this dark matter particle then decayed into a Standard Model one, which the NA62 detector was able to identify.

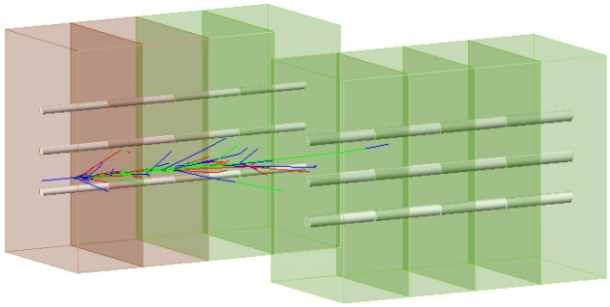

**Fig. 9:** TAX in BD configuration.

Anyway, in physics the ideal case is never the one that is found in nature, which is why the assumption that there should be none of the particles of the Standard Model downstream the beam dump has to be softened. In reality the experiment has to deal with a certain fraction of particles that are not blocked by the dump. This fraction is called a background of a specific particle type. Knowing the backgrounds is of first priority for a beam dump experiment like NA62-BD. Therefore it makes sense to introduce the backgrounds expected to be seen.

### 1.8.1. Discussion of backgrounds

Earlier it was found, that due to the kaon decay modes, the detection of muons and photons delivers valuable information for a kaon experiment. Also, in a dark matter experiment like NA62-BD the ability to detect these particles is an asset, however, for another reason.
Other than in kaon experiments one does not seek for information in the muons and photons created in the proton interactions, but they rather represent an undesirable background for the experiment. These backgrounds pose a threat to finding new particles and thereby new physics, which is why NA62-BD as all other dark matter experiments aim for minimizing all backgrounds as far as they can and furthermore knowing exactly what backgrounds they must expect. As a result, these backgrounds define the limit of the sensitivity of the experiment. This limit is also called energy threshold and means as much as the minimal energy at which it is still possible to distinguish a particle created in a dark matter decay from that of regular decays. For example, if at a certain energy one expects a mean background of 808 muons per million incident protons and measures 815 on average, he or she will not be able to find out whether the 7 additional detections are a fluctuation or the result of a dark matter decay. If one on the other hand knows he can expect a mean background of 8 muons per million incident protons and he measures 15 on average, this is way more suspicious.

### 1.8.2. Muon background

Compared to all other particles yet known, muons have two specific properties letting it become the worst nightmare of dark matter experiments. The first one is, that with a mean life span of about $2{,}2 \times 10^{-6}$ s [1] the muon due to its high velocity and time dilation is a long-lived particle. Because of that it lives long enough to move a far distance before it decays, enabling it to pass all stations of the detector of the experiment. The second property is, that due to its high mass, its mean energy loss per distance travelled traversing matter, which is described by the Bethe formula [2]

$$\frac{dE}{dx} \approx -4\pi\hbar^2 c^2 \alpha^2 \frac{nZ}{m_e v^2}\left(\ln\left[\frac{2\beta^2\gamma^2 c^2 m_e}{I_e}\right] - \beta^2\right) \text{ with } \beta\gamma = \frac{p}{mc}$$

is very low in the relevant momentum range of 100 MeV to 100 GeV enabling it to pass even

several metres of lead or concrete shielding without being stopped. Altogether, this means that high energetic muons are particles, that will live long enough to pass the whole detector and cannot be stopped. Additionally, they carry electromagnetic charge, which means they will be detected in a number of detector layers. Because of that, they represent an unwanted background and raise the energy threshold of the experiment.
Even though it is impossible to stop the muons, due to their electromagnetic charge it is possible to sweep them away from the detectors by the use of the K12's bending magnets. This of course has an impact on the other charged particles as well, making it quite a challenge to find an appropriate configuration for the beam line. However, in a beam dump experiment as NA62-BD most other particles should be already dumped in the TAX making this less of a problem. Even for particles, that would be created in dark matter decays, so those the experiment is particularly looking for, the sweeping fields are not an issue, since the decay would most likely happen only downstream the sweeping magnets. This means the fields have no impact on the events of interest but can only be beneficial in terms of background optimization at the detectors.
Since NA62 is expected to claim the observation of the decay with a statistical significance of $5\sigma$ after taking data during LHC's Run 3 (2021-2024), Run 4 will give rise to a new challenge in the K12 beam line. Even though it is not yet confirmed, which mode will be used in Run 4, currently NA62-BD is one of the possible options. Even a first period of data taking in NA62-BD was performed during Run 3, which will allow a comparison between the simulation results to actual measurement data and thereby to benchmark the simulation model.

## 1.9. The SHADOWS experiment

In late November 2021 an entirely new project started gaining momentum and receiving more and more attention. This project aims for the installation of an off-axis detector in the TCC8 tunnel, which should already get installed during LS3, the third long shut-down phase of the LHC currently scheduled from 12/2024 to 07/2027. It would be a parasitic experiment, that is able to take data, whenever the NA62 experiment runs in beam dump mode and would be able to search for feebly interacting particles, created in the beam dump. The name of this new initiative is SHADOWS.
Feebly interacting particles (FIPs) is a collective term for all particles whose interaction with Standard Model particles is very weak ($\alpha_f << 1$). Whether such a particle is a dark photon, a WIMP, a HNL etc. does not matter for this definition. Because of the weak coupling constant, an experiment that is looking for feebly interacting particles needs to be very sensitive and must therefore have extremely low, or better zero, background from Standard Model particles created in the TAX. Putting such an experiment off-axis can be the game-changer in that matter, which is why SHADOWS exactly aims for doing so.
Additionally, the SHADOWS detector would only be placed about 20 m downstream the TAX. Because of that, the dark matter particles and their decay products should still have relatively high energies at the SHADOWS detector compared to NA62 detectors, which are up to 220 m downstream the TAX. This also is the key difference between NA62-BD and SHADOWS. While NA62-BD takes data on-axis and over a long distance, SHADOWS can collect its off-axis and closer to the dump. Therefore, the two experiments together form an ideal symbiosis and their shared results could be extremely beneficial for the whole dark matter community.
However, such initiatives also bear possible complications, which must be understood in detail before realizing the project. It must be clarified, if one must make changes in the K12 beam line to install and position the SHADOWS detector appropriately. It is also necessary to find out about the backgrounds for this detector and whether it will be necessary to place additional elements for their reduction. Again, the muon background is expected to be of major concern here, especially because the detector is not far away from the TAX. For this purpose this thesis will explore the muon background and investigate measures to reduce it to a minimum.

# 2. Method

Before going into detail about the studies made for this thesis, an explanation of the method used to create their results shall be given. The experiments these studies are done for are not yet operational, which means these are preliminary studies. They shall enable the NA62 and SHADOWS collaborations to get an estimate on what backgrounds they must expect during their dark matter searches and give an idea on how to optimize the settings for their possible future beam dump experiments.
The common way to proceed in such a situation is via simulations and a first comparison to real data with an unoptimized setting to benchmark the simulation model before optimizing the settings to the needs of the experiment. Reduction of unwanted particle background is one of the needs of dark matter experiments.
The general approach for simulation studies is to start with the implementation of the geometry of the setup in the simulation software, once this is finalized to run the simulation and then to analyse the created simulation data in a framework of choice. In the studies for this thesis the simulations were performed in the Geant4-based [41] software BDSIM [42], which is optimized for beam physics. Geant4 is a code for Monte Carlo simulations that is commonly used in particle physics and it opens up the opportunity to build the geometry in the GDML framework [43]. As a result, the geometry building is done in GDML, the simulation will be performed with BDSIM and the created simulation data will be analysed by the use of REBDSIM and Python.
Fortunately, the geometry building in GDML for the simulations of the K12 beam line has already been achieved within the BE-EA-LE section at CERN. This BDSIM model of the K12 beam line was already available, when the work for this thesis started and it therefore is the backbone of these studies and the ones yet to come. Nonetheless, the goal of this thesis is to extend the model to make it more detailed, which means GDML geometry development has also been subject to this thesis.
To give a deeper insight in the process of model building, performing the simulations and the data analysis, the methods used in this thesis will be briefly explained in the following paragraphs.

## 2.1. Geometry building with GDML

The Geometry Description Markup Language (GDML) [43] is an XML based file format that enables the user to prepare geometries for applications that support it. It is developed and maintained at CERN and is commonly used in Geant4 or ROOT. Because of its clear structure it is a useful format for fast visualization.
A GDML file consists of five essential parts containing all necessary information for the read out.

**define**: The define environment enables to define variables, that can be used in the other four parts of the script. Apart from simple variables, it is also possible to predefine position or rotations, by giving them names that are callable later on. Often it is convenient to define the dimensions of the designed objects, so that there is no need to access the geometry again once it is built.

**materials**: In the materials environment all the elements and materials, that are used in the geometry are defined. These can later be attached to volumes, giving these volumes the properties needed for the simulations.

**solids**: The real geometry building is done in the solids environment. Here simple shapes, like cubes, cylinders etc. are used to build a more complex structure, which is later used in the final geometry. Via the set operations “union”, “subtraction” and “intersection” these simple shapes can be formed to the needs of the simulation.

**structure**: The structure environment enables the user to define (logical) volumes by referring to a created solid and the material it shall be filled with. These volumes can then be placed relative to each other as a physical volume in a larger volume, which represents the whole object. Most often this larger volume, where the single constituents of different material are placed, is called the world volume.

**setup**: Finally, in the setup environment the world volume is set and thereby the code gets to know, what it shall place in the simulation.

Appendix A shows an example for a GDML file.
In the beam line created in BDSIM, most of the single components are built as GDML and then placed at certain locations relative to one another. To give an example, the BEND1 configuration consists of four MTR-type magnets, where between the second and third one the two halves of the TAX (TAX1 and TAX2) are placed. Even though this makes a total of six components (BEND1A, BEND2, TAX1, TAX2, BEND1B, BEND1C), only three GDMLs (MTR, TAX1, TAX2) are needed, because the GDML file for the magnets can be placed four times, enabling the user to not only build one large geometry containing all six of the objects, but placing the same GDML files one after another. The described configuration can be seen in Figure 10. This reduces the effort in geometry building by far and makes it easier to change the geometry if necessary.

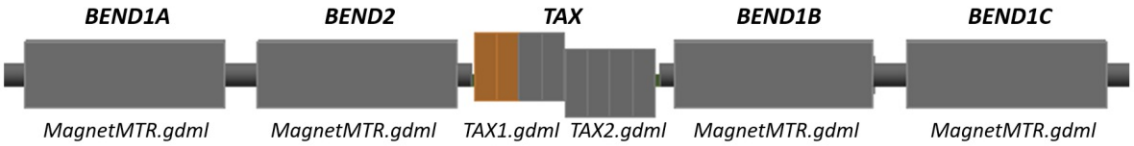


**Fig. 10:** GDML objects used for the BEND1 configuration.

## 2.2. Simulations in BDSIM

Beam Delivery Simulation (BDSIM) is a simulation software specializing on the movement of particles through a particle accelerator or a beam line [42]. By using standard software for high energy physics, like Geant4, ROOT or CLHEP, it enables the user to perform accurate Monte Carlo simulations that can be used for background simulations, radiation studies or particle tracking even over long distances without generating output that is too large to handle. Since Geant4 supports GDMLs for their geometry building, BDSIM is able to read them too.
Once the single components of the geometry are available as GDMLs, the simulation model can be prepared. In BDSIM there are several parameters one needs to specify before they can be started. All these parameters need to be defined in the GMAD file, the file type BDSIM is able to read and run. Those are beam, fields, components, sequence, options and the samplers. All of them are introduced in the present paper and by doing so an overview of the setting for the K12 model is given.

**beam**: This parameter defines the properties of the beam. It sets the starting position of the beam, its direction, the particles it consists of and their energy. To give the beam a more realistic shape, these parameters are not set to a specific value, but are defined in a particular range following a Gaussian distribution that has to be evaluated beforehand, for example via the use of the MAD-X software.
For the simulations in this thesis, the beam parameters for the 400 GeV primary proton beam from the SPS accelerator were already available from prior calculations. They were set to:

```
beam,
        distrType="gauss",
        X0=0.00*m,
        Xp0=0.0,
        Y0=0.000*m,
        Yp0=0.0,
        Z0=0.558*m,
        Zp0=0.0,
        sigmaX=0.0005,
        sigmaY=0.0005,
        sigmaXp=0.0027,
        sigmaYp=0.00135,
        sigmaE=0.15,
        energy=(400.001)*GeV,
        particle="proton";
```

**fields**: If some component of the beam line shall have a magnetic field, one has to define its parameters. This can be done via a text file that contains the field information. In fact, creating such files is not an easy task, because if one wants to have highly accurate magnets in his geometry, they have to be designed for every specific magnet separately to take note of their shape in terms of geometry and field strength. Fortunately, BE-EA-LE already had a ROOT tool [44], that manages to do that for magnets commonly used at CERN [45, 46]. The magnetic field for the first BEND1 magnet is for example read out from a file called "K12_B1_MTR_BDSIM.map", which can be done in BDSIM via:

```
mtr1_field: field, type="bmap2d",
        integrator = "g4classicalrk4",
        magneticFile = "bdsim2d:./FIELDS_QT/K12_B1_MTR_BDSIM.map",
        magneticInterpolator = "linear2D",
        bScaling=1;
```

After this definition the field "mtr1_field" can be attached to an element of the beam line.

**components**: The components describe the single geometries of each constituent of the beam line. It can either be a predefined object, like for example a simple drift, or it can be defined as an "element" and use a GDML file for its geometry. It is also possible to attach a magnetic field to the element, which is done via the "fieldAll" command by referring to a field, that was defined earlier on. For example, the first BEND1 magnet "mtr1" could be defined via:

```
mtr1: element, geometry=''./MAGNETS/MagnetMTR1.gdml'', l=3.6*m, tilt=1.57,
    fieldAll=''mtr1_field'';
```

where a new component called "mtr1" is introduced. This component is an "element" and refers to a GDML file that describes its geometry. Furthermore it is rotated by 90° (1.57 rad) and has a field attached to it, that was defined as "mtr1_field" in the fields.

**sequence**: The sequence marks a list of elements, that are placed in a line one after the other to define the beam line for the simulations. For example, the BEND1 configuration could be written as a sequence of components, that looks like this:

```
bend1: line = (dr1,mtr1,dr2,mtr2,dr3,TAX1,dr4,TAX2,dr5,mtr3,dr6,mtr4,dr7);
use, period=bend1;
```

where the "drN" are drifts, which secure that there is enough space between the MTR-type magnets of BEND1. All these objects had to be defined earlier on as components. The specifics for the space between the components can be derived from the corresponding BEATCH [47] or TRANSPORT files [48]. The "use" command defines which beam line BDSIM shall use for the simulation.

**samplers**: Samplers are objects that score data of particles passing through them. They are most often placed directly downstream a component, enabling the user to investigate the beam at certain spots in the beam line. If not specified further, this sampler will be a 5 m × 5 m square plane with its centre coinciding with that of the beam line. For example, if one wanted to know, what particles there will occur at the MUV3 detector, one would place a sampler directly after it via:

```
sample, range=muv3;
```

where "muv3" is the component representing the MUV3 detector in BDSIM. It is also possible to simply place samplers after all components of the beam line, which is often quite convenient. This can be done using:

```
sample, all;
```

However, for long beam lines this can lead to a huge amount of data that is stored, which means the files containing the data will be unnecessarily large. Because of that it can be more convenient to only place samplers after the components one is concerned with in the study.
It is also possible to place a sampler at a location of choice. This can be done via a samplerplacement and could look like:

```
plane1: samplerplacement, referenceElement=''muv3'', s=1*m, aper1=7.5*m;
```

This defines a samplerplacement object called "plane1", which is placed 1 m downstream the centre of the object "muv3". Contrary to a sampler, it by default has a circular shape and its radius has been set to 7.5 m.

**options**: The options open up the opportunity to give specifics for the simulations. There is a multitude of different options available that can be used depending on what one aims for. A common choice are always the ones that reduce the storage space needed for the output file and thereby reduce the duration of the simulation. For the simulations in this thesis the following settings were used:

```
option,
   minimumKineticEnergy=3.0*GeV,
   killNeutrinos=1;
option,
   storeELoss=0,
   storeElossHistograms=0,
   storeGeant4Data=0;
option,
   samplerDiameter=10*m,
   beampipeRadius=20*cm;
option,
   physicsList="g4FTFP_BERT";
option,
   geant4PhysicsMacroFileName="emextraphysics.mac";
```

In the first paragraph an energy cut-off for all particles with an energy below 3 GeV was set and the created neutrinos were killed without taking their interactions into account. By doing this it was possible to significantly reduce the runtime of the simulations and since the backgrounds of particles with energies lower then this cut-off are below the sensitivity of the NA62 detectors this component is not too interesting for the simulation anyway. In the second paragraph the storage of some non-relevant information is turned off to again reduce the runtime and also the size of the output files. In the third paragraph the diameter of the samplers is defined. Also the radius of the beam pipe along the drift segments of the beam is set. The fourth paragraph tells BDSIM, which Geant4 physics list it should use to run the simulation. It was chosen to use the default physics list "g4FTFP_BERT". The fifth paragraph introduces additional electromagnetic processes, which should add additional processes for muons, that might be relevant according to the BDSIM developers. It was only introduced with BDSIM version 1.5.0. An overview on the versions used for each study is given in appendix B.

Once all these parameters have been set the simulation can be started via a command in the Linux bash environment. The file containing the information about the K12 beam line is called "K12.gmad" and one possible command to run it is:

```
1 bdsim --file=''K12.gmad'' --ngenerate=250000 --outfile=data_bdsim --batch
```

Here the simulation of 250000 incident protons on the T10 target (POT) in the K12 beam line is started. The simulation data is saved in a file called "data_bdsim.root" and it is run in batch mode, which means that BDSIM will run without opening the GUI. To reach high statistics it most often is more convenient to use a cluster to run several of these jobs in parallel. CERN uses the HTCondor batch system to accomplish this. The simulation data created is then ready for analysis.

## 2.3. Data analysis with Python

Usually the data stored in the BDSIM output file - "data_bdsim.root" in the example above - contains a lot of information and the user will most likely not need most of it. Since these files use up a lot of storage it is necessary to process the data further by scraping off the relevant information contained in this file by the creation of a lighter file and deleting the original one to keep the final output manageable in size. This data processing can be performed conveniently in two ways, one is via ROOT and the other via REBDSIM and Python.

**ROOT**: On the one hand it is possible write a ROOT script that is able to directly create a lighter ROOT output file that only contains the information relevant for the study. Depending on the particular task, creating such a script can be quite time consuming, but once this is working it is a convenient and fast solution.

**REBDSIM and Python**: The second solution would be to use the data analysis tool provided by the BDSIM developers, which is called REBDSIM. Via REBDSIM it is possible to define specific histograms that are directly saved in the lighter file. This file then only contains the histograms read out from the original BDSIM data. Via the use of the "pybdsim" package in Python these histograms can be directly accessed and plotted. Therefore, obtaining straight forward results from the model used can be achieved quickly. This option most often is faster then the ROOT solution, since the user does not need to write a specific code to filter the relevant data. This can be simply done by defining the information one wants to see in a histogram.

For the data analysis performed for this thesis the second option has been used, which is why this method will be explained in a bit more detail
To create the lighter file "data_rebdsim.root" from scraping off the relevant information from "data_bdsim.root" via the REBDSIM and Python method the following command can be used in the Linux bash environment:

```
rebdsim rebdsim_analysis.txt data_bdsim.root data_rebdsim.root
```

Here "rebdsim_analysis.txt" is a text file that specifies the histograms that shall be extracted from the BDSIM data. It could look like as follows:

```
#Object treeName HistogramName #Bins Binning Variable Selection
Histogram2D  Event. tax2_Muon_x-y-Flux {250,250} {-5.0:5.0,-5.0:5.0} tax2.y
    :tax2.x 1&&abs(tax2.partID)==13
```

This REBDSIM analysis file will read out the distributions for the xy-flux of muons - muons have partID $\pm 13$ [1] - after the BDSIM component tax2 in the range of $\pm 5$ m around the centre of the beam line in x- and y-direction at a number of 250 bins in each direction. The histogram will be written into "data_rebdsim.root", which can be called in Python via its HistogramName and plotted as follows:

```
import pybdsim
import matplotlib.pyplot as plt

d = pybdsim.Data.Load(``data_rebdsim.root'')
h = d.histogramspy["Event/PerEntryHistograms/tax2_Muon_x-y-Flux"]
pybdsim.Plot.Histogram2D(h, logNorm=True)
plt.show()
```

This only shows a simple example of how the wanted output can be created. Of course Python contains a multitude of options to further analyse the output data, which one can use for the specific needs of the study.

Finally, with these prerequisites everything is set up to perform the simulations necessary for the studies in the P42 and K12 beam lines. The geometry building has been explained and also how it can be used to build a sufficient BDSIM model to perform simulations with. It has been shown how the simulation data is created and processed to receive the final output for the analysis.

# 3. Analysis

## 3.1. Developments for the P42 beam line in BDSIM

During the work for this thesis, components have been drawn for the P42 beam line. A model of this beam line would reflect the area between the T4 wobbling station and the T10 target and a detailed version of it does not yet exist in BDSIM. The reason for this is that several components of the beam line have not yet been implemented as GDML.
The main elements of the P42 beam line are its magnets. They have direct impact on the beam and the more advanced their geometry is the better they will reflect reality. To take the next step in creating this beam line, it is particularly necessary to design the magnet geometries. Fortunately, some of them, namely MTN, MDX and QNL, were already available from the model of the K12 beam line, the others MBN, MBW, MCW and QSL were built as part of this thesis. This was achieved by investigating the technical drawings of these magnets and designing the GDMLs based on them. The GDMLs reflect the geometry of the main constituents of these magnets, which are the iron yoke and the coils. The first three magnets that start with M are bending magnets and QSL is a quadrupole. Figure 11 shows the GDML geometries of these magnets.
Now that there are the GDML geometries available, it is necessary to also attach the fields for each type of magnet. For the commonly used magnets in the beam lines at CERN a ROOT script [44] enables to create their fields for FLUKA within the BE-EA-LE section. There are also Python scripts available, that are able to convert the FLUKA field map format into the BDSIM format. A tool named “fieldcreator” was written that makes use of the existing scripts to enable the user to do both steps in one making the creation of field maps for BDSIM more comfortable. A tutorial for this tool can be found in appendix C.
With the fieldcreator tool, it was possible to create the fields for the four new magnet geometries of the P42 beam line. Figure 12 shows an example for the magnetic fields inside the magnet geometries.

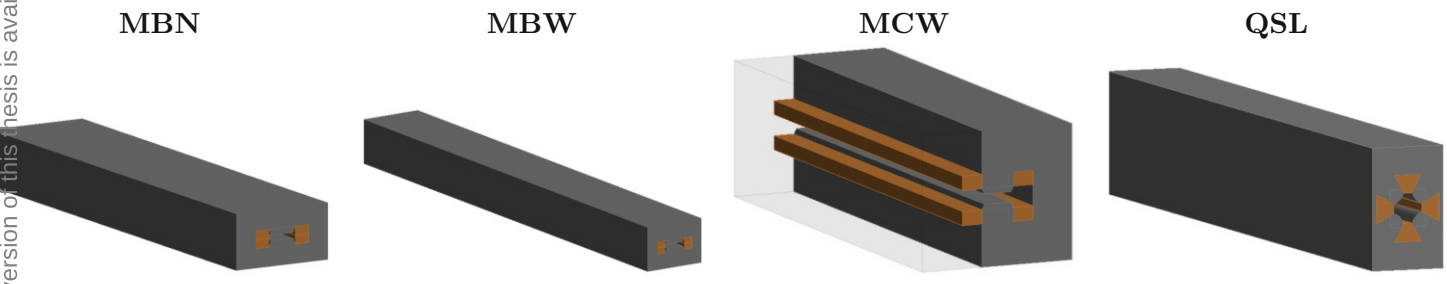


**Fig. 11:** GDML geometries of the newly created P42 magnets. Type of the magnet from left to right: MBN, MBW, MCW, QSL. One can see the iron yokes in grey, the copper coils in brown and the transparent air.

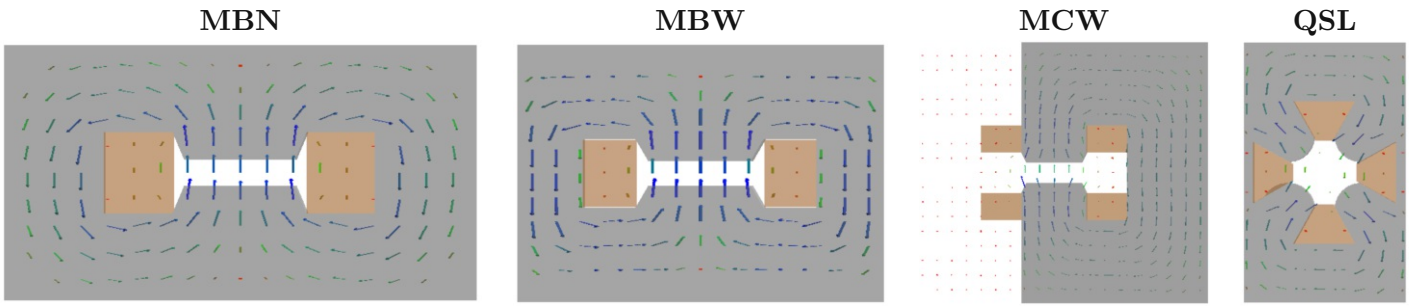


**Fig. 12:** Magnetic field lines of the newly created P42 magnets inside the GDML. Type of the magnet from left to right: MBN, MBW, MCW, QSL. One can see the iron yokes in grey, the copper coils in brown and the transparent air.

Finally, a first attempt for building the P42 beam line has been made. A beam line was designed, that reflects the last six magnets of P42, which are the three QNL-type quadrupoles Q19, Q20 and Q21, two MBN-type bending magnets B10 and B11 and the MCW-type bending magnet B12. These six magnets represent the last part of P42 and therefore the beam line directly upstream the T10 target, which marks the start of the K12 beam line. This beam line was called "P42BeamlineEnd" and it is shown in Figure 13.
It is possible to place it directly upstream the BDSIM model of the K12 beam line enabling simulations with more flexible parameters, since the six new magnets give more options for the variation of the beam properties in the model.

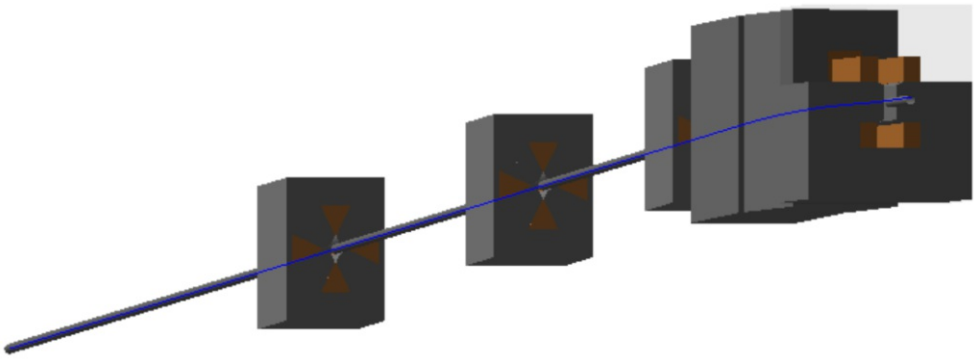

**Fig. 13:** BDSIM model of the beam line containing the last six magnets of P42 (P42BeamlineEnd). The blue line represents an example of a proton trajectory.

## 3.2. Introducing the Beam Dump Mode to the K12 Model

The first step to prepare the beam dump simulations in the K12 beam line is putting the BDSIM model of K12 from the $K^+$ mode to the beam dump mode. This is achieved by removing the Beryllium target T10 and by shifting the TAX to beam dump mode. To remove the target, the Physical Volume of the Beryllium cylinder in "BAC_T10.gdml" was commented out and the beam dump mode of the TAX was introduced by setting the offset in y-direction in "K12_components.gmad" to +140 mm for TAX1 and to -140 mm for TAX2, as described in Table 3.
Now without any other changes in the geometry a comparison between the simulation results of the K12 model in $K^+$ mode and beam dump mode can be done. The particle fluxes (xy-fluxes) at four locations in the beam line are compared to each other in order to point out the differences in the particle distributions. The four locations and the reason for choosing them are described in Table 4.

| z-location [m] | Reference point | Importance |
|---|---|---|
| 26.2 | After TAX | Particle creation in the beam dump |
| 34.4 | After last BEND1 magnet | Effect of the dipole field on the created particles |
| 55.3 | After second BEND3 magnet | Possible location of the SHADOWS spectrometer<br>Detector region (x,y) [m]: ([1.0, 4.0],[-0.5, 2.5]) |
| 246.9 | After MUV3 | Location of the last NA62 detector able to detect charged particles<br>Detector region (x,y) [m]: ([-1.32, 1.32],[-1.32, 1.32]) |

**Tab. 4:** Locations in the K12 beam line relative to the centre of the Beryllium target and their relevance in the beam dump studies.

The discussion of the particle distributions at these location will be split up in one for the muon distributions and one for those of all the other particles. The reason for this is clarified below.

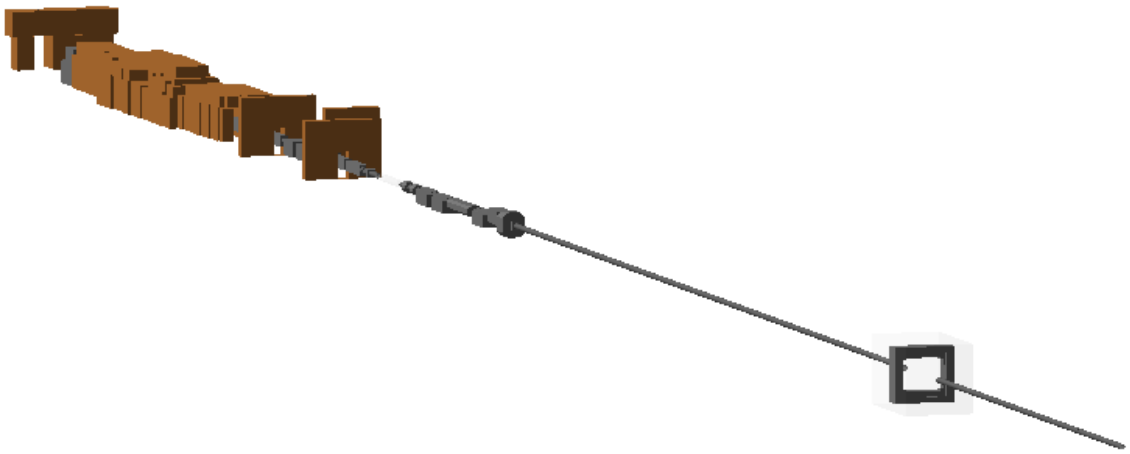

**Fig. 14:** BDSIM model of the K12 beam line including the shielding walls around the TAX. The shielding is visualized in brown colour ("shielding.gdml").

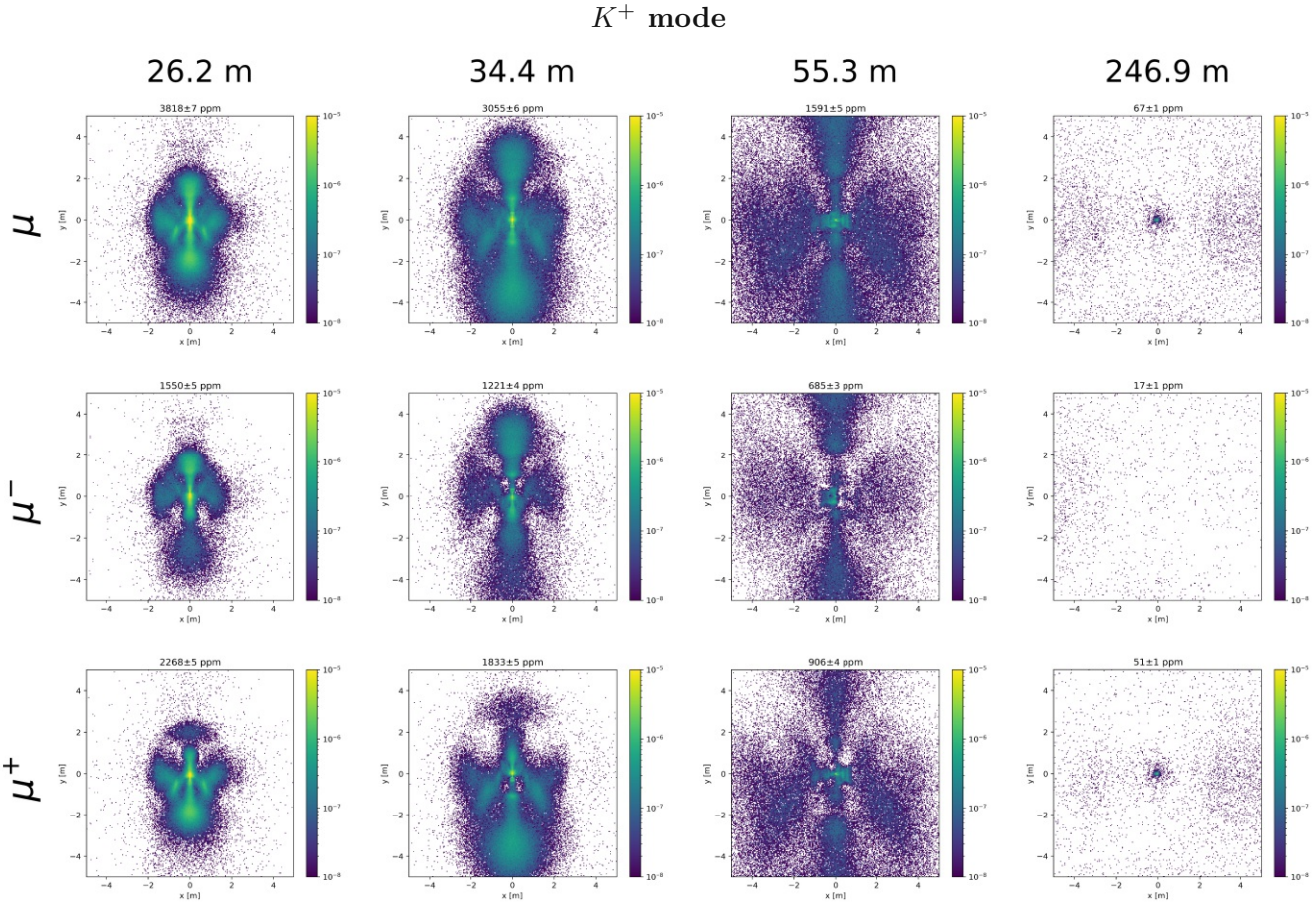


**Fig. 15:** Transversal muon distributions (xy-flux) at selected locations in the K12 beam line in $K^+$ mode. The investigated locations (left to right) are introduced in Table 4. The muons are viewed separated as for both polarities (top), negatively charged (mid) and positively charged (bottom). The colorbar refers to the number of particles per 4 cm × 4 cm large bin per number of incident protons. The heading of each plot shows the total number of particles per million incident protons.

From Figure 15 one can find the starting position for the muon studies in this thesis. It shows the muon distributions in the $K^+$ mode at several locations along the beam line in a square of 10 m × 10 m. This is the mode, that NA62 is running in since 2016. As for this mode the model has already been validated in terms of kaons, the experiment can expect to see about $67 \pm 1$ muons at the plane directly after the MUV3 for every million incident protons on the target (POT).

Directly after the TAX at 26.2 m the muons form four different higher populated regions, which are symmetric along the y-axis. The reason for this is that the BEND1 magnets alter the $K^+$ flux only in ±y-direction. The two regions that developed in horizontal direction, are most likely caused by the return yokes of the BEND1 magnets as illustrated in Figure 16. With rising distance from the TAX the muon distribution opens up until it covers almost the whole area around the beam line at 55.3 m.

One can see that the magnetic fields of the BEND1 additionally cause the positive and negative muons to separate. The reason for that is again the magnetic field inside the return yokes of the MTR-type magnets. To create the homogeneous field in the centre of the magnet for the sweeping of the $K^+$ the field lines in the upper and lower half of the magnet run in the opposite direction. These fields cause a separation of the positively and negatively charged muons as

indicated in Figure 16. While the upper half traps the $\mu^+$ inside the yoke, it pushes the $\mu^-$ outwards. The lower half has the complementary effect. Since the magnetic field of the first two BEND1 magnets before the TAX have fields in opposite direction, this muon separation happens at different z-locations in the beam line. This means that muons of one polarity should have had more time to open up than the other, which would be seen in a larger spread for one polarity. In fact one can see, that the upper half of the $\mu^+$ is more widespread, than the lower half of the $\mu^-$, for example at 26.2 m. One can see that the $mu^+$ have got their outward push earlier, since their distribution is wider than that of the $\mu^-$, which supports this theory.
The described effect is of course stronger for lower energetic muons because of their lower beam rigidity. In principle this separative effect occurs for all charged particles and not only muons. However these particles have a higher interaction cross section in the TAX material, which means on the other side of the TAX they should no longer be visible.

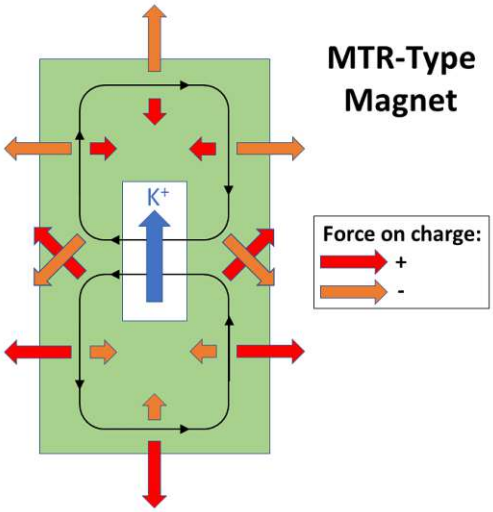


**Fig. 16:** Schematic overview of the impact of a MTR-type magnet on charged particles.

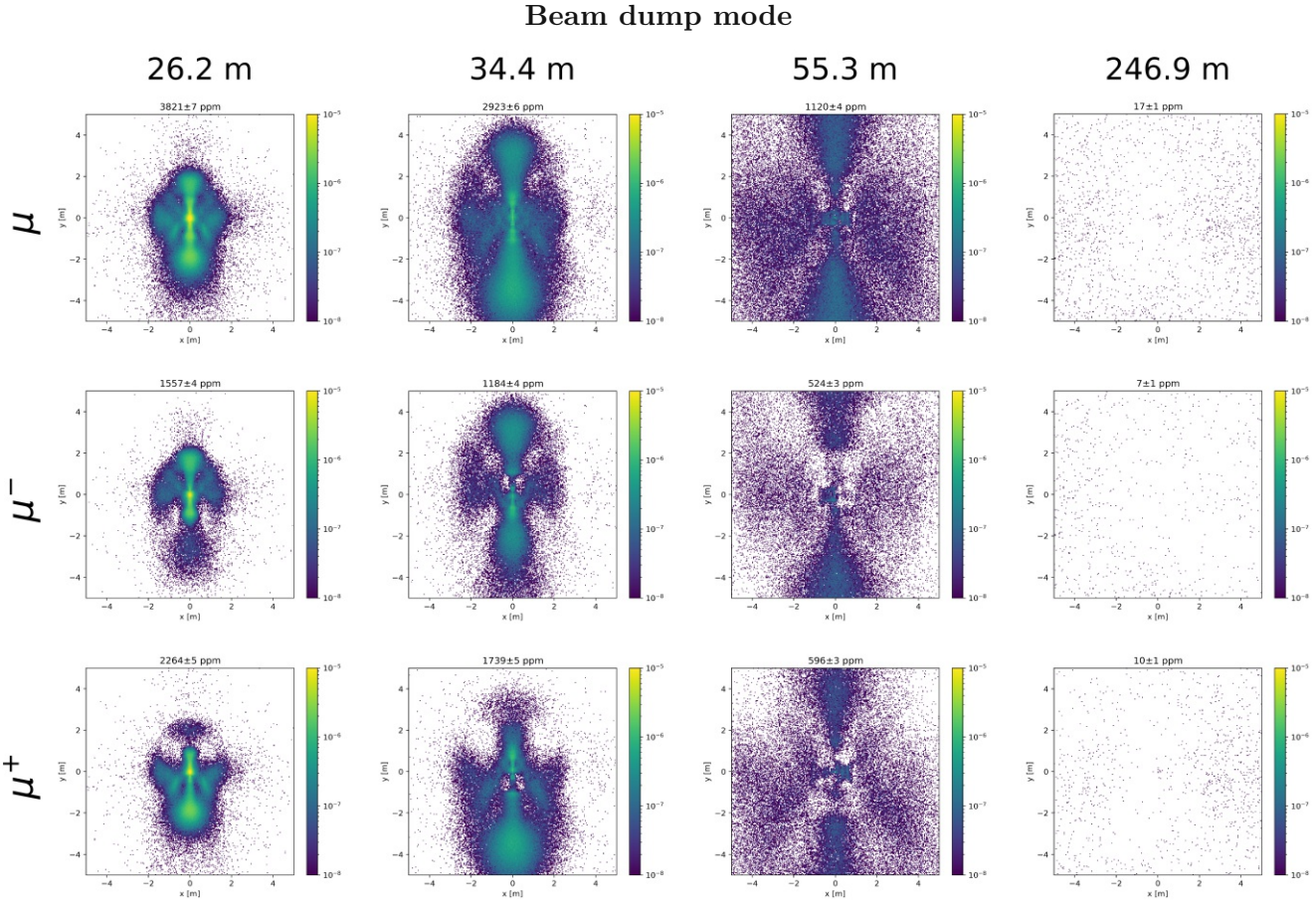


**Fig. 17:** Transversal muon distributions (xy-flux) at selected locations in the K12 beam line in beam dump mode. The investigated locations (left to right) are introduced in Table 4. The muons are viewed separated as for both polarities (top), negatively charged (mid) and positively charged (bottom). The colorbar refers to the number of particles per 4 cm × 4 cm large bin per number of incident protons. The heading of each plot shows the total number of particles per million incident protons.

By having a look at the muon distributions in beam dump mode as shown in Figure 17 it can be seen that the distributions look very much alike, especially directly after the TAX. Due to the same electromagnetic field configuration the distributions are similar for both, $K^+$ and beam dump mode. This is a bit surprising because now the protons do no longer hit the target, but will directly interact with the TAX material. It seems like the particles that created the muons seen after the TAX in the $K^+$ mode were not so much created in the target, but at other places in the beam line or by protons, that did not interact with the Beryllium target in the first place. If one takes a closer look at the number of muons per million incident protons, further downstream the TAX one can see that the numbers differ more and more. This is caused by the TAX, which is now closed. A closed TAX means that the kaon component will no longer reach the downstream regions of the beam line and therefore neither of its decay products, which are most often muons. This means the number of muons that were created downstream the TAX is much lower for the beam dump mode. The muon rate at 55.3 m is decreased by 30% and at the MUV3 at 246.9 m even by 75%. Here especially the $\mu^+$ component in the centre has vanished entirely, which should be even more beneficiary for the detector, which covers only a range between ± 1.32 m in x- and y-direction around the centre of this plot.

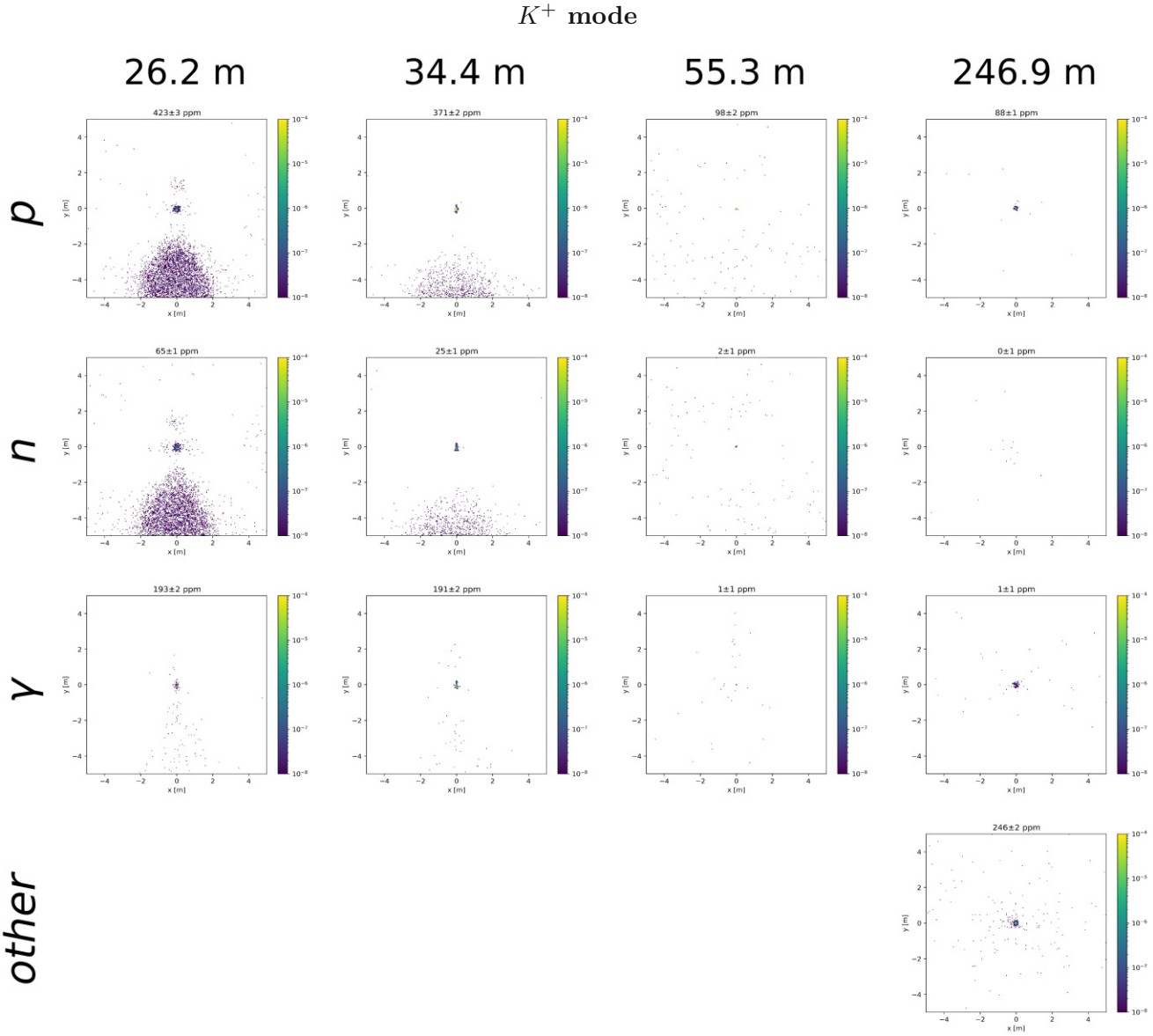


**Fig. 18:** Transversal particle distributions (xy-flux) at selected locations in the K12 beam line in $K^+$ mode. The investigated locations (left to right) are introduced in Table 4. The particles discussed include protons, neutrons, photons and all the other particles (top to bottom), where the other particles contain all particles except protons, neutrons, photons and muons. The colorbar refers to the number of particles per 4 cm × 4 cm large bin per number of incident protons. The heading of each plot shows the total number of particles per million incident protons.

In a next step one can have a look at other particles then muons. For the $K^+$ mode this is shown in Figure 18. These plots show the xy-distributions of protons, neutrons, photons and all other particles then those or muons at the locations from Table 4.
It is found that after the TAX the only other particles than muons can be expected to be protons, neutrons and photons. The denser region in the lower half of the plots is caused by fields of the first two BEND1 magnets, which bend the protons in the negative y-direction. Some of these particles will leave the displayed region already before 55.3 m and the central ones soon lose energy in interactions in the shielding material around the TAX region or other components of

the K12 beam line, so that at 55.3 m the total number of these particles is already reduced by a large factor, which is about 4 for protons, 30 for neutrons and 200 for photons.
However, the particle decays that happen along the beam line lead to a larger number of particles other than muons, protons, neutrons and photons at the MUV3.

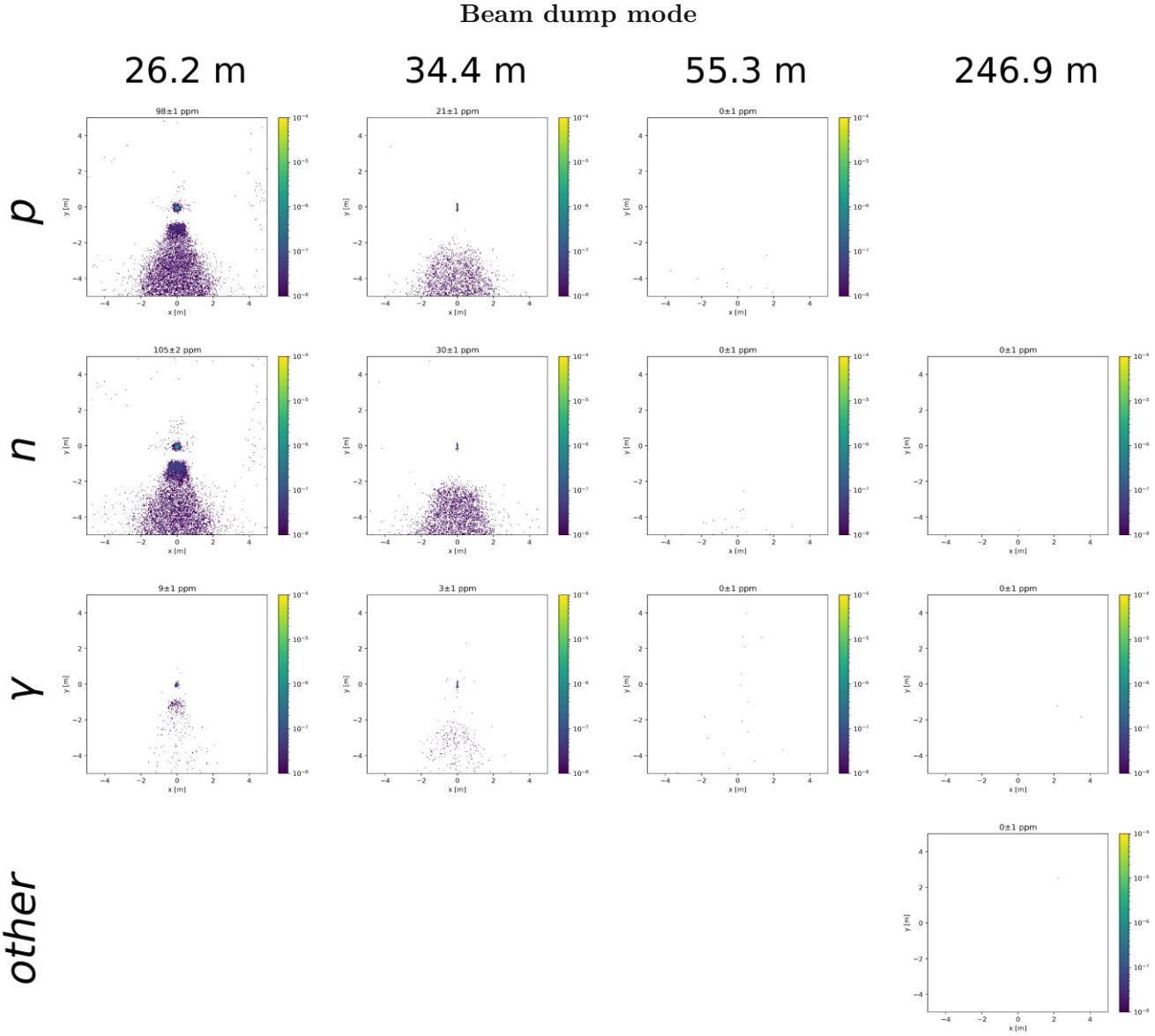


**Fig. 19:** Transversal particle distributions (xy-flux) at selected locations in the K12 beam line in beam dump mode. The investigated locations (left to right) are introduced in Table 4. The particles discussed include protons, neutrons, photons and all the other particles (top to bottom), where the other particles contain all particles except protons, neutrons, photons and muons. The colorbar refers to the number of particles per 4 cm × 4 cm large bin per number of incident protons. The heading of each plot shows the total number of particles per million incident protons.

In beam dump mode the number of protons downstream the TAX is reduced by a factor 4 due to the closed TAX and the therefore now missing momentum selected proton component. Even though the number of neutrons initially is higher, since the closed TAX means more proton interactions and thereby more neutrons that are crated, there is nearly no particle left to be seen at the locations relevant for the detectors.
This important result shows first evidence that whenever the K12 beam line is run in beam dump mode the only background a dark matter experiment needs to worry about will be the muon background, on- and off-axis.

## 3.3. K12 Model Extensions

The previous section introduced results from simulations with the BDSIM model of K12 in $K^+$ mode and in beam dump mode. In doing so, a comparison between the two modes could be made that led to the conclusion that the muon background should be the only noteworthy background for the beam dump mode.
Now that a first idea of the simulation results exists, extensions will be added to the BDSIM model, whose impact has to be evaluated afterwards. There are two extensions expanding the model. The first one is adding the TCC8 tunnel and ECN3 cavern around the K12 beam line and the second one is introducing the NA62 detector after the GTK (see Figure 8) to the model. Both extensions and their impact on the simulation results will be discussed in separate subsections, which start with information about the geometry building and finally have a look at the impact on the simulation results.

### 3.3.1. Model Extension: TCC8 Tunnel and the ECN3 cavern

So far the BDSIM model of the K12 beam line (see Figure 14) did not contain a surrounding, which means the effect of the TCC8 tunnel and the ECN3 cavern, where K12 and the NA62 experiment are placed, is not reflected in the simulated data one gets from the model. The expected impact of adding such a geometry are interactions of the particles in the walls, the ceiling or the floor of the tunnel and the experiment cavern. Since this surrounding can be interpreted as some sort of additional shielding it should lead to a change in the particle distributions, which are like TCC8 and ECN3 themselves not symmetric around the beam line any more. Particles hitting the cavern could also backscatter and add an additional component to the expected background.
Via the introduction of the TCC8/ECN3 geometry, radiation studies in BDSIM become available, that can later be compared to CERN's standard tool for that kind of simulation, FLUKA, in which such a geometry already exists.

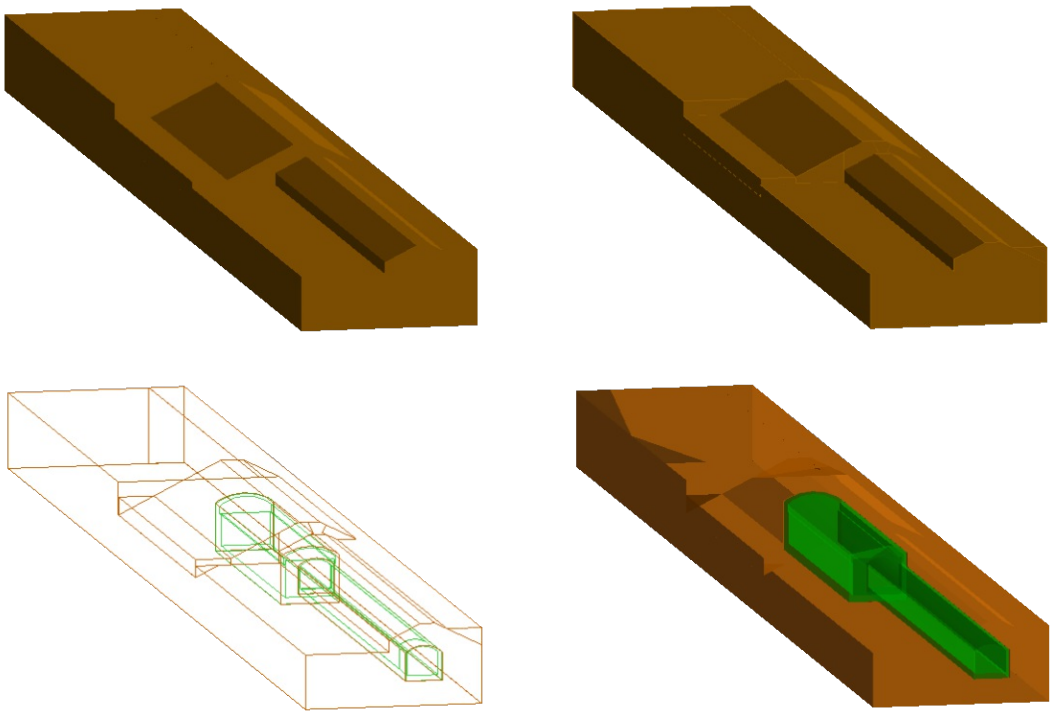

**Fig. 20:** GDML geometry of the TCC8 tunnel and the ECN3 cavern. The concrete tunnel walls are marked green and the soil is marked brown in the drawing.

The geometry of this surrounding was built in GDML ("ECN3.gdml") and can be seen in Figure 20. It is based on the original plans of TCC8 and ECN3 and was additionally compared to the already existing FLUKA geometry [44]. The GDML contains the most important parts of the building, namely the tunnel and cavern themselves made from concrete and their surrounding of soil. Positioning it around the K12 beam line enables using the BDSIM model for radiation studies if necessary in the future for benchmarking the FLUKA simulations.
After the TCC8/ECN3 geometry was finished, it of course was necessary to place it around the K12 beam line. Therefore the beam line and the shielding walls around them, which are introduced via the "shielding.gdml", had to be correctly positioned relative to the surrounding in "ECN3.gdml". To achieve this, two options described below have been considered, where only the last of which was found suitable:

**Assembly volumes:** Using the Python tool pyg4ometry [49] enables the user to combine and place different GDMLs in a shared world volume. The sub-volumes are called assembly volumes and having the option to do this can be a great advantage in GDML development, since it is quite easy to use and in many cases, it is easier to handle one GDML file that contains all the parts than a multitude of single GDMLs, especially when one does not plan on changing this geometry very often. Discovering this opportunity led to the development of a Python script for the BE-EA-LE section, that specialises on exactly that purpose, the "pyg4ometry_toolbox".
The script contains a function called "gdmlAssemblyMerge" that places one GDML with respect to another GDML in a shared world volume. The input parameters it takes, are described in Table 5.

| **Parameter** | **Meaning** |
|---|---|
| filename1 | name of the first file (e.g. "name1.gdml") |
| filename2 | name of the second file (e.g. "name2.gdml") |
| xpos | x-position of the second gdml in [m] relative to the first one, which stays at (0,0,0) |
| ypos | y-position of the second gdml in [m] relative to the first one, which stays at (0,0,0) |
| zpos | z-position of the second gdml in [m] relative to the first one, which stays at (0,0,0) |
| worldlengthx | length of the surrounding volume in x direction in [m] (it is placed at (0,0,0) ) |
| worldlengthy | length of the surrounding volume in x direction in [m] (it is placed at (0,0,0) ) |
| worldlengthz | length of the surrounding volume in x direction in [m] (it is placed at (0,0,0) ) |
| outfilename | name one wants want to give the merged gdml (e.g. "AssemblyConversion.gdml") |
| vis | set to True if one wants to visualize the merged geometry |
| interactive | set to True if one wants the visualized, merged geometry to be interactive (rotating with the mouse and zooming) |

**Tab. 5:** Input arguments for the function "gdmlAssemblyMerge" in the pyg4ometry_toolbox.

However, to avoid overlaps between the beam line elements and the shielding, the "shielding.gdml" had a cut-out from its world volume so that the single elements of the K12 beam line could be placed inside the shielding without overlapping. Because of that merging into a larger shared world volume was not an option and the assembly volume method therefore was not suitable for the task at hand.

**Placements:** In BDSIM there are objects called "placement", in which a GDML or another object, can be placed at a certain point in the geometry. To avoid overlaps between the elements of the K12 beam line with the TCC8/ECN3 geometry it was necessary to cut out the inner volume of the tunnel from the world volume of "ECN3.gdml". After placing the GDML accordingly the cavern was successfully added to the K12 model.

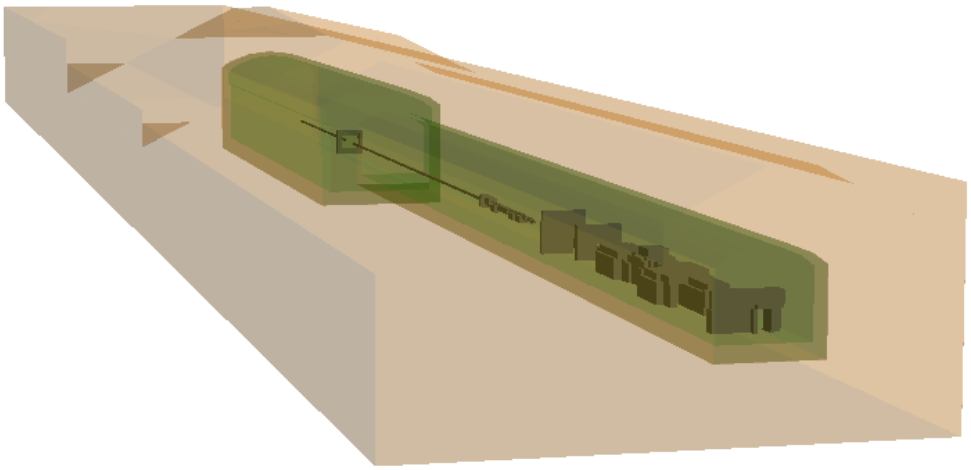

**Fig. 21:** BDSIM Model of the K12 model with TCC8 tunnel and the ECN3 cavern. The green tunnels are made of concrete and the brown region around it is soil. "ECN3.gdml" positioned around K12 as BDSIM placement.

The final placement of the TCC8/ECN3 geometry around the beam line can be seen in Figure 21. This newly introduced geometry can now be tested for its effect on the beam. This is done similar to the simulation discussion in Section 3.2 by an investigation of the particle distributions described in Table 4.

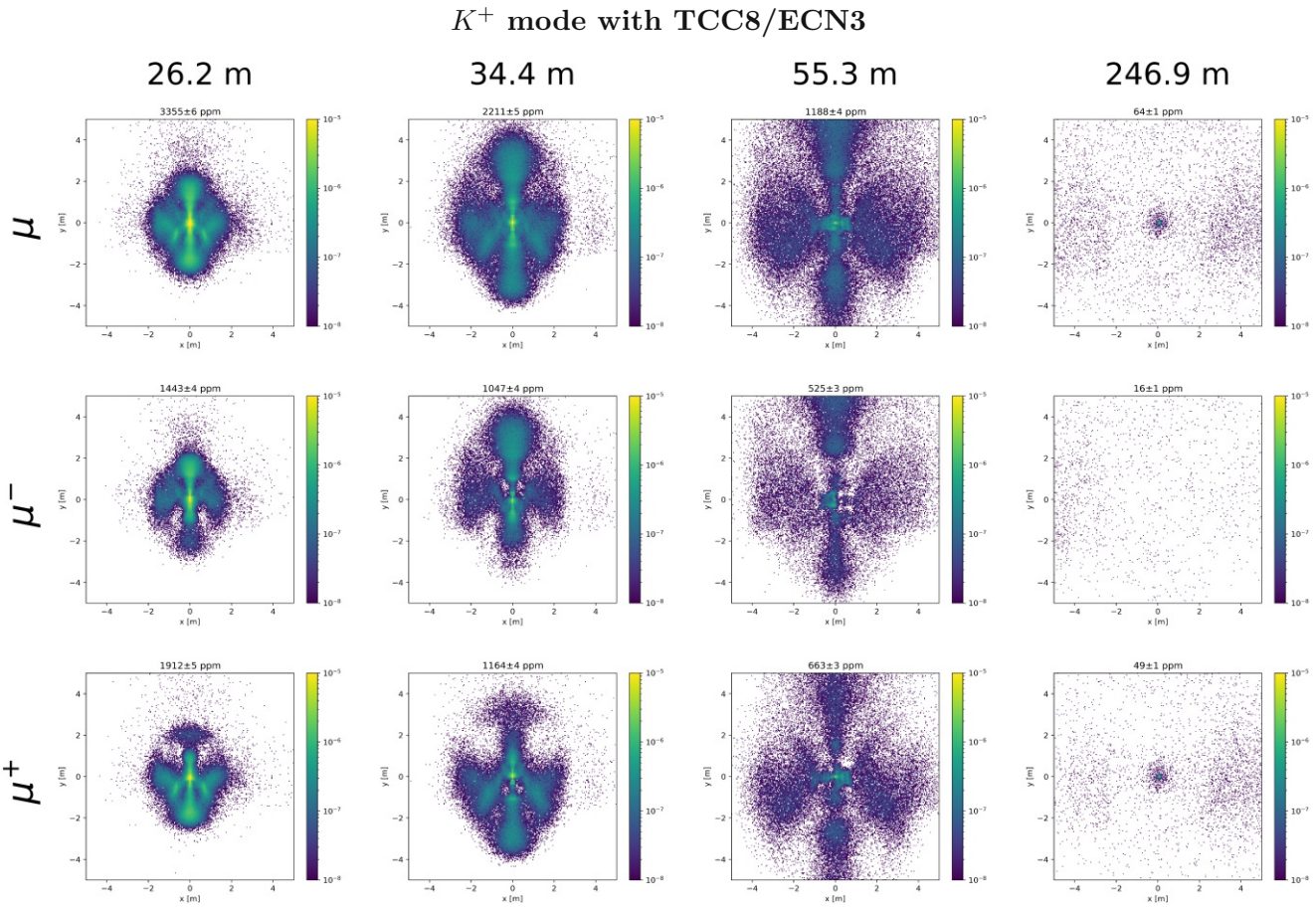


**Fig. 22:** Transversal muon distributions (xy-flux) at selected locations in the K12 beam line in $K^+$ mode after introducing the TCC8 tunnel and ECN3 cavern. The investigated locations (left to right) are introduced in Table 4. The muons are viewed separated as for both polarities (top), negatively charged (mid) and positively charged (bottom). The colorbar refers to the number of particles per 4 cm × 4 cm large bin per number of incident protons. The heading of each plot shows the total number of particles per million incident protons.

By comparing Figure 15 and 22 one is able to find out about the impact of adding the TCC8/ECN3 geometry to the BDSIM model in terms of the muon distributions in $K^+$ mode. It is found that the outer regions are less densely populated once the surrounding is included. This is of course caused by the particle interactions in the concrete of the building around the beam line, which therefore works as additional shielding for the outer regions. The distribution in the inner region of the building, however, stays the same. This means one may not expect some dramatic effect on the muon distribution from backscattering at the walls, floor or ceiling. Especially in the further downstream area at 246.9 m the distributions are nearly the same. Thereby, it can be concluded that the muon distribution in the relevant detector regions inside the building is not affected by introducing this geometry.

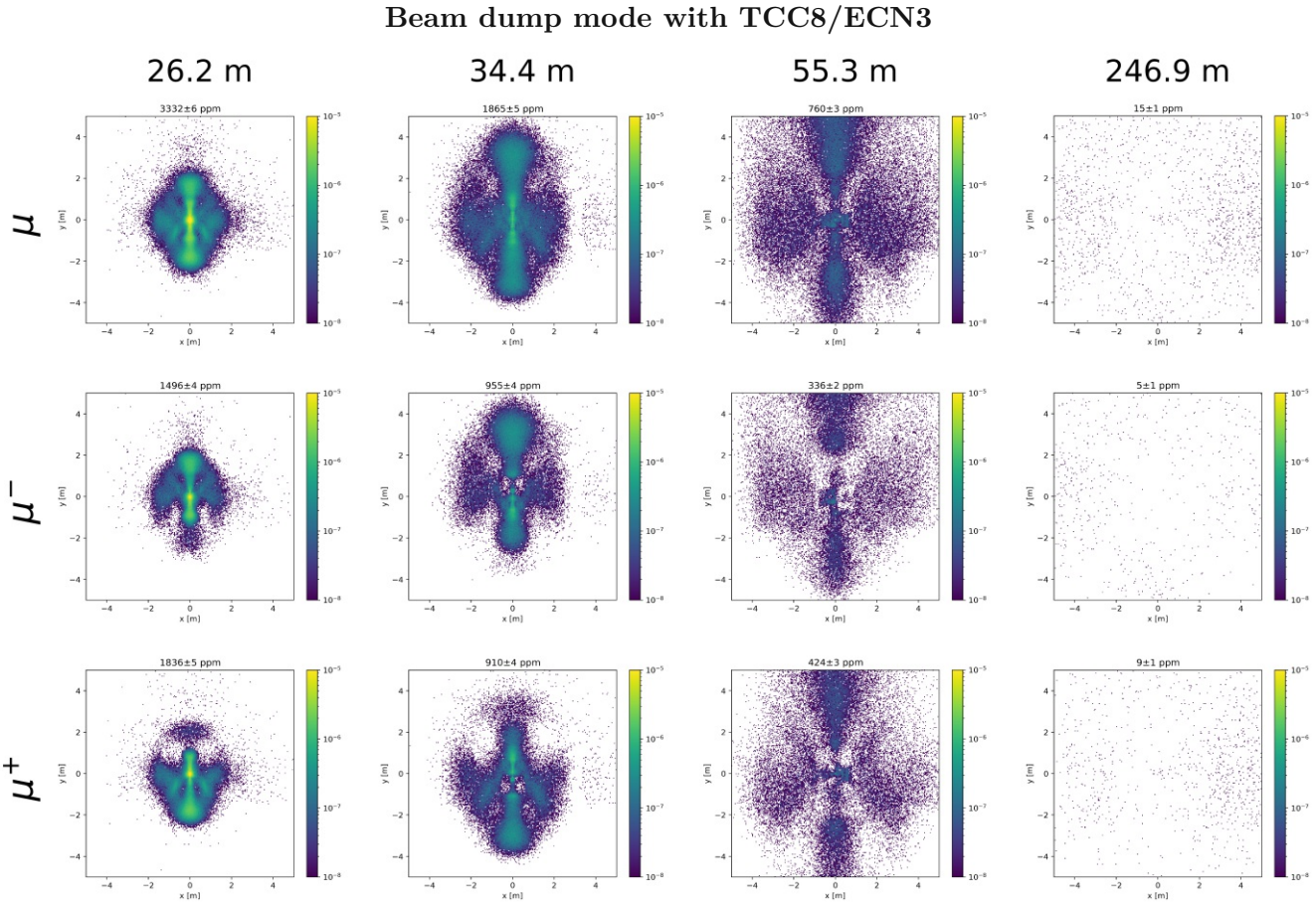


**Fig. 23:** Transversal muon distributions (xy-flux) at selected locations in the K12 beam line in beam dump mode after introducing the TCC8 tunnel and ECN3 cavern. The investigated locations (left to right) are introduced in Table 4. The muons are viewed separated as for both polarities (top), negatively charged (mid) and positively charged (bottom). The colorbar refers to the number of particles per 4 cm × 4 cm large bin per number of incident protons. The heading of each plot shows the total number of particles per million incident protons.

The same is true if one compares the simulation results for muons with and without TCC8/ECN3 (see Figure 23 and 17) in beam dump mode. Again the outer regions are cleaned by the concrete, but the distribution inside the building stays the same.

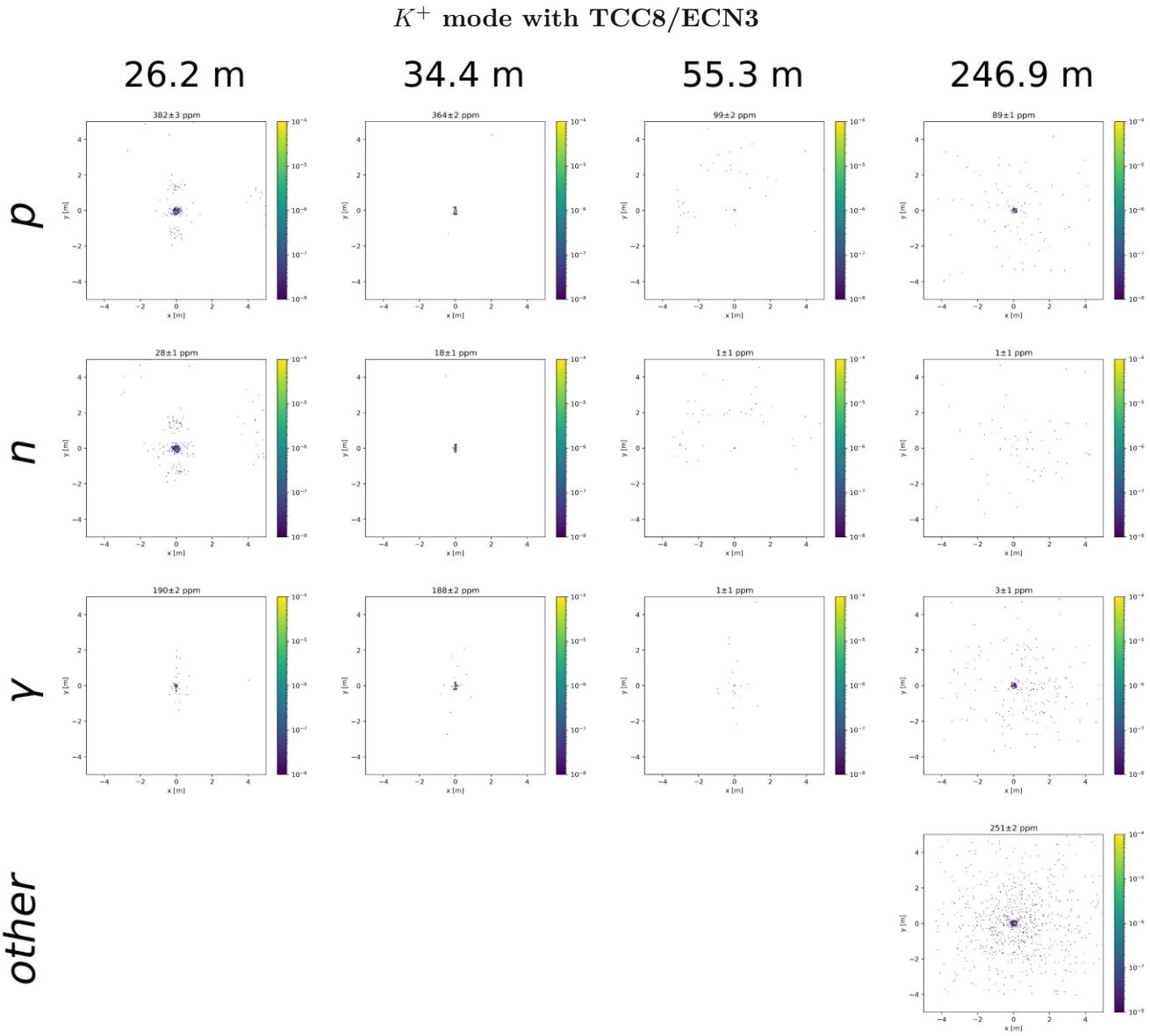


**Fig. 24:** Transversal particle distributions (xy-flux) at selected locations in the K12 beam line in $K^+$ mode after introducing the TCC8 tunnel and ECN3 cavern. The investigated locations (left to right) are introduced in Table 4. The particles discussed include protons, neutrons, photons and all the other particles (top to bottom), where the other particles contain all particles except protons, neutrons, photons and muons. The colorbar refers to the number of particles per 4 cm × 4 cm large bin per number of incident protons. The heading of each plot shows the total number of particles per million incident protons.

The plots for the particles other than muons show similar differences, as a comparison between Figure 24 and 18 points out. Directly after the TAX the components in the lower half of the plots vanish. Here the introduction of the floor at about -1 m in y-direction causes these particles to interact and the particles will be stopped. Apart from the reduction in the outer region, the distributions for protons, neutrons and photons are the same as without the surrounding and in particular in the detector regions there are no obvious changes.
The most interesting plot in this Figure is the one for all other particles than muons, protons,

neutrons or photons. Here it can be seen that even thought the absolute number of particles reaching 246.9 m is not much higher, but their distribution changes. This is most likely caused by backscattering from the walls. Due to this additional material in the far downstream beam line, the particles hitting the walls are able to create others, that then might be seen by the detectors. This is even more likely since the region around the centre of the beam line is more dense now, which is exactly the place, where the MUV3 is placed. The MUV3 has a hole with a radius of 10.6 cm in its centre, which prevents high energetic protons that might pass the TAX from interacting directly with the detector material and hence from causing damage. This means the particles in the centre will not trigger a detection, the particles around the centre on the other hand might do so.

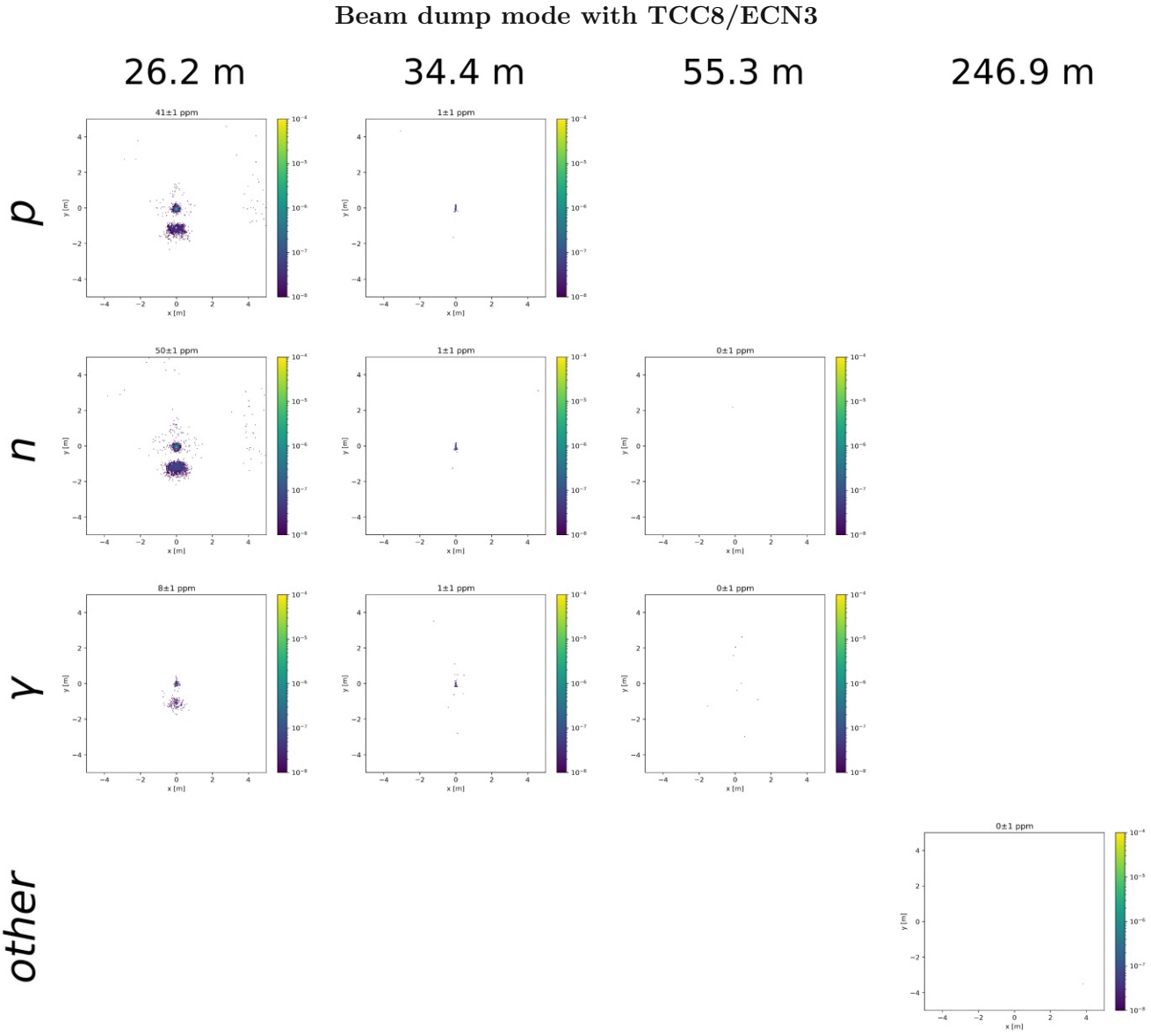


**Fig. 25:** Transversal particle distributions (xy-flux) at selected locations in the K12 beam line in beam dump mode. The investigated locations (left to right) are introduced in Table 4. The particles discussed include protons, neutrons, photons and all the other particles (top to bottom), where the other particles contain all particles except protons, neutrons, photons and muons. The colorbar refers to the number of particles per 4 cm × 4 cm large bin per number of incident protons. The heading of each plot shows the total number of particles per million incident protons.

In beam dump mode the impact of the surrounding is the same as for the $K^+$ mode, but since there are not many particles reaching the downstream region anyway, this effect is negligible. This is shown in Figure 25 and 19. Again one finds, that all backgrounds apart from the muon one are expected to be negligible for possible dark matter experiments after the beam dump.

### 3.3.2. Model Extension: NA62 detector

The second extension added to the model is a simplified version of the NA62 detector. This extension will enable the BDSIM model to reflect the presence of the experiment. Possibly, it might work as further shielding for the downstream region and probably also add new beam components due to interactions in the detector material.
The single components of the detector geometry are based on the properties given in technical papers from the NA62 collaboration [39]. Their correct placement was made via the use of the BEATCH and TRANSPORT files corresponding to the K12HIKA+ beam line layout version [47, 48].
The exact same detector geometry has already been developed for FLUKA within the BE-EA-LE section and during the creation of this GDML geometry, the FLUKA model was double-checked in its correctness.
In contrast to the "shielding.gdml" the NA62 detector geometry between the CHANTI and the MUV3 detectors was introduced as part of the beam line in BDSIM and not as a placement. It was split up in several components to simplify placing samplers in BDSIM after the detectors. The detectors were described in more detail in section 1.6. Most of their materials are not very dense, which is why their effect on the beam should be moderate, but the vacuum tubes and the MUV filter could have quite an impact on the particle distributions near the centre.
In Figure 26 it can be seen how the beam line after the GTK3 looked like in original BDSIM model and how it changes with adding the detector geometry. The only component, that was already there is the MNP33 spectrometer magnet because it has a magnetic field and thereby contributes to the beam optics.

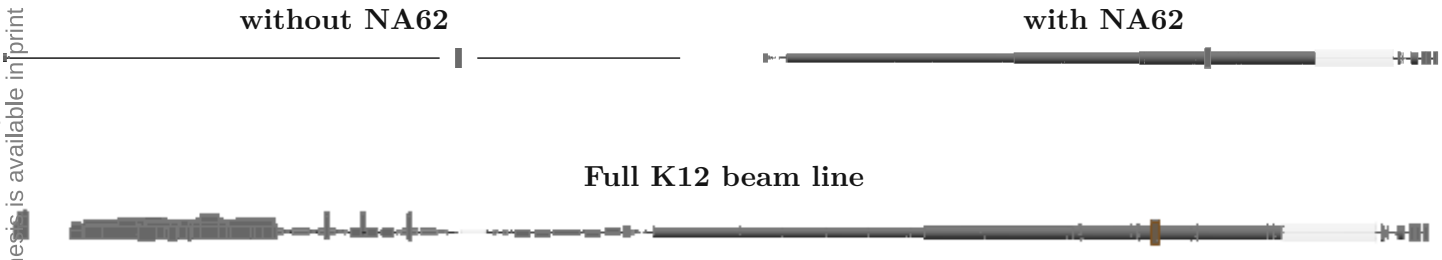


**Fig. 26:** BDSIM geometry of the NA62 detector region without (upper left) and with (upper right) the detector and the full beam line with detector (below).

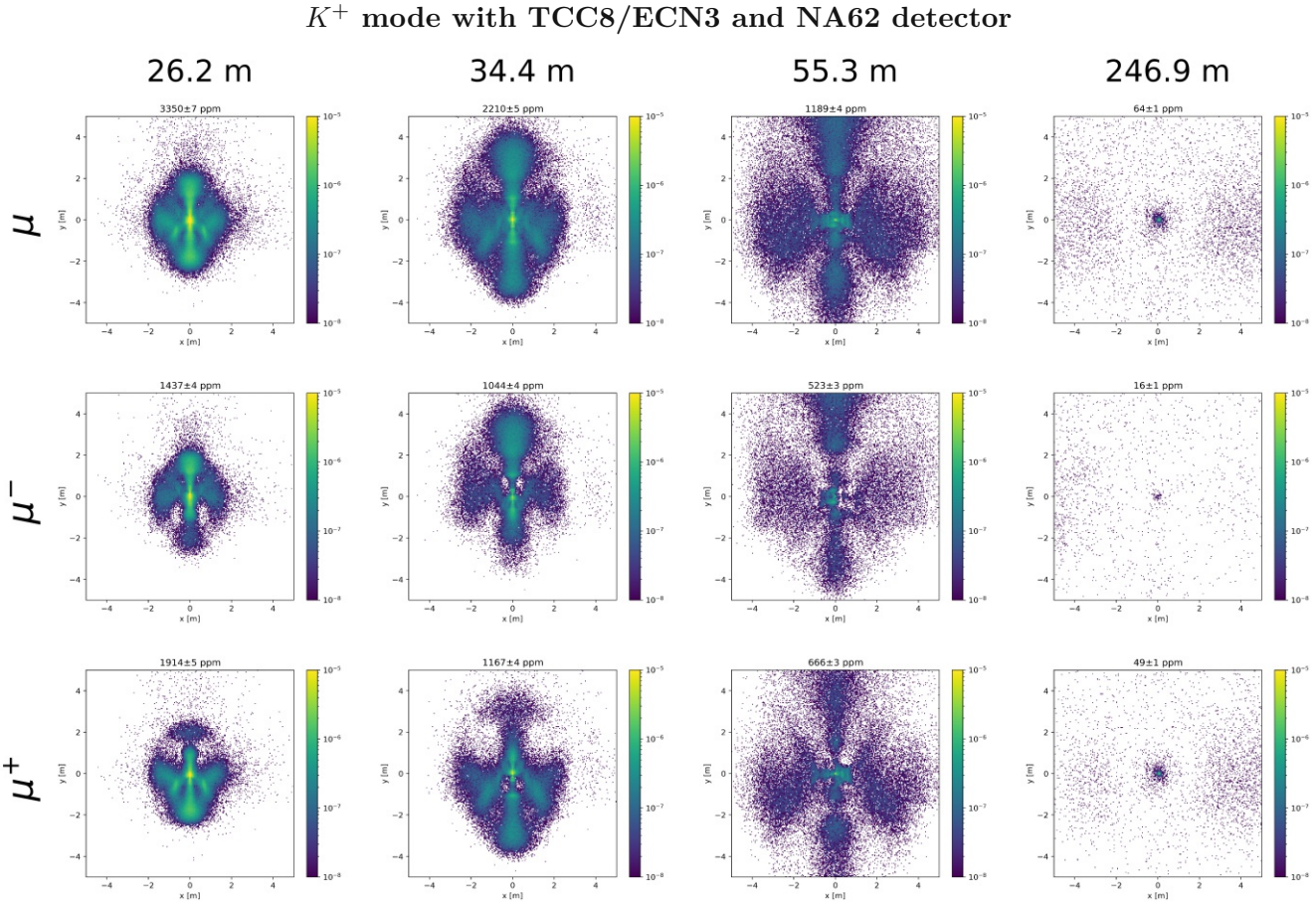


**Fig. 27:** Transversal muon distributions (xy-flux) at selected locations in the K12 beam line in $K^+$ mode after introducing the TCC8 tunnel and ECN3 cavern and the NA62 detector. The investigated locations (left to right) are introduced in Table 4. The muons are viewed separated as for both polarities (top), negatively charged (mid) and positively charged (bottom). The colorbar refers to the number of particles per 4 cm × 4 cm large bin per number of incident protons. The heading of each plot shows the total number of particles per million incident protons.

The next step is to inspect the impact of this model extension. After additionally introducing the geometry of the NA62 detector to the model in $K^+$ mode, a comparison between Figure 22 and 27 can be made. Thereby the effect on the muon distributions is visualized. Since the NA62 detector is only introduced downstream of 55.3 m it should in principle only affect the last column of the plots, which indeed is the case.
The only difference between these plots is that the distribution of the $\mu^-$ is denser in the centre, where there is the hole of the MUV3. The reason for this is most likely that there have been beam interactions with the detector material, that caused the creation of negative muons on the way to 246.9 m. Because the absolute number of $\mu^-$ remains constant, it seems the $\mu^-$ created near the centre were able to pass through, while the material even stopped others in the outer regions. The vacuum tubes and the MUV filter - an 80 cm iron wall right before MUV3, which also has a hole in its centre - are most likely the cause of this, since their density is higher then the other materials and therefore has a higher stopping power.

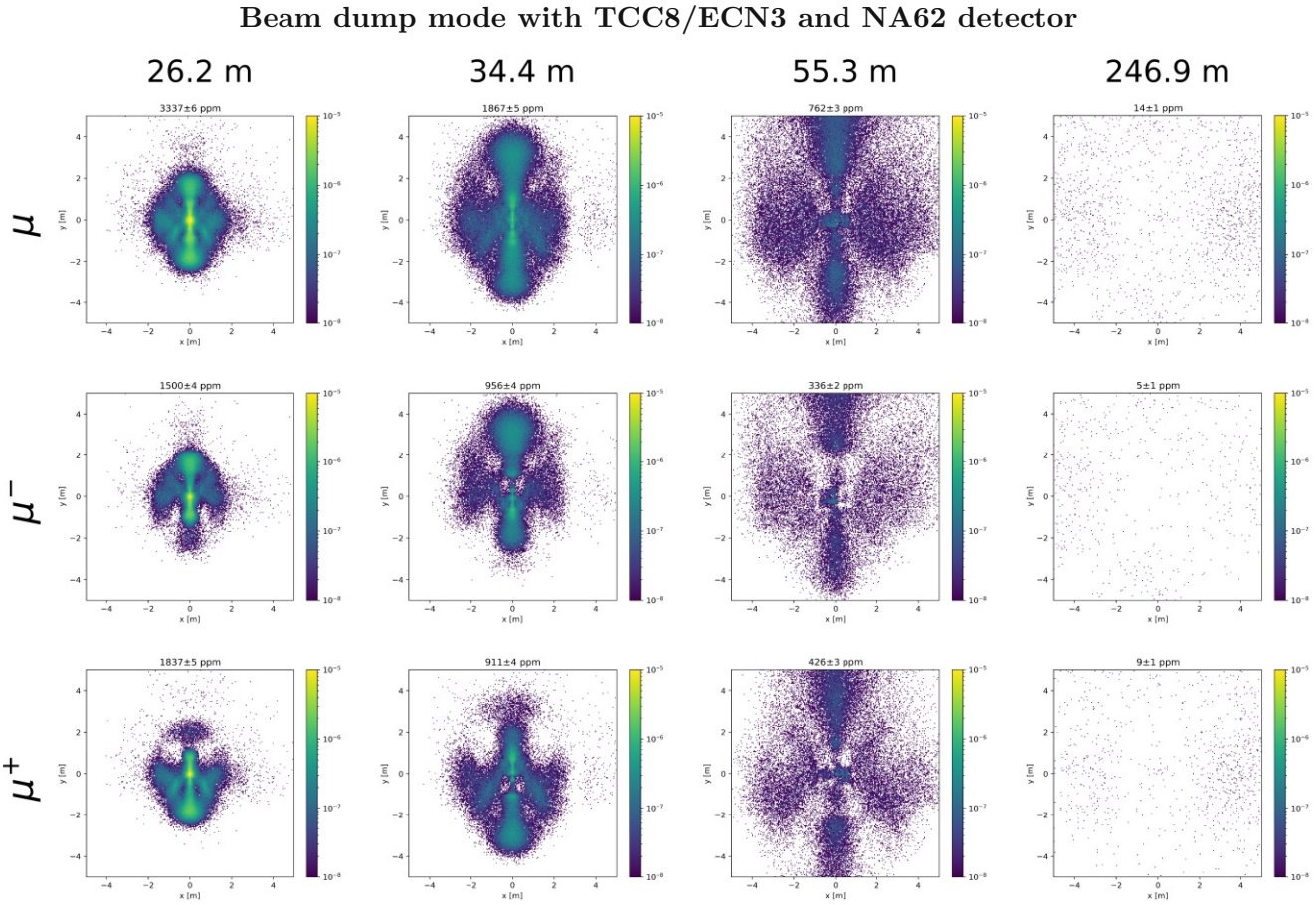


**Fig. 28:** Transversal muon distributions (xy-flux) at selected locations in the K12 beam line in beam dump mode after introducing the TCC8 tunnel and ECN3 cavern and the NA62 detector. The investigated locations (left to right) are introduced in Table 4. The muons are viewed separated as for both polarities (top), negatively charged (mid) and positively charged (bottom). The colorbar refers to the number of particles per 4 cm × 4 cm large bin per number of incident protons. The heading of each plot shows the total number of particles per million incident protons.

Putting the NA62 detector to the model in beam dump mode (see Figure 22 and 27) does not have any influence on the muon background. Here this additional central muon component does not develop, because with the closed TAX there are not any particles to decay any more. In particular, the muon background looks the same with and without NA62 detector.

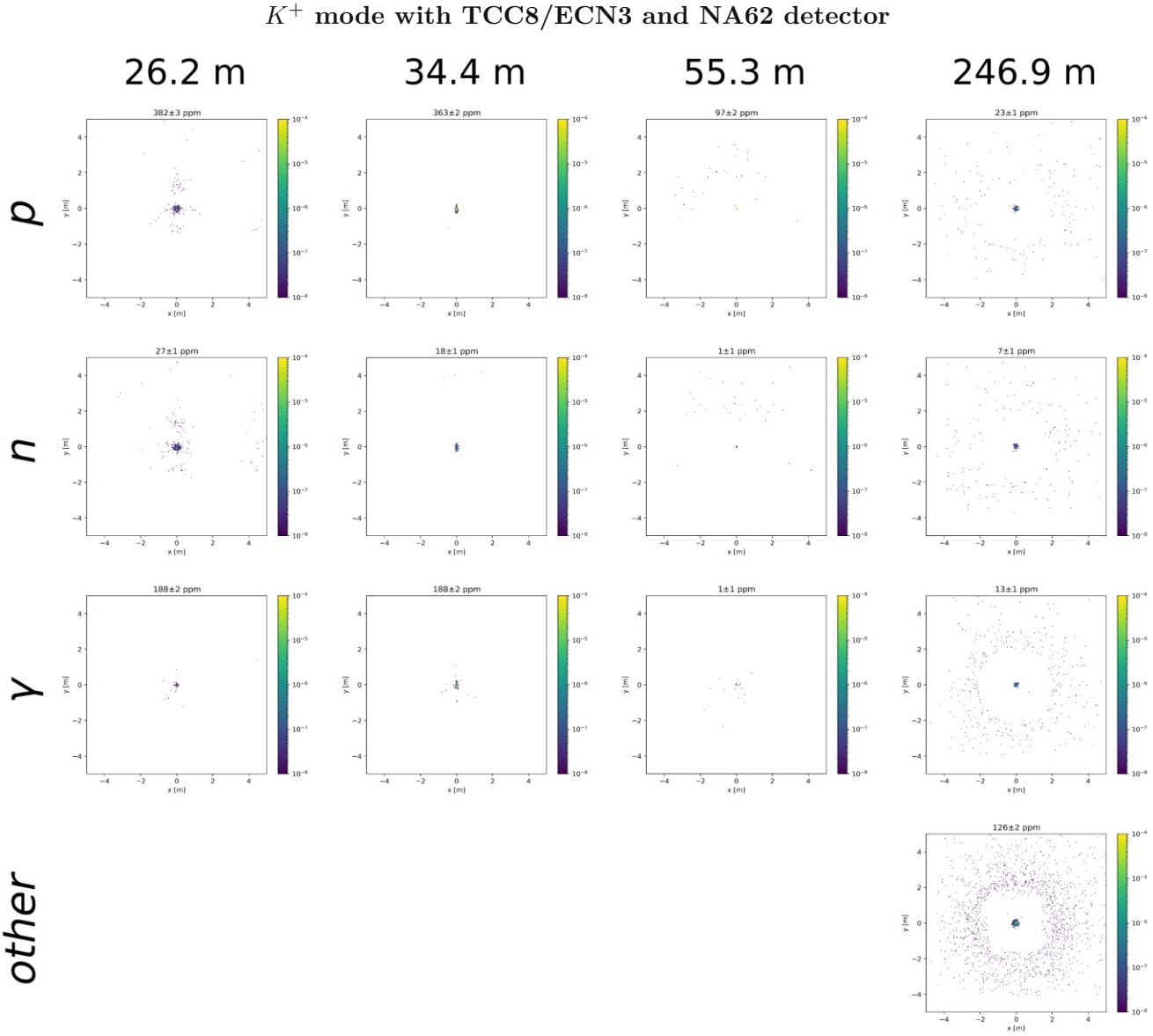


**Fig. 29:** Transversal particle distributions (xy-flux) at selected locations in the K12 beam line in $K^+$ mode after introducing the TCC8 tunnel and ECN3 cavern and the NA62 detector. The investigated locations (left to right) are introduced in Table 4. The particles discussed include protons, neutrons, photons and all the other particles (top to bottom), where the other particles contain all particles except protons, neutrons, photons and muons. The colorbar refers to the number of particles per 4 cm × 4 cm large bin per number of incident protons. The heading of each plot shows the total number of particles per million incident protons.

The comparison between Figure 29 and 24 seems to be the most interesting one for this model extension. Here the distributions of all particles other than muons are compared for the K12 model in $K^+$ mode. The last column of Figure 29 reveals a dramatic change in the angular distribution of these particles at the MUV3 plane. The particles created along the beam line will interact with the detector material and thereby no longer propagate there. Only the particles, that could move outside of the vacuum tube are able to reach this plane. The reason for this is, that particles other than muons are more likely to interact and therefore the NA62 detector has

an influence on their lateral distribution downstream of it. Since the MUV3 detector is placed in the centre of the beam line with a hole in its centre, this new angular distribution benefits the detector, because the number of particles arriving there is minimized, making it easier to veto the muons.

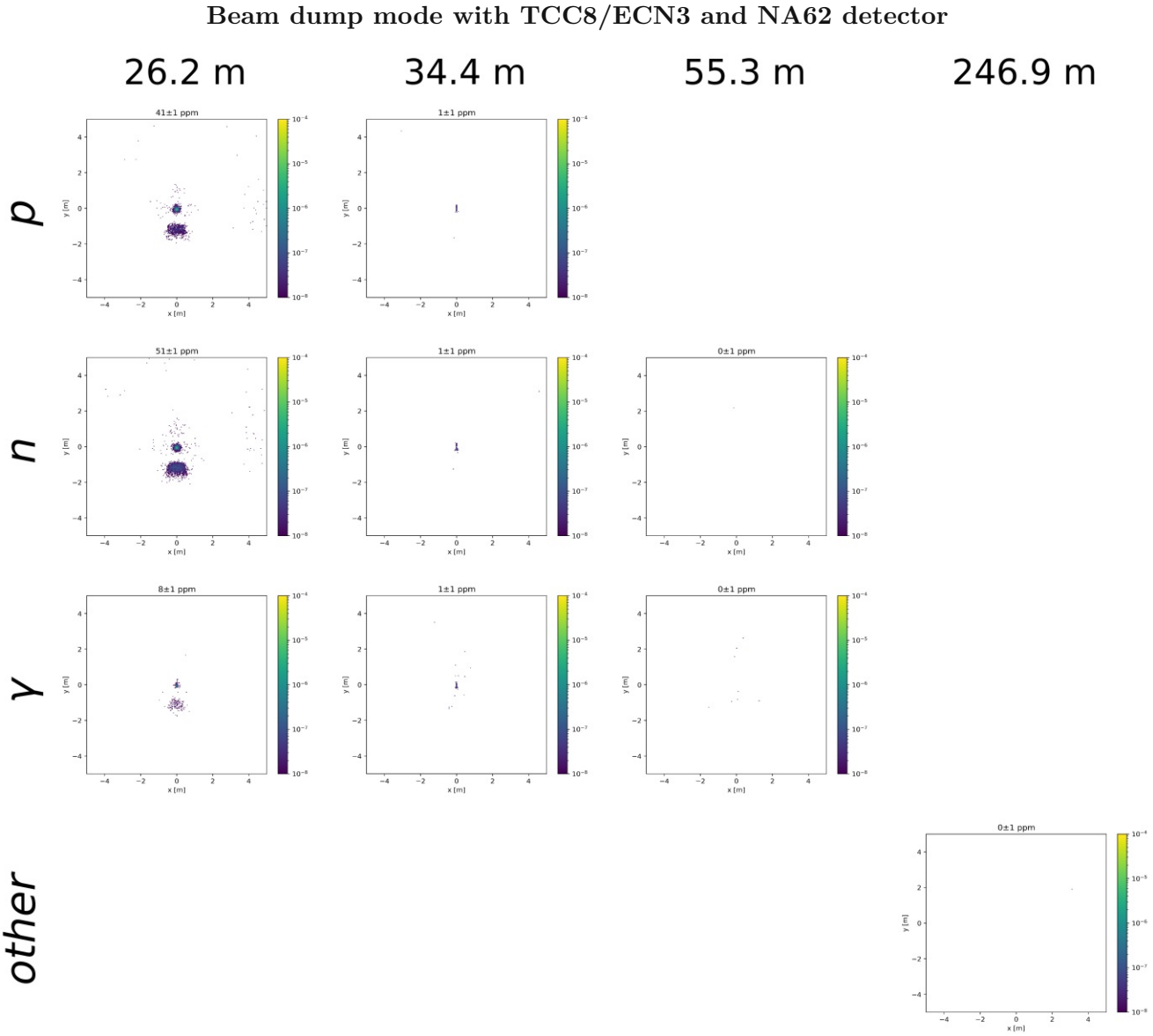


**Fig. 30:** Transversal particle distributions (xy-flux) at selected locations in the K12 beam line in beam dump mode after introducing the TCC8 tunnel and ECN3 cavern and the NA62 detector. The investigated locations (left to right) are introduced in Table 4. The particles discussed include protons, neutrons, photons and all the other particles (top to bottom), where the other particles contain all particles except protons, neutrons, photons and muons. The colorbar refers to the number of particles per 4 cm × 4 cm large bin per number of incident protons. The heading of each plot shows the total number of particles per million incident protons.

Finally, one can also have a look at the non-muonic distributions for the K12 model including the NA62 detector in beam dump mode. Since there has not been a noteworthy background from these particles after the TAX, there is also none after placing the NA62 detector. As expected the muons do not interact very much with the material, which means not even they create a new component that reaches the MUV3.

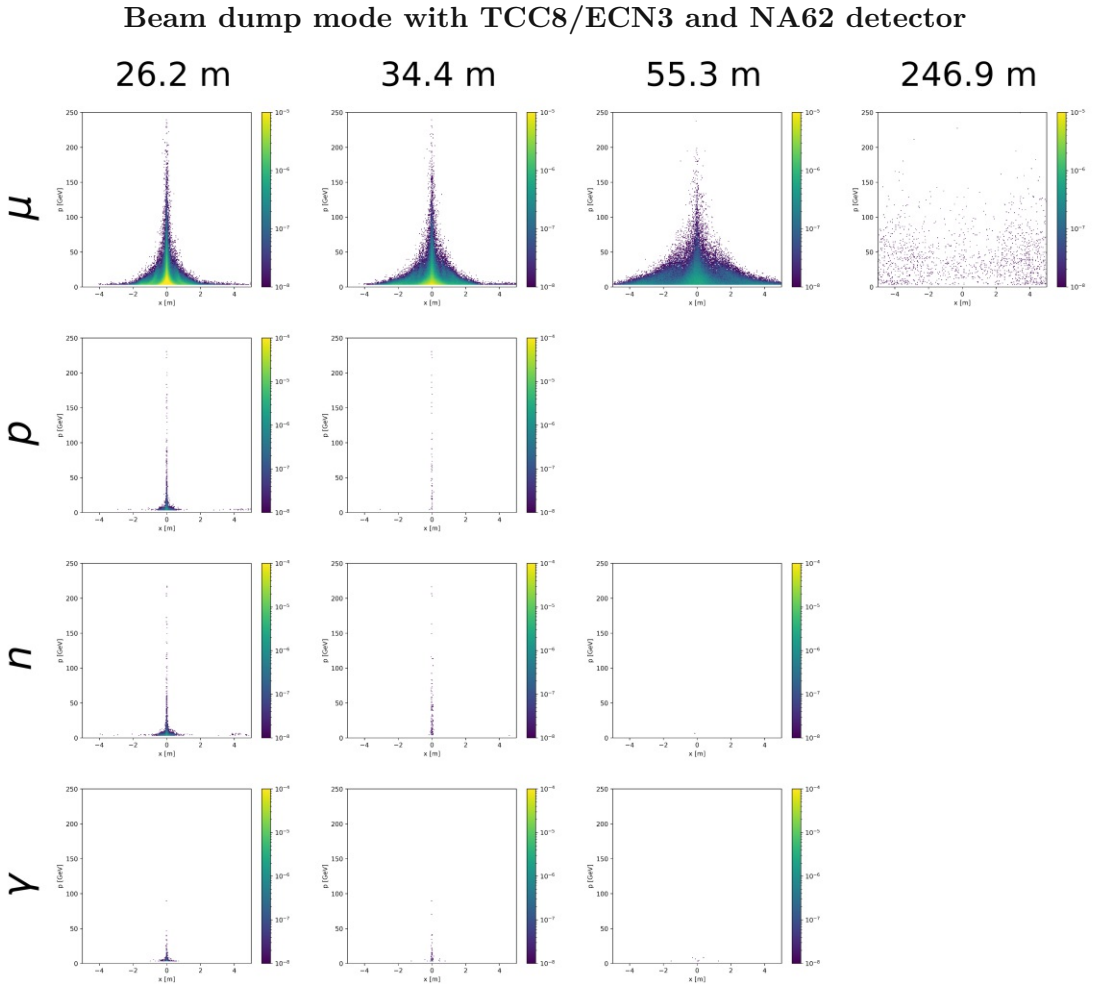


**Fig. 31:** Histogram of beam momentum plotted vs the particle position in the x-plane at selected locations in the K12 beam line in beam dump mode after introducing the TCC8 tunnel and ECN3 cavern and the NA62 detector. The investigated locations (left to right) are introduced in Table 4. The particles discussed include muons, protons, neutrons and photons (top to bottom). The colorbar refers to the number of particles per 4 cm in x-direction and per GeV (4 cm × 1 GeV bins) per total number of incident protons.

Since this model of K12 in beam dump mode, where the surrounding and the NA62 detector are included, will be the one used for the simulations in the upcoming sections of this thesis, it makes sense to investigate it a bit further. In particular it might be interesting to have a look at the momentum distributions in the relevant detector regions at 55.3 m and 246.9 m. These can be seen in Figure 31 and 32 for the x- and y-direction.
As it was mentioned earlier the fields of the bending magnets should only change the distribution in y-direction, which means the x-direction should be quite symmetric around 0 m. This in fact seems to be the case, while for the y-direction one can see the influence of the fields in the protons, neutrons and photons, which is most obvious after the TAX. The fields cause the muons to open up more and more the further downstream they go and in the muon distribution at 34.4 or 55.3 m one can even see some missing components, which occur due to the additional interactions in the iron yoke of the magnet, which works as a shielding and therefore decreases the momentum. Apart from that it is found, that the momentum of the particles behind the TAX is much higher near 0 m, because the protons will mostly hit the dump exactly there.
Since the only noteworthy background at the detectors will be muons, it is reasonable to take

a deeper look into their momentum distribution. For the SHADOWS detector at 55.3 m the interesting region in x will be between 1 m and 4 m. It becomes clear, that the momenta that have to be expected in that region are mostly lower than 50 GeV and that their energy gets lower with higher x. This means placing the detector further off-axis would naturally lead to a background reduction. However, this would come at a price, namely that one would also loose dark matter events, which are of course more likely to be seen near the axis.
In the MUV3 region a different behaviour occurs. Since this is already far away from the TAX the high energetic muons could spread over the whole x- and y-range, which means the high energetic muons are more evenly distributed. Because of that, the experiment has to expect, that the MUV3 detector will detect muons in all energy ranges up to 400 GeV of course with a trend to lower energetic ones.

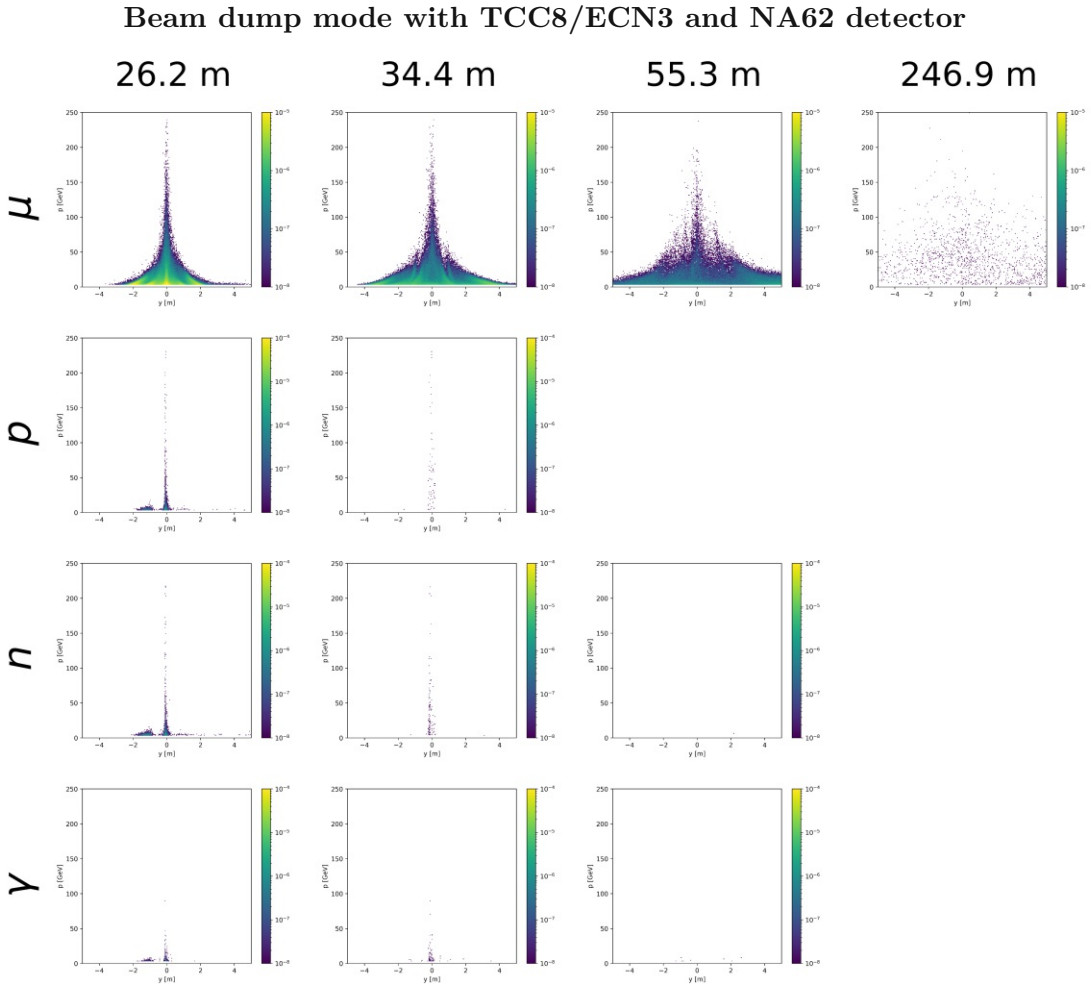


**Fig. 32:** Histogram of beam momentum plotted vs the particle position in the y-plane at selected locations in the K12 beam line in beam dump mode after introducing the TCC8 tunnel and ECN3 cavern and the NA62 detector. The investigated locations (left to right) are introduced in Table 4. The particles discussed include muons, protons, neutrons and photons (top to bottom). The colorbar refers to the number of particles per 4 cm in y-direction and per GeV (4 cm × 1 GeV bins) per total number of incident protons.

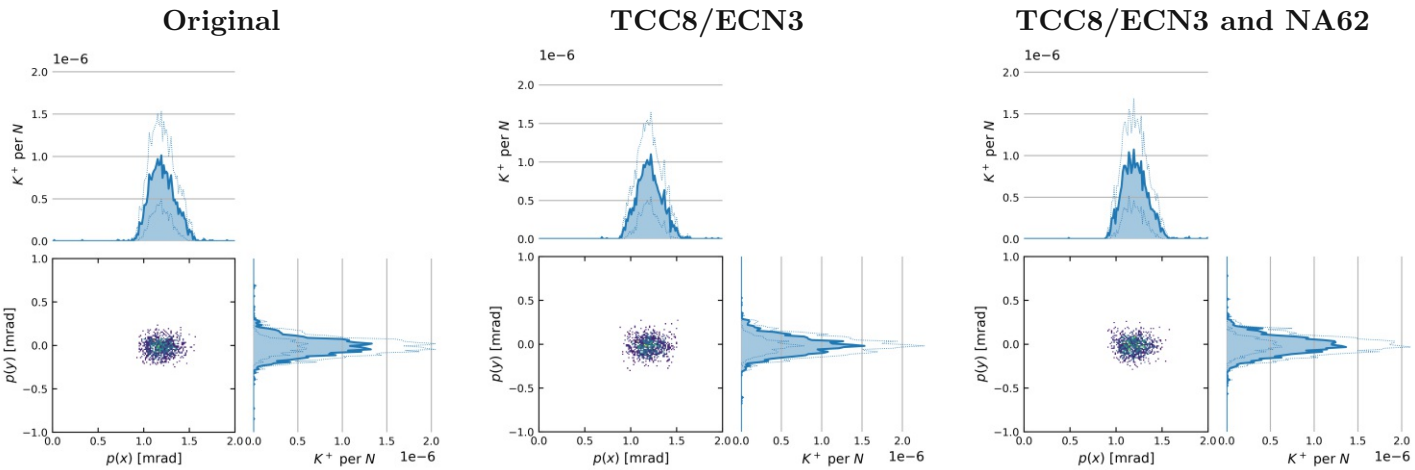


**Fig. 33:** Kaon momentum angle scatter plot as well as the histograms after the GTK for K12 in $K^+$ mode. Comparison of the original model (left), the one including TCC8/ECN3 (mid) and the one including TCC8/ECN3 and the NA62 detector (right).

Finally, an inspection of the impact of the model extensions on the kaons is made. In Figure 33 the distribution of the kaons in terms of their momentum angles in x- and y-direction directly after the GTK3 is displayed. Investigating the kaons here is particularly interesting because the kaons are finally identified at this location. The histograms show the total number of kaons with a momentum in a certain angle in bins of the size of 13.3 $\mu$rad. Immediately it becomes clear, that the distribution looks very much alike even after introducing the model extensions, which leads to the conclusion that the kaon physics up to the GTK3 is not influenced by their introduction to the K12 model.

## 3.4. Validation of the BDSIM model of NA62-BD

In a next step it is necessary to validate the accuracy of the simulation data created with the BDSIM model of the K12 beam line. Such a validation study has already been performed for the $K^+$ mode in terms of the kaons within the BE-EA-LE section and it showed a good agreement with the measurement data. Now that the model was put in beam dump mode, the simulation data should be benchmarked by a comparison with measurement data too. Fortunately, the NA62 collaboration already did a trial run of this setup during Run 2 in 2018 and with the received data this comparison comes within reach.
For a benchmarking of the K12 model in beam dump mode the natural choice is to investigate the muon background. It will be the largest background for the experiment and because of that it can be expected, that it will deliver the highest statistics in the detector region compared to all other particles. Therefore, using the muon background for this task is only reasonable.
During the data taking in 2018 in beam dump mode, plots were created that show the muon distributions at 180 m downstream the usual centre of the T10 target. It contains only those particles, that are in the acceptance of a detector called newCHOD [50] - a charged-particle hodoscope that is able to detect and veto muon decays - and the collected data contained also their momentum enabling a comparison of not only the lateral distribution in the transverse direction, but also the momentum distribution in terms of the radius from the transverse centre of the beam line.
The configuration of the K12 beam line for these measurement has not been changed from the K12HIKA+ setting in any other way then putting the TAX in beam dump mode and removing the Beryllium target T10, which means a comparison with Monte Carlo data from the BDSIM model of K12 in beam dump mode (as described in Section 3.3.2) is valid and should lead to the same results as in the experiment.

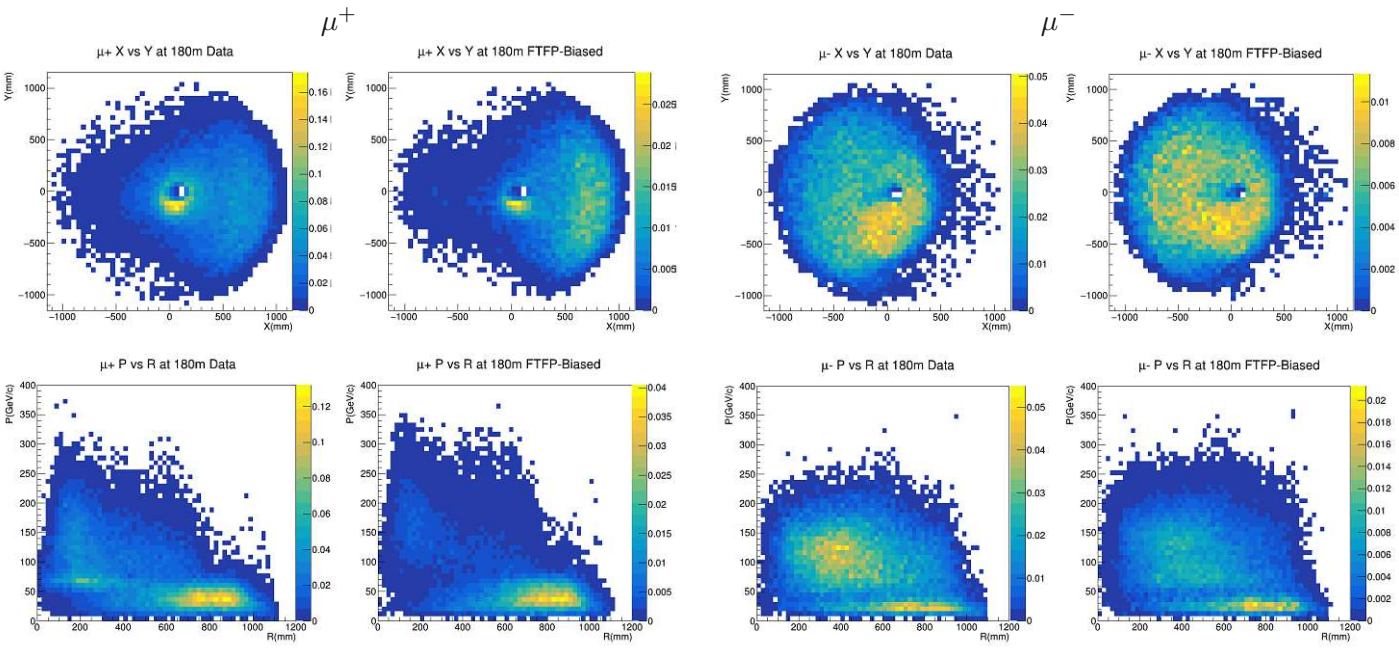


**Fig. 34:** Comparison between measurement data and simulated Monte Carlo data for the BDSIM model validation of the K12 beam line in beam dump mode. The plots show the scatter plot (top) and the momentum distributions of the particles in terms of radius (bottom) for positively (left) and negatively (right) charged muons at 180 m after the centre of T10, which are in the acceptance of the newCHOD detector.

Figure 34 shows the plots created for the BDSIM model validation. It shows a comparison between the measurement data and the simulation data. The plots were created with the use of biassing techniques for the FTFP physics list to create the statistics needed for these plots. The FTFP physics list in Geant4 is the one that is recommended by the Geant4 developers and should therefore be the most accurate one available. All the simulations done for this thesis are based on it. The left and right hand side plots show the transverse and momentum distributions for the positively and negatively charged muons, respectively.
it can be seen that qualitatively the measurement data and the FTFT-biased simulation data look very much alike. This is true for all four plots. It is found that the density of the $\mu^+$ is higher at the right side of the detector and that of the $\mu^-$ higher at the left. Also the $\mu^+$ tend to reach higher energies than the $\mu^-$. The denser areas are similarly distributed in the measurement and simulation data. Of course, they are not exactly the same, like one can see in the higher densities of the simulation at the right of the $\mu^+$ and at the left of the $\mu^-$ plot, but the trend is correct.
These results clarify that qualitatively simulations with the BDSIM model of K12 show the same results as the measurement data. Thereby, the model validation was successfully achieved. Because of that, it is valid to optimize the magnetic field configuration via simulations with the K12 model in BDSIM.

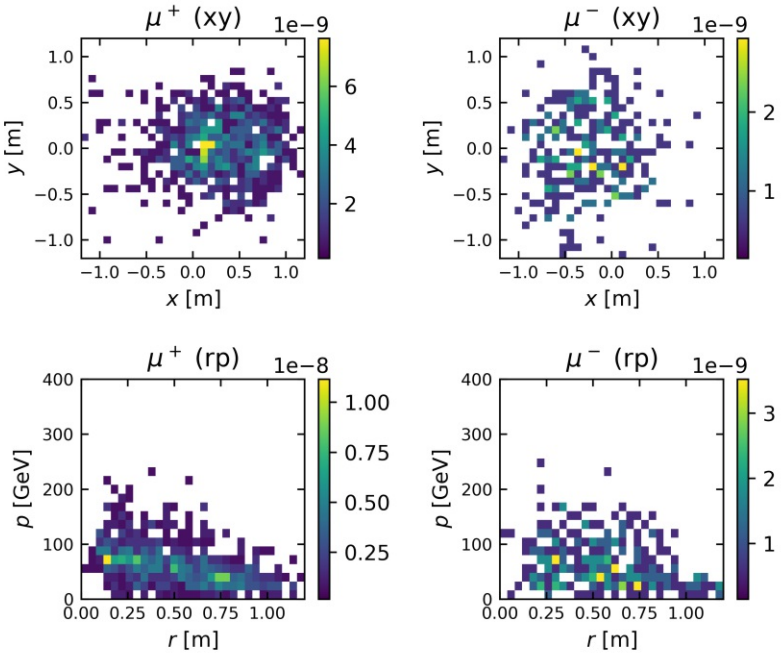


**Fig. 35:** Brute force simulation data created with the BDSIM model of K12 in beam dump mode. The plots show the scatter plot (top) and the momentum distributions of the particles in terms of radius (bottom) for positively (left) and negatively (right) charged muons at 180 m after the centre of T10, which are in the acceptance of the newCHOD detector.

Furthermore, it was also tried to achieve this validation simply by using a brute force method, namely by propagating enough protons to the dump, so that the same picture develops without any use of biassing. Since biassing always results in some sort of information loss, unbiased simulation data would be more accurate. Therefore it is interesting to see results of a brute force method. However, this comes at the cost of lower statistics, which remains to be seen if it is sufficient.
The results for this can be found in Figure 35. Note that the binning was chosen differently than in Figure 34 to increase the density of the plot. As one can see the trend seems to go into the right direction. Nonetheless, the statistics are too low to make meaningful statements. It became clear that the number of particles one would need to run is simply too high to create sufficiently meaningful graphs. Because of that, this approach was not considered feasible.

## 3.5. Optimization of the magnetic field configuration at the BEND1

So far the magnetic field configuration for all the simulations has still been the same as that used in K12HIKA+, which was optimized for NA62 using the $K^+$ mode. Because NA62-BD has different goals than NA62, the magnetic field configuration has to be optimized for the task at hand. For a dark matter experiment optimization initially means the reduction of the backgrounds at the detectors of the experiment. As it was already discussed in Section 1.8.2 and as it could be seen in Figure 28 and 30, the muon background is expected to be the most critical one, which means this optimization boils down to the reduction of the muon background.
The K12 beam line has three options to sweep the muons out of the detectors acceptance, namely BEND1, BEND3 and the scraper magnet. Figure 7 in section 1.6 indicates their location in the beam line. The most effective muon sweeping is expected to be achieved by an optimization of the magnetic fields of the last two magnets in the BEND1 configuration. This is because these two are bending magnets that are located directly downstream the TAX. Since the TAX is the place, where most of the muons will be created, the muons will still be quite central giving those magnets a high potential of sweeping them away from the detectors and in particular from MUV3. Because of that, their optimization will be the main priority of this section.
To achieve this goal all magnets downstream BEND1C and also BEND1A and BEND2 - the first two magnets of BEND1 - were switched off in the simulations. This means the proton beam will directly hit the TAX and the created muons only see the effect of BEND1B and BEND1C. The comparison between the different magnetic field constellations of the two will be made in terms of the respective muon ratios with respect to the nominal configuration, where the nominal configuration is B(BEND1B) = -1.65 T and B(BEND1C) = 1.65 T. Figure 36 sketches the magnetic field configuration for this study.
The last detector of NA62 that is able to detect charged particles like muons is MUV3. Because of that, it will be the final detector that is able to veto muons and therefore the best choice for a reference point in the optimization process. With this choice the remaining muon rate with respect to the nominal configuration directly after the MUV3 is used as figure of merit (FOM). Previous investigations based on simulations performed in G4Beamline already delivered insights on minimizing the background for NA62-BD [51, 52]. Therefore, this study shall not only inspect the optimal BEND1 configuration for NA62-BD via BDSIM simulations, but also take SHADOWS into account. Therefore, for SHADOWS the FOM is defined in the same way only at another location in the beam line, namely at the possible future location of the SHADOWS detector mentioned in Table 4.
The MUV3 detector is expected to only be sensitive to charged particles with momenta higher than 5 GeV. However, the simulations set a more generous cut-off for particles with momenta lower than 3 GeV.

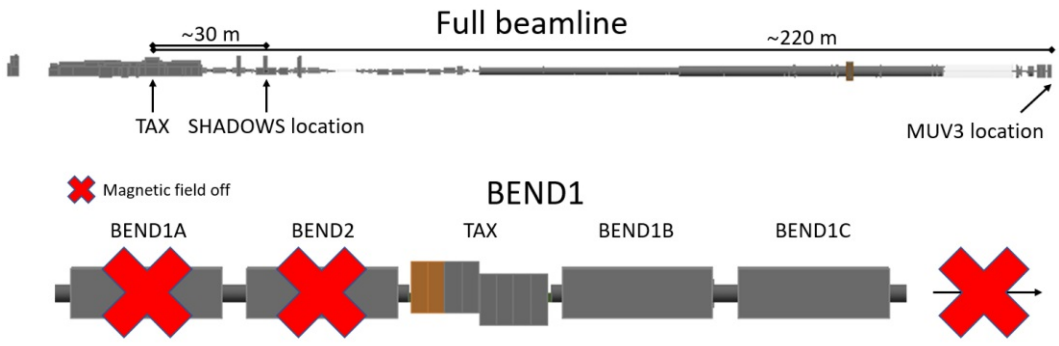


**Fig. 36:** Detector location in the beam line (top) and magnetic field configuration (bottom) of the K12 beam line in the BEND1 study. The magnetic fields of BEND1B and BEND1C are varied.

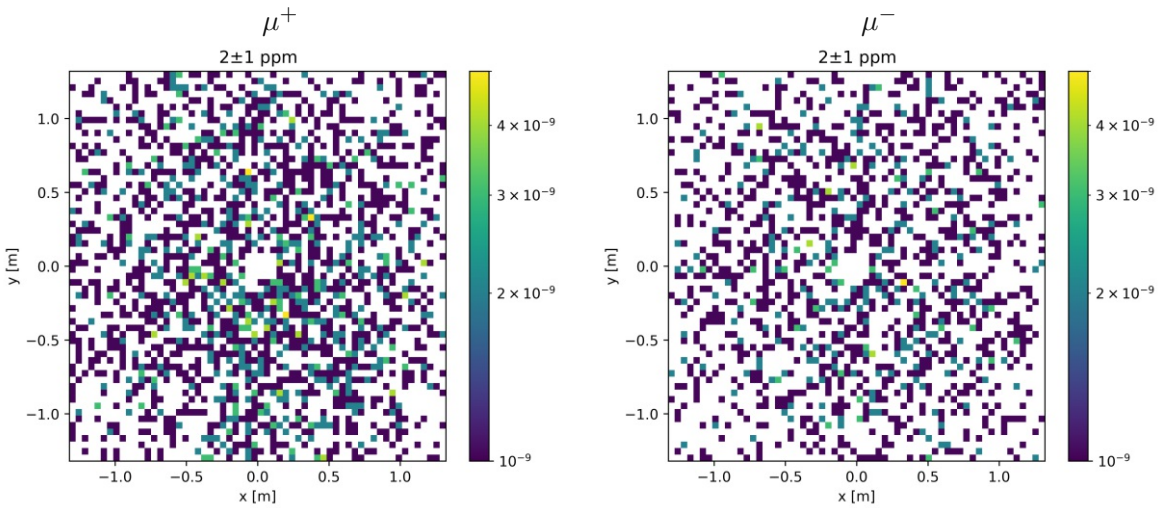


**Fig. 37:** Transverse muon distribution at the MUV3 detector separated into positively (left) and negatively (right) charged muons.

The distributions of the positively and negatively charged particles at the MUV3 with BEND1B and BEND1C in the nominal configuration can be seen in Figure 37. BEND1A, BEND2 as all magnets downstream of BEND1C were switched off. These pictures show that for every million POT one can expect to see $2\mu^+$ and $2\mu^-$. It also can be seen that the muon density is higher near the centre of the beam. Since the MUV3 has a hole with radius of 10.6 cm in its centre, this region shows no muon detections.
Now that an overview of the results in the nominal BEND1B and BEND1C configuration was given, it is possible to start the discussion of the results for other ones.

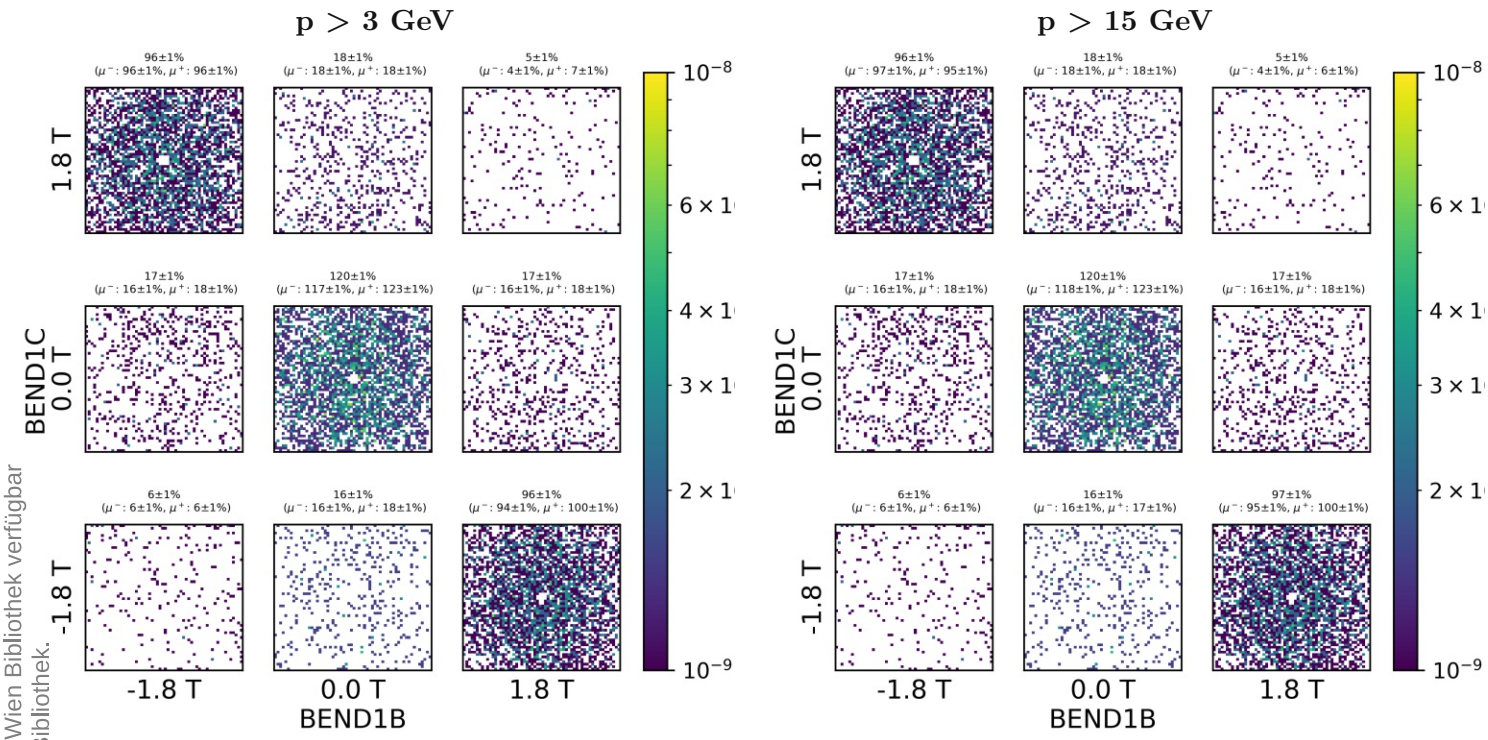


**Fig. 38:** Transverse muon distribution at the MUV3 for different magnetic field configurations of BEND1B and BEND1C and different low momentum cut-off (left: p > 3 GeV, right: p > 15 GeV). The numbers show the remaining muon rate with respect to the nominal configuration for different field constellations of BEND1B and BEND1C.

The left-hand side of Figure 38 shows the transverse muon distributions at the MUV3 and the remaining rate with respect to the nominal configuration for all combinations of -1.8, 0 and 1.8 T fields, where 1.8 T (-1.8 T) was chosen since it is the maximal (minimal) field, that can be generated with the currently used MTR magnets. A low momentum cut-off was set at 3 GeV. The plots show that the highest reduction of the muon background can be achieved by using high magnetic fields with same polarity. Here the number of muons will be only about 5% of that of the nominal configuration, which means the muon background could be reduced up to a factor 20 simply by using this BEND1 configuration. If only one of the magnets were switched on with high field, this should already lead to a muon background reduction of about a factor 5. Unsurprisingly, the most critical configuration is the one where both magnets are switched off. Here the muons created in the TAX will reach the MUV3 without being swept by any fields. Because of that, it is expected to see a large muon background for this configuration. However, the background for this configuration would only rise by 20% compared to the nominal configuration, which implicates that using fields with opposite polarities, like the nominal configuration, is not much better for muon sweeping in NA62-BD than having no field at all. This is supported by the large number of muons that can be seen in the off-diagonal plots.
Muons with energies larger than 15 GeV are especially problematic for the detection. These so-called “hard muons” are able to access decay processes that make it hard to distinguish between electrons and muons if the decay happens in late stages of the detector. Because of that it is important to know the background for these muons and to reduce it as much as possible. Therefore, the right-hand side of Figure 38 shows the remaining rate with respect to the nominal configuration for muons with momenta larger than 15 GeV. It is found that the hard muons behave the same as if the lower energetic component were included.
The results are in good agreement with the outcome of the previous studies [51, 52].

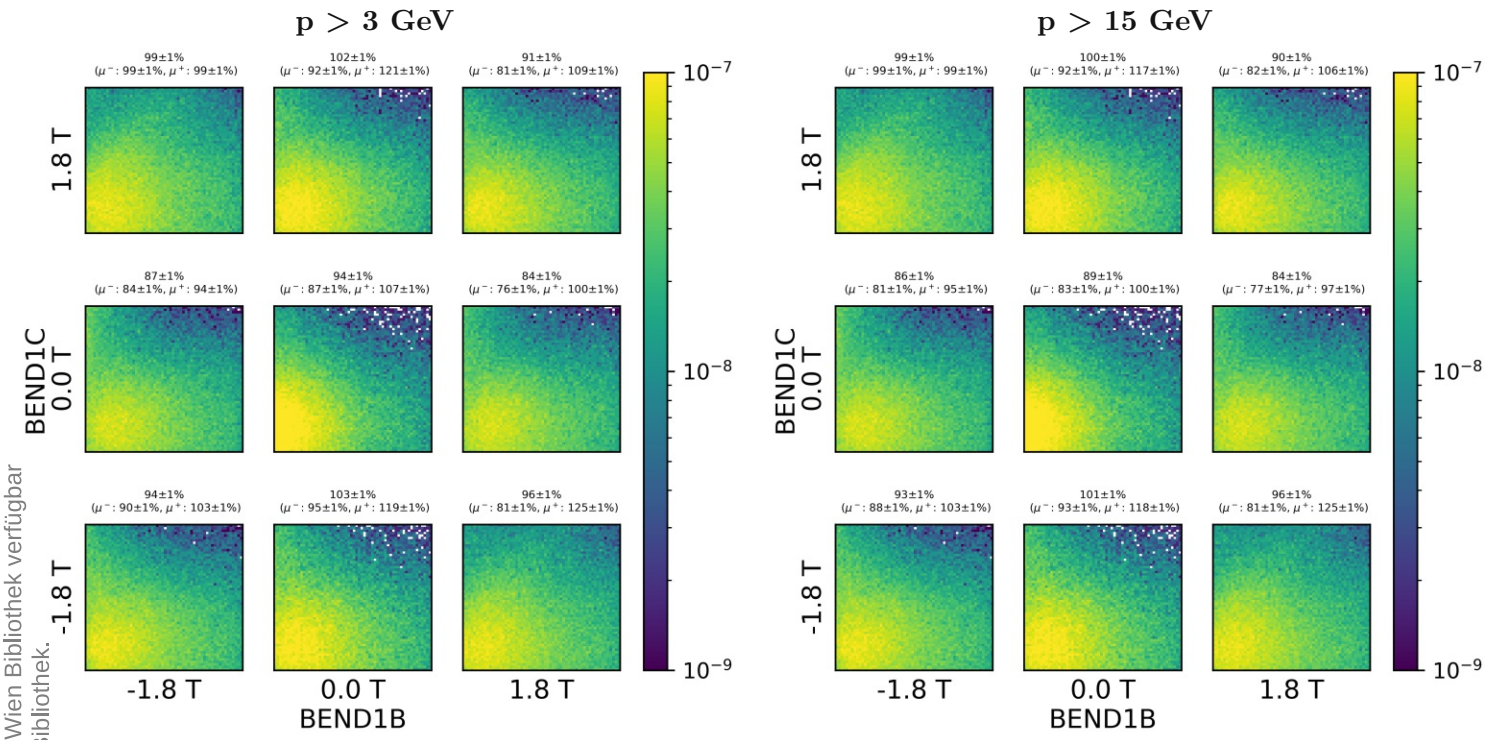


**Fig. 39:** Transverse muon distribution at the possible location of the SHADOWS detector for different magnetic field configurations of BEND1B and BEND1C and different momentum cut-off (left: p < 3 GeV, right: p < 15 GeV). The numbers show the remaining muon rate with respect to the nominal configuration for different field constellations of BEND1B and BEND1C.

Via Figure 39 it is possible to find out about the impact of the BEND1 configurations at the possible future location of the SHADOWS detector at 55.3 m in the beam line starting at 1 m off axis in x-direction. The Figure displays the transverse muon distributions and the remaining rate with respect to the nominal configuration for muons as for positively charged and negatively charged muons. Furthermore, the plot is shown for muons with momenta larger than 3 GeV and for the hard muons with momenta larger then 15 GeV.
It can be seen that the effect of BEND1B and BEND1C is smaller for the SHADOWS detector than for the MUV3. The reason for this is that the detector is not far downstream the TAX, only about 30 m. Because of that, the deflection angle of the muons did not have enough time to evolve along the beam line. The maximal background reduction of 16%, which is reached for B(BEND1B) = 1.8 T and B(BEND1C) = 0.0 T will only enable the experiment to reduce it by a factor 1.2 making BEND1 optimization less useful for SHADOWS than for NA62-BD.
Furthermore, it is found that the plots for the different momentum cut-off show the same results, except for the configuration where both magnets are switched off. Here a higher momentum cut-off leads to an about 5% better background suppression for hard muons as if the lower energetic ones were included. The reason for that might be that the lower energetic muons leaving the beam dump have already undergone more interactions inside its material, meaning they are more likely to leave the TAX at higher angles that allow the muons to reach the off-axis SHADOWS detector.
Unsurprisingly, the distributions show a higher density nearer the centre of the beam line, which is at the lower left side of the plots and 1 m away from the detector. Since muon sweeping with the BEND1 does not seem to be a sufficient solution for the background optimization in SHADOWS, other options have been evaluated that will be presented in the next section.

Finally, it is possible to define a combined FOM for both experiments. A convincing definition is the root mean square of the gain factors of the FOMs for the single experiments. The gain factor in this context is the factor by which the muon background could be reduced for a certain BEND1 configuration. For example at the MUV3 at B(BEND1B) = 1.8 T and B(BEND1C) = 1.8 T (see Figure 38) the background is only 5% with respect to the nominal one, which means a factor of 20 was gained. Therefore, the combined FOM can be defined as:

$$FOM_{combined} = \sqrt{\left(\frac{1}{FOM_{NA62BD}}\right)^2 + \left(\frac{1}{FOM_{SHADOWS}}\right)^2} \tag{4}$$

leading to Table 6.

| **p > 3 GeV** | | | |
|---|---|---|---|
| | **-1.8 T** | **0.0 T** | **1.8 T** |
| **1.8 T** | 1.5 | 5.6 | 20.0 |
| **0.0 T** | 6.0 | 1.4 | 6.0 |
| **-1.8 T** | 16.7 | 6.3 | 1.5 |

| **p > 15 GeV** | | | |
|---|---|---|---|
| | **-1.8 T** | **0.0 T** | **1.8 T** |
| **1.8 T** | 1.5 | 5.6 | 20.0 |
| **0.0 T** | 6.0 | 1.4 | 6.0 |
| **-1.8 T** | 16.7 | 6.3 | 1.5 |

**Tab. 6:** Combined Figure of merit for NA62-BD and SHADOWS at different BEND1 configurations for momentum cut-off at 3 GeV and 15 GeV.

This table shows the combined gain factors at the two detectors. The higher this value is, the more beneficial the BEND1 configuration will be with respect to both experiments. It is found that the momentum cut-off does not change this table at all. From this table it can be derived that the optimal BEND1 configuration with respect to the FOM defined in Equation 4 is B(BEND1B) = 1.8 T and B(BEND1C) = 1.8 T.

## 3.6. Evaluation of a muon sweeping system for further muon background reduction at SHADOWS

SHADOWS is a new experiment that aims for placing an off-axis detector alongside the K12 beam line to search for feebly interacting particles near the beam dump. The project was presented in the March 2021's Physics Beyond Colliders workshop at CERN [53] and it is currently in a state of preliminary studies. One of these studies is that of the backgrounds and in particular the muon background.

The previous section showed that for SHADOWS the muon background cannot be heavily reduced only by optimizing the BEND1 configuration. The SHADOWS detector is possibly located about 55 m downstream the centre of T10, which is in the same region as the BEND3 configuration, meaning that BEND3 or the even further downstream scraper magnet will not be an option for a further optimization of this background.

The solution to this problem is to introduce a muon sweeping system that is dedicated to optimize the muon background for SHADOWS. In the simplest form this muon sweeping system could consist of an additional off-axis bending magnet upstream the SHADOWS detector, but after the BEND1 magnets to also minimize the fraction of muons that are swept into the SHADOWS acceptance due to the effect that was illustrated in Figure 16 in section 3.2. The sweeping magnets used in the simulations for this study are scaled versions of the scraper magnet (introduced in Figure 7). The reason behind this is, that for the scraper magnet there is already a field map available, that can be used in BDSIM. The GDML of the scraper and its field are shown in Figure 40. For the simulations it was assumed that the muon sweeping magnet reaches up to B = 1.7 T in the centre of the yoke and the direction of the field was chosen to be upwards at the side near to the beam line.

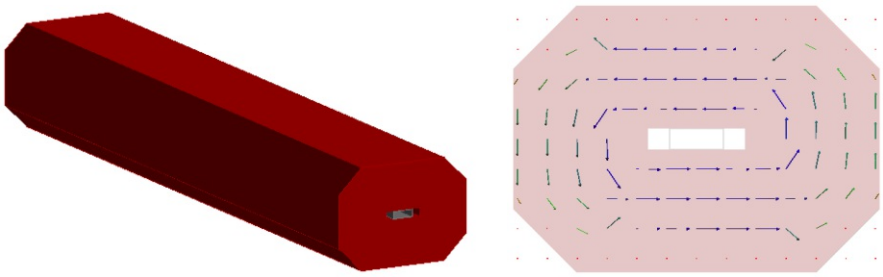

**Fig. 40:** GDML geometry of the scraper magnet (left) and its magnetic field (right).

For the magnetic field configuration in the K12 model it was chosen to use the BEND1 configuration that was optimized with respect to both experiments in the previous section, which means BEND1A and BEND2 as all magnets downstream BEND1C are switched off, while B(BEND1B) = B(BEND1C) = 1.8 T. The discussion will be based on the transverse muon distributions at the locations introduced in Table 7.

| z-location [m] | Reference point | Importance |
|---|---|---|
| 42.8 | After Q5 magnet | Location about 3 m downstream the end of the muon sweeping magnet where its effect on the muon distribution is more prominent |
| 55.3 | After second BEND3 magnet | Possible location of the SHADOWS spectrometer Detector region (x,y) [m]: ([1.0, 4.0],[-0.5, 2.5]) |

**Tab. 7:** Locations in the K12 beam line relative to the centre of the Beryllium target and their relevance in the SHADOWS studies.

**Fig. 41:** Shielding at the possible location for the muon sweeping system.

To introduce the sweeping magnet at a location near the BEND1C, it would be necessary to adjust the shielding that is surrounding this area. A picture of the current shielding can be seen in Figure 41. Since the magnet itself is made from iron, it is expected to have stopping power too, which means placing the magnet instead of the shielding blocks should not lead to a higher background in the later regions of the NA62 detector. It is even possible that the dense material of the magnet will increase the stopping power and reduce the background. Of course this has to be evaluated with simulations in the future.

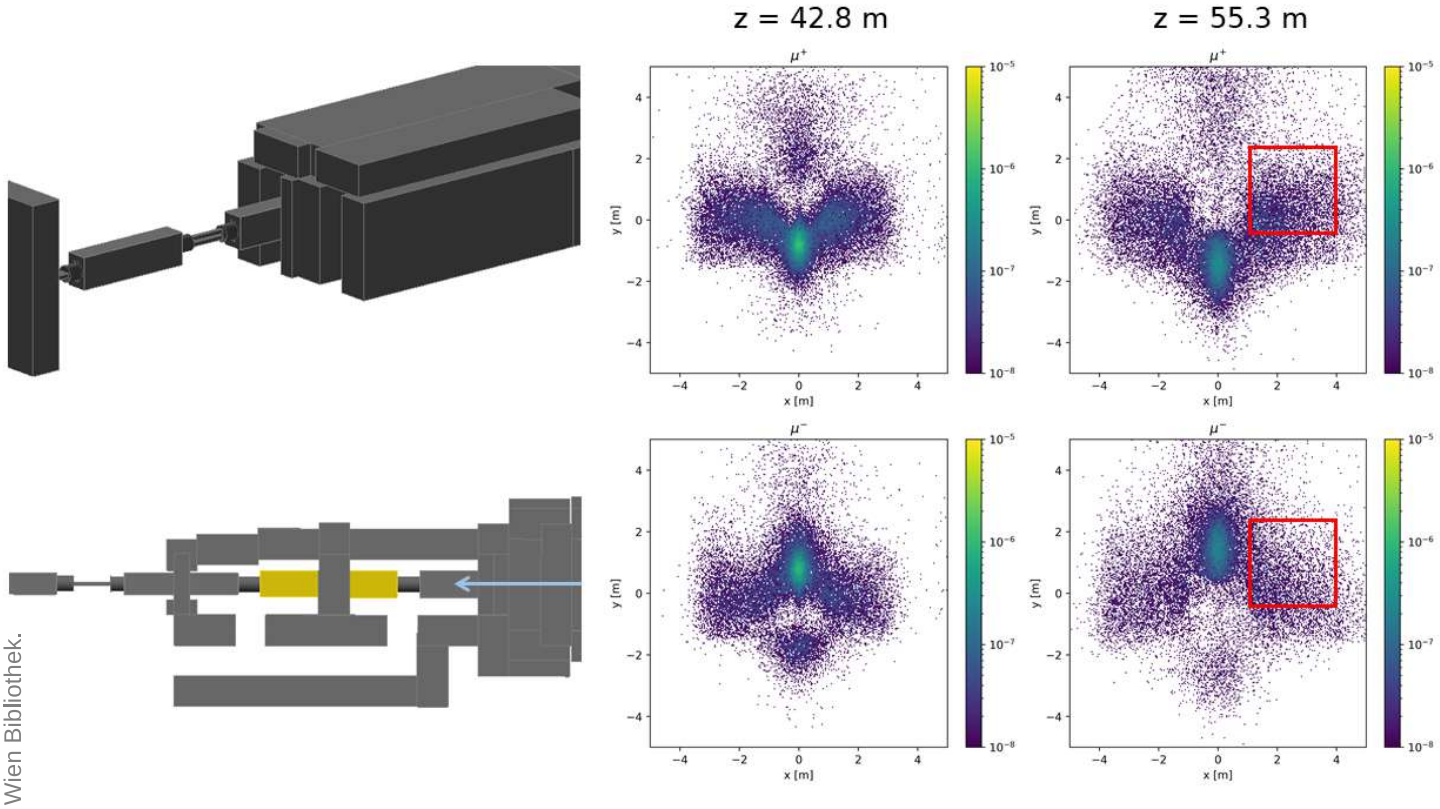


**Fig. 42:** Geometry and muon distributions without a SHADOWS dedicated muon sweeping system. The geometry (left) displays the layout of the shielding and BEND1C in yellow. The beam direction is indicated by the blue arrow. The plots on the right show the transverse distributions of positively (top) and negatively (bottom) charged muons at the locations described in Table 7. The red rectangle marks the possible location of the SHADOWS detector.

Figure 42 marks the starting point of this study. It shows the geometry of the relevant region at the left and the muon distributions at the locations mentioned in Table 7 at the right. This setup is equivalent to the one used in section 3.5 with the optimized magnetic field configuration. It is found that in x-direction the muon distributions are more or less mirror-symmetric around the centre of the beam line. In y-direction the magnetic field of the BEND1 magnets separates the positively charged from the negatively charged muons. The return yokes of the MTR magnet also give the muons a momentum in x-direction pushing them into the SHADOWS acceptance. This effect was already described in section 3.2 via Figure 16.
From inspecting these pictures it once more becomes evident, that a muon sweeping system will be necessary to reduce the background for SHADOWS.

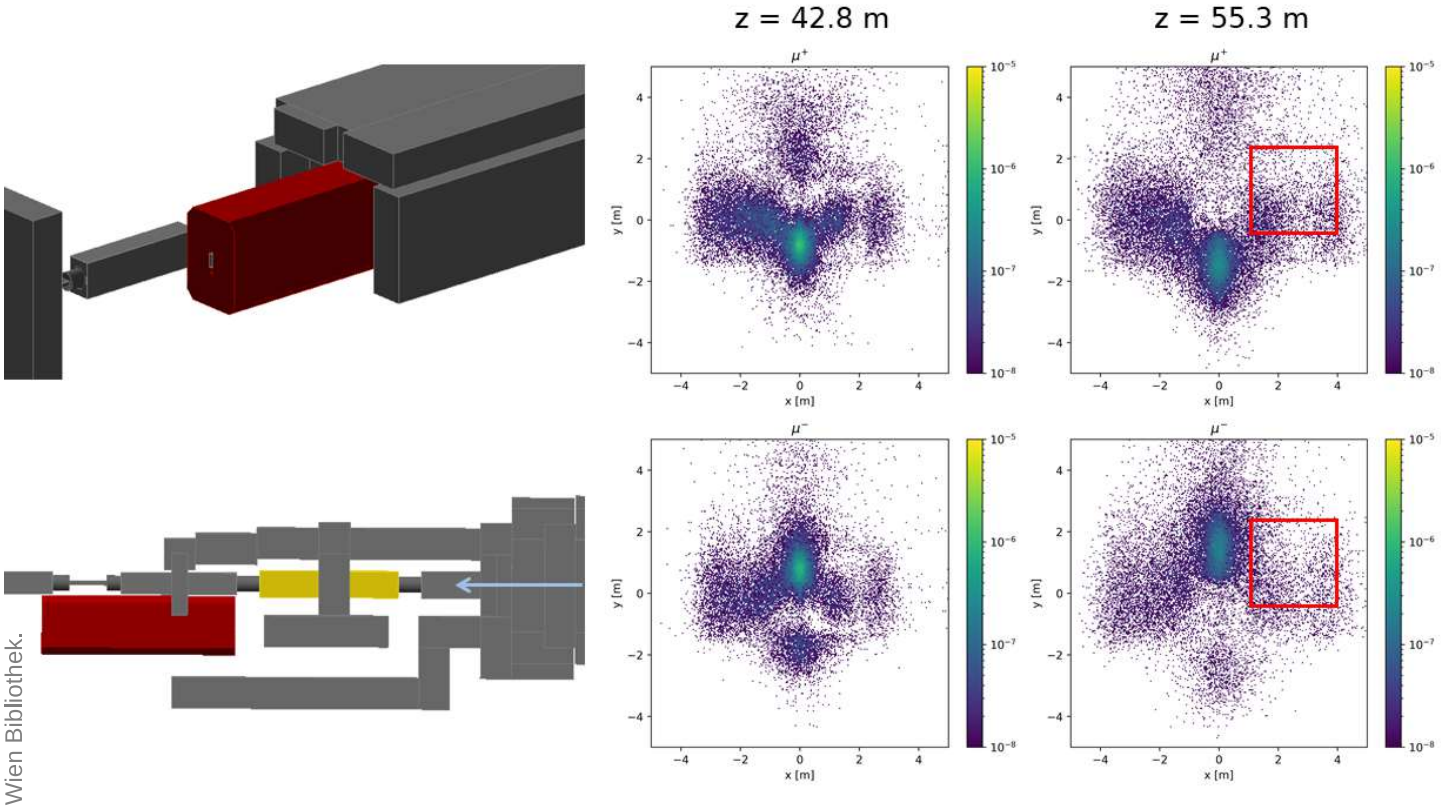


**Fig. 43:** Geometry and muon distributions with a scraper-like off-axis magnet of dimensions (xyz) = (1.5m×2.1m×5.0m) with its field switched off. The geometry (left) displays the sweeping magnet in red, the altered layout of the shielding and BEND1C in yellow. The beam direction is indicated by the blue arrow. The plots on the right show the transverse distributions of positively (top) and negatively (bottom) charged muons at the locations described in Table 7. The red rectangle marks the possible location of the SHADOWS detector.

As a first attempt to improve the muon background only placing the magnet alongside the beam line without using any magnetic field is a reasonable approach. By doing this it can be evaluated whether the dense iron material already helps minimizing the muon background in the SHADOWS region. A possible configuration for this and the results for running a simulation with such a setup is shown in Figure 43. The magnet in this geometry is a version of the scraper magnet, that was scaled to the dimensions of (xyz) = (1.5m×2.1m×5.0m) and it is placed as near to the beam line as possible. The results in the plots at the right can be directly compared to Figure 42 and the following ones.
It is found that the yoke material already reduces the background in the relevant detector region by a factor of 2 even in the absence of a magnetic field. Still, the muon background remains non-negligible and therefore a magnetic field will be necessary to reduce the background even further.

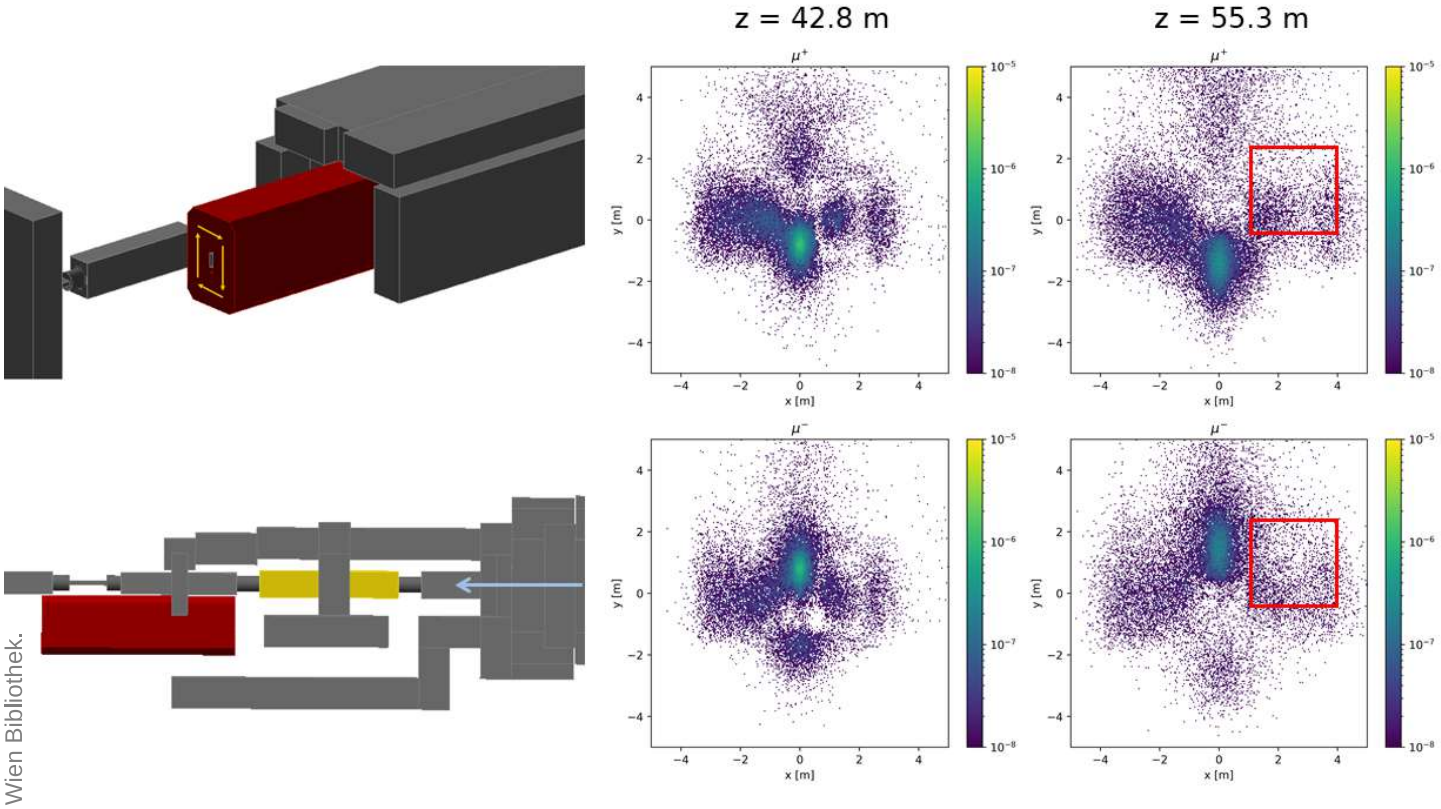


**Fig. 44:** Geometry and muon distributions with a scraper-like off-axis magnet of dimensions (xyz) = (1.5m×2.1m×5.0m) with its field of B = 1.7 T switched on. The geometry (left) displays the sweeping magnet in red, the altered layout of the shielding and BEND1C in yellow. The beam direction is indicated by the blue arrow. The plots on the right show the transverse distributions of positively (top) and negatively (bottom) charged muons at the locations described in Table 7. The red rectangle marks the possible location of the SHADOWS detector.

Since it became clear that the 5 m of dense iron alone will not be enough to achieve a sufficient suppression of the muon background, the next step is to turn on the magnetic field in the off-axis magnet. The magnet in this geometry remains at the dimensions of (xyz) = (1.5m×2.1m×5.0m), which with a magnetic field of B = 1.7 T leads to a field strength of BL = 8.5 Tm. The polarity of its field was chosen such that the field lines in the yoke near to the beam line point upwards. This is indicated in Figure 44, which also shows the results for the simulations in BDSIM for this configuration.

Compared to the configuration without the magnetic field, the muon distributions look very much alike. The main difference is that at 42.8 m there is are two gaps between the central muons and the ones along the positive x-direction. The reason for this shape is, that the muons that hit the sweeping magnet at its centre, will not be affected very much by its magnetic field, since in the centre of the magnet the force acting on the muons is about zero. The muons that move through one of the two sides of the iron yoke, where there is a magnetic field, are swept away thereby creating the gaps seen in x-direction.

The problem is that the centre of the magnet is not far enough off-axis, because if it were, the high population of muons there would also be bent away. However, simply moving the magnet further off-axis in x-direction is not an option, since thereby only the gaps would move, but the background would not be further reduced. Therefore, another solution for this has to be found.

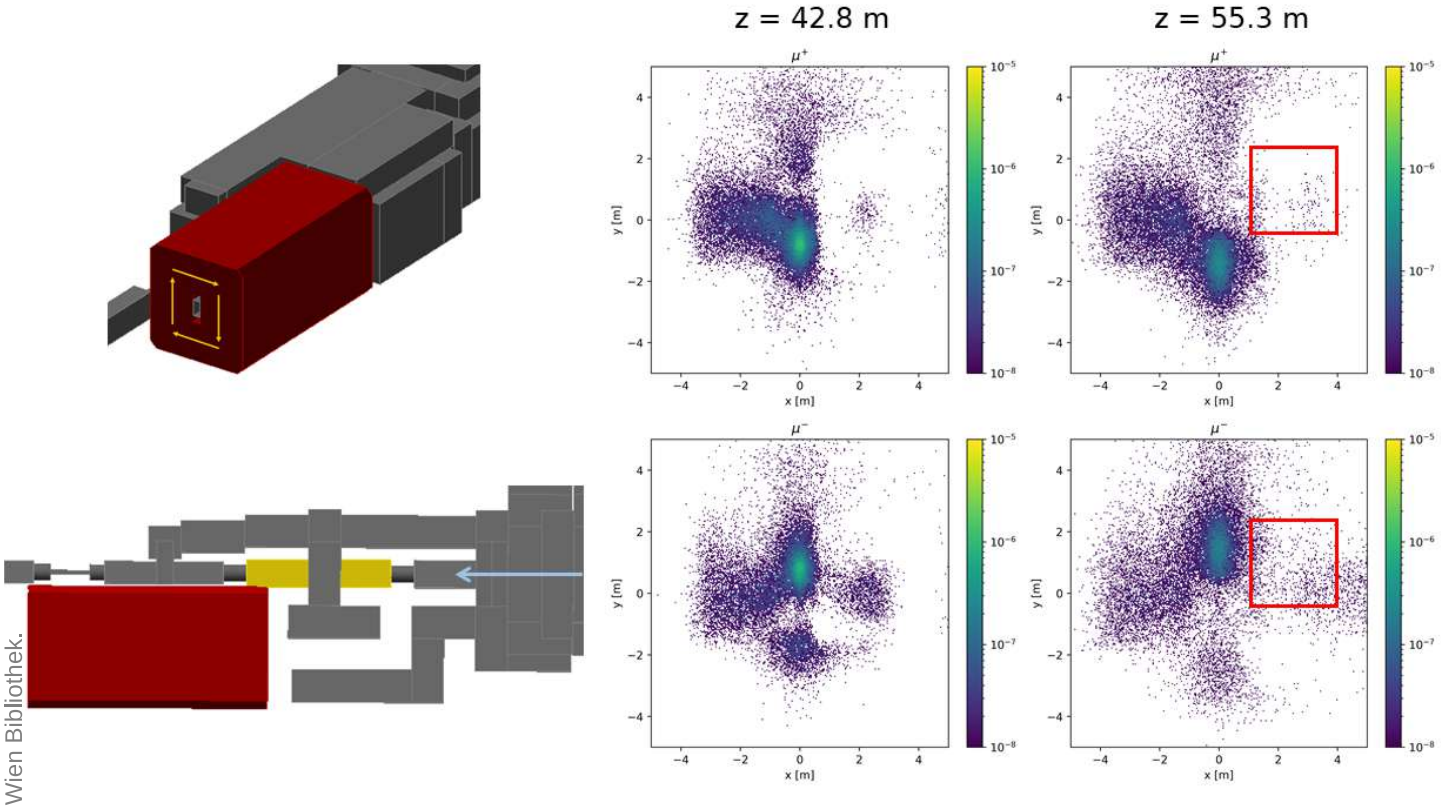


**Fig. 45:** Geometry and muon distributions with a scraper-like off-axis magnet of dimensions (xyz) = (3.0m×3.1m×6.0m) with its field of B = 1.7 T switched on. The geometry (left) displays the sweeping magnet in red, the altered layout of the shielding and BEND1C in yellow. The beam direction is indicated by the blue arrow. The plots on the right show the transverse distributions of positively (top) and negatively (bottom) charged muons at the locations described in Table 7. The red rectangle marks the possible location of the SHADOWS detector.

The simplest solution to the mentioned problem is to increase the transverse size of the off-axis magnet. With a larger magnet more muons will be affected by the near yoke. These muons are then swept in x-direction and therefore miss the SHADOWS detector. Also an additional meter in magnet length should add more stopping power to the muon sweeping magnet. The configuration shown in Figure 45 uses a larger scaled version of the scraper magnet, which now has the dimensions of (xyz) = (3.0m×3.1m×6.0m) with B = 1.7 T leading to a field strength of BL = 10.2 Tm. The results for a simulation with this setup are also displayed in Figure 45.
The plots show that for this configuration finally the muon background could be reduced drastically. Compared to the original setup shown in Figure 42 the number of muons in the relevant SHADOWS detector region could be reduced by a factor of 7 in the relevant SHADOWS region.
Furthermore, by having a look at the charge of the muons as it is displayed in Figure 45 one finds that the tested muon sweeping system is able to reduce the positive muons far better than the negative ones. In fact the background of $\mu^+$ would decrease by a factor of 18, while the $\mu^-$ backgound is reduced by a factor of 4 compared to the simulation without sweeping system. It can be expected that if the field had the opposite polarity, this effect would be the same only with complementary muon charges. The reason for that is shown in Figure 46. The left side of the magnet is the one responsible for the sweeping and is therefore the main reason for the background reduction. While the positive muons are swept away from the SHADOWS detector, the negative muons are swept into the direction of the return yoke. This return yoke,

however, also sweeps the negatively charged muons to the centre of the magnet meaning that these muons are trapped inside the magnet and therefore eventually reach the SHADOWS detector. Nonetheless, it is possible that this separation of the positive and negative muons might deliver the opportunity to even further optimize of the muon background. By doing so it might also be possible to reduce the size of the sweeping system and to avoid having this effect from the return yoke entirely.

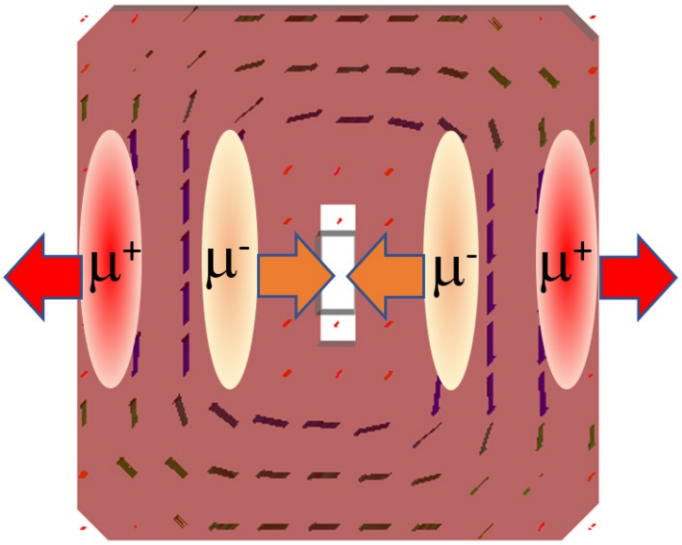


**Fig. 46:** Muon separation due to the magnetic field of the SHADOWS muon sweeping system.

# 4. Conclusion

The work for this thesis addresses the studies for possible future beam dump experiments in the P42 and K12 beam lines and for further developments in the BDSIM infrastructure of the BE-EA-LE section. The know-how gained during these studies shall deliver useful insights for the NA62-BD and SHADOWS experiments, help them understand the problems they might face and propose solutions on how to solve them. This last chapter shall draw the conclusions from the scientific work done and thereby pointing out questions that might be worth having a closer look at in succeeding studies.

Magnet geometries for the P42 beam line have been created as GDML files. They are now available for simulations in Geant4 and BDSIM. A Python tool called "fieldcreator" has been introduced to simplify the creation of magnetic field maps for BDSIM. Using these magnets and the Python tool, a beam line covering the last six magnets of the P42 beam line has been created in BDSIM that can be combined with the already existing model of the K12 beam line opening up the opportunity to test more parameters for possible future optimization studies. With the newly introduced magnets also the creation of a complete model of the P42 beam line in BDSIM comes within reach.

The beam dump mode has been successfully introduced to the BDSIM model of the K12 beam line. A discussion of the simulated backgrounds at relevant locations within the beam line revealed that the only relevant background for experiments using this setup will be the muon background. This is true for detectors that are placed on- or off-axis.

Furthermore, the model of the K12 beam line has been extended by two new elements. First of all, the environment surrounding the beam line, namely the TCC8 tunnel and experimental cavern ECN3, has been placed around the beam line thereby enabling to perform radiation studies with the BDSIM model for benchmarking the FLUKA simulations, which are CERN standard for these kinds of studies. It was found that backscattering at the walls of the cavern does not result in an additional muon background component in the relevant detector regions. Secondly, the NA62 detector downstream the GTK3 has been added to the model. In $K^+$ mode the additional material alongside the beam results in a decrease of the backgrounds other than muons, since the dense materials of the vacuum tube and the MUV filter work as additional shielding. It was found that in beam dump mode these backgrounds are again negligible, even after adding the model extensions. The newly introduced NA62 detector now opens up the opportunity to investigate the influence of the single detectors on the beam and evaluate what they might detect in $K^+$ mode as in beam dump mode.

The BDSIM model of K12 was benchmarked to data provided by NA62. This data was taken during CERN's Run 2 and the beam line was already put in beam dump mode for this first acquisition. A comparison of the simulated data with the measurement data showed a good qualitative agreement. Because of that, performing optimization studies with the BDSIM model became a valid approach.

Subsequently, an optimization study for the magnetic field configuration of BEND1B and BEND1C was performed. The results of this study propose that for NA62-BD the muon background can be reduced by a factor of 20 at the MUV3 detector if the optimized BEND1 configuration of B(BEND1B) = B(BEND1C) = $\pm$1.8 T is used. These results are in good agreement with previous studies that were based on G4Beamline simulations and have been carried out within the BE-EA-LE section at CERN [51, 52]. Additionally, the magnetic field configuration optimized for the possible location of the SHADOWS detector was found to be B(BEND1B) = 1.8 T and B(BEND1C) = 0.0 T. However, this configuration only reduces

the background by a factor 1.2, which clarified that the muon background minimization for SHADOWS demands further measures.

Because of that, several possibilities for a muon sweeping system upstream the SHADOWS detector have been tested and their effectiveness was evaluated. A configuration using a scaled version of K12's scraper magnet with the size of (xyz) = (3.0m×3.1m×6.0m) and a magnetic field of B = 1.7 T that is placed off-axis and upstream the relevant SHADOWS detector region was found to be a promising candidate for further muon suppression. An additional background reduction by a factor of 7 could be achieved with this configuration. Furthermore, it was found that the magnetic field of the off-axis magnet results in a charge separation in the muon background leading to the fact that the remaining background will mainly consist of muons of the same charge. Which one depends on the polarity of the magnet. It is possible that this charge separation could be used to design a more complex muon sweeping system that not only would be able to better sweep the muons, but also to reduce the magnet size and therefore the cost of such a sweeping system, which might be interesting to have a look at in future studies. Once the magnet geometry of the sweeping system becomes more concrete it will also be necessary to evaluate its impact on the NA62-BD experiment and whether the SHADOWS dedicated muon sweeping has an effect on the backgrounds that are seen at the MUV3 detector. An optimization of the magnetic field configuration in BEND3 poses another option for further muon sweeping for NA62-BD and could also improve the muon background when including the SHADOWS muon sweeping system.

# Appendices

## A. Example of a GDML file

The following example for the form of a GDML file was retrieved from the GDML manual [54]:

```
<?xml version="1.0" encoding="UTF-8"?>
<gdml xsi:noNamespaceSchemaLocation="schema/gdml.xsd">
   <define>
      ...
      <position name="TrackerinWorldpos" unit="mm" x="0" y="0" z="100"/>
   </define>
   <materials>
      ...
      <element name="Nitrogen" formula="N" Z="7.">
         <atom value="14.01"/>
      </element>
      <material formula=" " name="Air" >
         <D value="1.290" unit="mg/cm3"/>
          <fraction n="0.7" ref="Nitrogen" />
          <fraction n="0.3" ref="Oxygen" />
       </material>
   </materials>
   <solids>
      ...
      <box lunit="mm" name="Tracker" x="50" y="50" z="50"/>
   </solids>
   <structure>
      ...
      <volume name="World" >
         <materialref ref="Air" />
         <solidref ref="world" />
         <physvol>
            <volumeref ref="Tracker" />
            <positionref ref="TrackerinWorldpos"/>
            <rotationref ref="TrackerinWorldrot"/>
         </physvol>
      </volume>
   </structure>
   <setup name="Default" version="1.0" >
      <world ref="World" />
   </setup>
</gdml>
```

## B. Simulation Specifics

Software versions used for the studies described in the single sections:

| Section | BDSIM version | Geant4 version | Geant4 physics list |
|---|---|---|---|
| 3.2 | 1.4.develop | 10.6.1 | g4FTFP_BERT |
| 3.3 | 1.4.develop | 10.6.1 | g4FTFP_BERT |
| 3.4 | 1.5.0 | 10.6.2 | g4FTFP_BERT & emextraphysics.mac |
| 3.5 | 1.5.0 | 10.6.2 | g4FTFP_BERT & emextraphysics.mac |
| 3.6 | 1.5.0 | 10.6.2 | g4FTFP_BERT & emextraphysics.mac |

**Tab. 8:** Software versions used for the studies in this thesis.

## C. Tutorial: fieldcreator

The fieldcreator is a python tool that enables the user to create magnetic field maps for magnets that are commonly used at CERN, which are necessary for the geometry preparations in FLUKA and BDSIM. At the moment the tool consists of three functions:

**CreateFieldFluka("magnet", "strength", "source")**: This function can be used to create a FLUKA field map by making use of the already existing ROOT scripts, which it inherently calls within the script. To run these scripts three input parameters, which are "magnet", "strength" and "source" have to be inserted. "magnet" is the name of the magnet one wants to create a field map for, "strength" defines the field strength - defined for bending magnets in equation 2 and for quadrupole magnets in equation 3 - and "source" tells the function, which source script there should be used - there are two options "halo" and "schwarz". For the field strength the "halo"-script uses linear interpolation from one underlying field map file, while the "schwarz"-script uses several of them at different field strengths making it possible to take into account their flattening at high values. This means the field maps created with the "schwarz"-option are more detailed, but currently not all magnets are available with this script, which is why the "halo"-option can be used for the remaining magnets.

**CreateFieldBDSIM("magnet", "strength", "duplicates")**: This function converts an existing FLUKA field map of the form $(x, y, Fx, Fy)$ to a BDSIM field map of the form $(x', y', Fx', Fy', Fz')$. This is done by adding a fifth column that reflects the field in z-direction. Since the field of the magnets will not have a z-component, it is filled with zeros. However, this is not the only difference between the FLUKA and the BDSIM field map. While the field map in FLUKA will only cover a part of the magnet, that is later duplicated and mirrored for the other parts of the magnet via symmetry conditions inside FLUKA, this has to be done manually for BDSIM. Depending on the magnet this needs to be done differently depending on the underlying FLUKA field map. Figure 47 shows the three options that have been implemented for fieldcreator. While "B" and "Q" declare whether the magnet is a bending or a quadrupole magnet and thereby change the field direction of the duplicated fields, "2" and "4" tell whether the FLUKA field map represents a half of the magnet or a quarter, or in other words how many duplicates there are needed. One of the three options "B2", "B4" and "Q4" has to be set in the "duplicates" input variable. Furthermore, "magnet" and "strength" have to be set again. Finally, the BDSIM field map will be created.

**CreateField("magnet", "strength", "source", "duplicates")**: This function calls the first two to create the BDSIM field map directly from the input variables. Therefore, all four input variables are needed.

This script can also be expanded to do the same for other simulation environments.

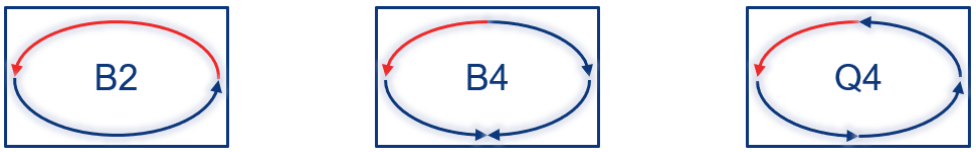


**Fig. 47:** Options for the "duplicates" input variable. The red arrow marks the region reflected by the FLUKA field map. Depending on the specific magnet, one of the three options will be correct.

## References


[1] P. A. Zyla *et al.*, "Review of particle physics," *Progress of Theoretical and Experimental Physics*, vol. 2020, 08 2020. 083C01.

[2] M. Thomson, *Modern particle physics*. New York: Cambridge University Press, 2013.

[3] "Standard model of elementary particles," 2021. File: Standard Model of Elementary Particles.svg.

[4] P. W. Higgs, "Broken symmetries and the masses of gauge bosons," *Phys. Rev. Lett.*, vol. 13, pp. 508–509, Oct 1964.

[5] G. Aad, T. Abajyan, B. Abbott, *et al.*, "Observation of a new particle in the search for the standard model higgs boson with the atlas detector at the lhc," *Physics Letters B*, vol. 716, pp. 1–29, Sep 2012.

[6] S. Chatrchyan, V. Khachatryan, A. Sirunyan, *et al.*, "Observation of a new boson at a mass of 125 gev with the cms experiment at the lhc," *Physics Letters B*, vol. 716, pp. 30–61, Sep 2012.

[7] G. Anzivino, "Measurement of direct cp violation by na48," *Multiparticle Dynamics*, Mar 2002.

[8] W. John, "What cp violating processes do we know of?." Physics Stack Exchange.

[9] M. Tanabashi *et al.*, "Review of particle physics," *Phys. Rev. D 98*, 2018.

[10] S. Profumo, *An Introduction to Particle Dark Matter*. WORLD SCIENTIFIC (EUROPE), 2017.

[11] S. Price, "Galaxy masses," 2015.

[12] V. C. Rubin, "The rotation of spiral galaxies," *Science*, vol. 220, no. 4604, pp. 1339–1344, 1983.

[13] S. Hawking, "Gravitationally Collapsed Objects of Very Low Mass," *Monthly Notices of the Royal Astronomical Society*, vol. 152, pp. 75–78, 04 1971.

[14] A. Hanslmeier, *Einführung in die Astronomie und Astrophysik*, vol. 2. Berlin Heidelberg: Spektrum Akademischer Verlag, 2007.

[15] C. Alcock, R. Allsman, D. Alves, *et al.*, "Eros and macho combined limits on planetary-mass dark matter in the galactic halo," *The Astrophysical Journal Letters*, vol. 499, p. L9, 01 2009.

[16] R. D. Peccei, "The strong cp problem and axions," *Axions*, pp. 3–17, 2008.

[17] H. Noh, J. C. Hwang, and C. G. Park, "Axion as a cold dark matter candidate: Proof to fully nonlinear order," *The Astrophysical Journal*, vol. 846, p. 1, Aug 2017.

[18] P. Sikivie, "Experimental tests of the "invisible" axion," *Phys. Rev. Lett.*, vol. 51, pp. 1415–1417, Oct 1983.

[19] V. Anastassopoulos, S. Aune, K. Barth, *et al.*, "New cast limit on the axion-photon interaction," *Nature Physics*, vol. 13, pp. 584–590, May 2017.

[20] T. Braine, R. Cervantes, N. Crisosto, *et al.*, "Extended search for the invisible axion with the axion dark matter experiment," *Physical Review Letters*, vol. 124, Mar 2020.

[21] M. D. Ortiz, J. Gleason, H. Grote, *et al.*, "Design of the alps ii optical system," 2021.

[22] P. W. Graham, I. G. Irastorza, S. K. Lamoreaux, *et al.*, "Experimental searches for the axion and axion-like particles," *Annual Review of Nuclear and Particle Science*, vol. 65, pp. 485–514, Oct 2015.

[23] M. Drewes, "The phenomenology of right handed neutrinos," *International Journal of Modern Physics E*, vol. 22, p. 1330019, Aug 2013.

[24] S. Lazanu, I. Lazanu, and G. Ciobanu, "Modelling the transient processes produced under heavy particle irradiation," *Nuclear Instruments and Methods in Physics Research Section B: Beam Interactions with Materials and Atoms*, vol. 269, pp. 498–503, Feb 2011.

[25] A. Abdelhameed, G. Angloher, P. Bauer, *et al.*, "First results from the cresst-iii low-mass dark matter program," *Physical Review D*, vol. 100, Nov 2019.

[26] E. Aprile, J. Aalbers, F. Agostini, *et al.*, "The xenon1t dark matter experiment," *The European Physical Journal C*, vol. 77, Dec 2017.

[27] R. Agnese, A. Anderson, T. Aralis, *et al.*, "Low-mass dark matter search with cdmslite," *Physical Review D*, vol. 97, Jan 2018.

[28] M. Fabbrichesi, E. Gabrielli, and G. Lanfranchi, "The physics of the dark photon," *SpringerBriefs in Physics*, 2021.

[29] B. Holdom, "Two u(1)'s and $\epsilon$ charge shifts," *Physics Letters B*, vol. 166, no. 2, pp. 196–198, 1986.

[30] G. L. D'Alessandro, "Lecture notes of summer students lecture of be-ea-le," October 2020.

[31] J. Pinson, "The power of attraction: magnets in particle accelerators (fermilab)," 2020.

[32] "The Compact Linear Collider (CLIC) - Project Implementation Plan," vol. 4/2018, 12 2018.

[33] CERN, "Computing: Storage," 2021.

[34] CERN, "Accelerator complex," 2021.

[35] CERN, "Schematic of the north area beam lines," 2007.

[36] G. L. D'Alessandro, "K12 beam line," October 2020.

[37] E. C. Gil, E. M. Albarran, E. Minucci, *et al.*, "The beam and detector of the na62 experiment at cern," *Journal of Instrumentation*, vol. 12, May 2017.

[38] Q. H. Cao, G. Li, B. Yan, *et al.*, "Double higgs production at the 14 tev lhc and a 100 tev pp collider," *Physical Review D*, vol. 96, Nov 2017.

[39] F. Hahn, F. Ambrosino, A. Ceccucci, *et al.*, "NA62: Technical Design Document," tech. rep., CERN, Geneva, Dec 2010.

[40] E. Cortina Gil, "Measurement of the very rare $K^+ \to \pi^+\nu\bar{\nu}$ decay," tech. rep., CERN, Geneva, Mar 2021.

[41] S. Agostinelli, J. Allison, K. Amako, *et al.*, "Geant4 - a simulation toolkit," *Nuclear Instruments and Methods in Physics Research Section A: Accelerators, Spectrometers, Detectors and Associated Equipment*, vol. 506, no. 3, pp. 250–303, 2003.

[42] L. Nevay, S. Boogert, J. Snuverink, *et al.*, "Bdsim: An accelerator tracking code with particle-matter interactions," *Computer Physics Communications*, vol. 252, p. 107200, 2020.

[43] R. Chytracek, J. Mccormick, W. Pokorski, and G. Santin, "Geometry description markup language for physics simulation and analysis applications," *IEEE Transactions on Nuclear Science*, vol. 53, no. 5, pp. 2892–2896, 2006.

[44] M. Van Dijk *et al.*, "The K12 beamline for the KLEVER experiment," *J. Phys. Conf. Ser.*, vol. 1350, no. 1, p. 012092, 2019.

[45] CERN, "Secondary beams and areas: Bending magnets," 2017.

[46] CERN, "Secondary beams and areas: Quadrupole magnets," 2017.

[47] BE-EA-LE, "K12hika+ beatch-file," 2019.

[48] BE-EA-LE, "K12hika+ transport-file," 2007.

[49] S. Boogert, A. Abramov, J. Albrecht, *et al.*, "Pyg4ometry : A Tool to Create Geometries for Geant4, BDSIM, G4Beamline and FLUKA for Particle Loss and Energy Deposit Studies," in *10th International Particle Accelerator Conference*, 6 2019.

[50] S. Fedotov, A. Kleymenova, and A. Khotjantsev, "New chod detector for the na62 experiment at cern," *Physics of Particles and Nuclei*, vol. 49, pp. 26–29, 01 2018.

[51] M. Rosenthal, D. Banerjee, J. Bernhard, *et al.*, "Single-muon rate reduction for beam dump operation of the k12 beam line at cern," *International Journal of Modern Physics A*, vol. 34, no. 36, p. 1942026, 2019.

[52] L. Gatignon, D. Banerjee, J. Bernhard, *et al.*, "Report from the Conventional Beams Working Group to the Physics beyond Colliider Study and to the European Strategy for Particle Physics," tech. rep., CERN, Geneva, Dec 2018.

[53] G. Lanfranchi, A. Gerbershagen, F. Stummer, *et al.*, "Shadows (pbc workshop)," 2021.

[54] B. Lloyd, "Gdml manual," 2021.